CHAPTER

11

Instability

CHAPTER OBJECTIVES

- To present the mathematical theory of temporal flow instability

- To illustrate how this theory may be applied in a variety of confined and unconfined flows

- To present classic theoretical results for parallel flows

- To describe results for viscous flows

- To discuss nonlinearity and the possible role of chaos in the transition to turbulence

11.1. INTRODUCTION

Many phenomena that satisfy the conservation laws exactly are unobservable because they are unstable when subjected to the small disturbances that are invariably present in any real system. Consider the stability of two simple mechanical systems in a vertical gravitation field. A sharpened pencil may, in theory, be balanced on its point on a horizontal surface, but any small surface vibration or air pressure disturbance will knock it over. Thus, sharpened pencils on horizontal surfaces are commonly observed lying horizontally. Similarly, the position of a smooth ball resting on the inside surface of a hemispherical bowl is stable provided the bowl is concave upwards. However, the ball's position is unstable to small displacements if placed on the outer side of a hemispherical bowl when the bowl is concave downwards (Figure 11.1). In fluid flows, smooth laminar flows are stable to small disturbances only when certain conditions are satisfied. For example, in the flow of a homogeneous viscous fluid in a channel, the Reynolds number must be less than some critical value for the flow to be stable, and in a stratified shear flow, the Richardson number must be larger than a critical value for stability. When these conditions are not satisfied, infinitesimal disturbances may grow spontaneously and completely change the character of the original flow. Sometimes the disturbances can grow to finite amplitude and reach a new steady-state equilibrium. The new state may then become unstable to other types of disturbances, and may evolve to yet another steady state, and so on. As a limit of this situation, the
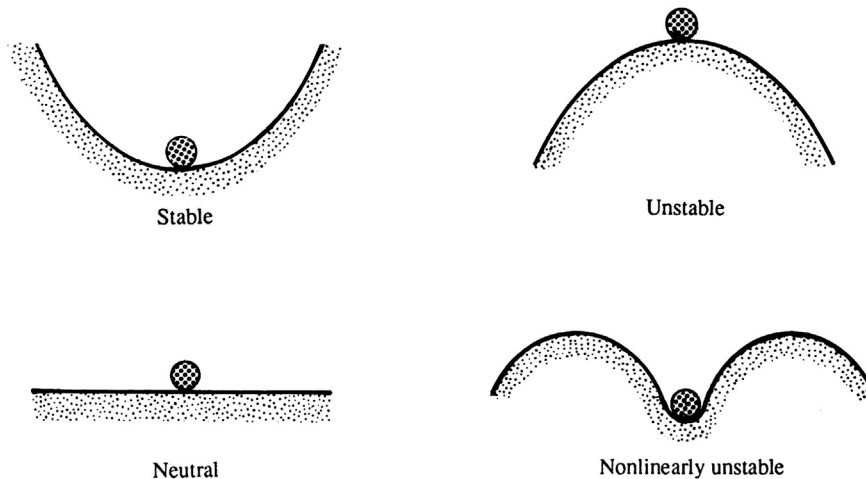
FIGURE 11.1 Stable and unstable mechanical systems. Here, gravity is presumed to act downward. In the upper left and lower right panels, a small displacement of the round object away from equilibrium will be opposed by the action of gravity and the object will move back toward its equilibrium location. These are linearly stable situations. In the upper right panel, a small displacement of the object will be enhanced by the action of gravity and the object will move away from its equilibrium location, an unstable situation. In the lower left, a small displacement of the object does not produce a new force, thus the situation is neutrally stable. In the lower right panel, a sufficiently large displacement of the object may place it beyond its region of stability; thus this situation is nonlinearly unstable.

flow becomes a superposition of a variety of interacting disturbances with nearly random phases, a state of chaotic or nearly chaotic fluctuations that is commonly described as *turbulence*. In fact, two primary motivations for studying fluid-flow stability are: 1) to understand the process of laminar to turbulent transition, and 2) to predict the onset of this transition. Finite-amplitude effects, including the development of chaotic solutions, are examined briefly later in this chapter.

The primary objective of this chapter, however, is the examination of stability of certain fluid flows with respect to infinitesimal disturbances. We shall introduce perturbations on a particular flow, and determine whether the equations of motion predict that the perturbations grow or decay. In this analysis, the perturbations are commonly assumed to be small enough so that linearization is possible through neglect of quadratic and higher order terms in the perturbation variables and their derivatives. While such linearization fruitfully allows the production of analytical results, it inherently limits the applicability of such results to the *initial* behavior of infinitesimal disturbances. The loss of stability does not in itself constitute a transition to turbulence since the linear theory can, at best, describe only the very beginning of the transition process. In addition, a real flow may be stable to infinitesimal disturbances (linearly stable), but may be unstable to sufficiently large disturbances (nonlinearly unstable); this is schematically represented in Figure 11.1.

In spite of these limitations, linear stability theory enjoys considerable success. There is excellent agreement between experimental results and the theoretical prediction of the onset of thermal convection in a layer of fluid, and of the onset of Tollmien-Schlichting waves in a viscous boundary layer. Taylor's experimental verification of his own theoretical prediction of the onset of secondary flow in a rotating Couette flow is so striking that it has led people to suggest that Taylor's work is the first rigorous confirmation of the Navier-Stokes equations on which the calculations are based.

This chapter describes the temporal instability of confined and unconfined flows where spatially extended perturbations decay, persist, or grow in time. The complimentary situation where spatially confined disturbances decay, persist, or grow while traveling in space is more complicated and is described elsewhere (see Huerre & Monkewitz, 1990). The primary analysis technique used here, the method of normal modes, is described in the next section. The third through eleventh sections of this chapter utilize this technique to illustrate basic flow physics and to present results for a variety of flows important in engineering applications and geophysical situations. The final few sections describe transition and the onset of turbulence. None of the flow situations discussed in this chapter contains Coriolis forces. *Baroclinic instability*, which does contain the Coriolis frequency, is discussed in Chapter 13. The books by Chandrasekhar (1961, 1981) and Drazin and Reid (1981) provide further information on flow instability. The review article by Bayly, Orszag, and Herbert (1988) is recommended as well.

11.2. METHOD OF NORMAL MODES

Basic linear stability analysis consists of presuming the existence of sinusoidal disturbances to a *basic state* (also called a background, initial, or equilibrium state), which is the flow whose stability is being investigated. For example, the velocity field of a basic state

involving a flow parallel to the x-axis and varying along the z-axis is $\mathbf{U} = U(z)\mathbf{e}_x$. On this background flow we superpose a spatially extended disturbance of the form:

$$u(x,y,z,t) \;=\; \widehat{u}(z)\,\exp\{ikx + imy + \sigma t\} \;=\; \widehat{u}(z)\,\exp\{i|\mathrm{K}|(\mathbf{e}_K\boldsymbol{\cdot}\mathbf{x} - ct)\} \qquad (11.1)$$

where $\hat{u}(z)$ is a complex amplitude, $i = \sqrt{-1}$ is the imaginary root, $\mathbf{K} = (k, m, 0)$ is the disturbance wave number, $e_K = \mathbf{K}/|\mathbf{K}|$, $\mathbf{x} = (x, y, z)$, σ is the temporal growth rate, c is the complex phase speed of the disturbance, and the real part of (11.1) is taken to obtain physical quantities. The complex notation used here is explained in Section 7.7. The two forms of (11.1) are useful when the disturbance is stationary, and when it takes the form of a traveling wave, respectively. The reason solutions exponential in (x, y, t) are allowed in (11.1) is that, as we shall see, the coefficients of the differential equation governing the perturbation in this flow are independent of (x, y, t). The flow field is assumed to be unbounded in the x and y directions, hence the wave number components k and m can only be real (and $|\mathbf{K}|$ positive real) in order that the dependent variables remain bounded as $x, y \rightarrow \pm\infty$; however, $\sigma = \sigma_r + i\sigma_i$ and $c = c_r + ic_i$ are regarded as complex.

The behavior of the system for *all* possible wave numbers, $\mathbf{K}$, is examined in the analysis. If σ_r or c_i are positive for *any* value of the wave number, the system is unstable to disturbances of this wave number. If no such unstable state can be found, the system is stable. We say that

$$\sigma_r < 0 \quad \text{or} \quad c_i < 0 \text{ implies a } \textit{stable} \text{ flow,}$$

$$\sigma_r = 0 \quad \text{or} \quad c_i = 0 \text{ implies a } \textit{neutrally stable} \text{ flow, and}$$

$$\sigma_r > 0 \quad \text{or} \quad c_i > 0 \text{ implies an } \textit{unstable} \text{ flow.}$$

The method of analysis involving the examination of Fourier components such as (11.1) is called the *normal mode method*. An arbitrary disturbance can be decomposed into a complete set of normal modes. In this method the stability of each of the modes is examined separately, as the linearity of the problem implies that the various modes do not interact. The method leads to an eigenvalue problem.

The boundary between stability and instability is called the *marginal state*, for which $\sigma_r = c_i = 0$. There can be two types of marginal states, depending on whether σ_i or c_r is also zero or nonzero in this state. If $\sigma_i = c_r = 0$ in the marginal state, then (11.1) shows that the marginal state is characterized by a *stationary pattern* of motion; we shall see later that the instability here appears in the form of *cellular convection* or *secondary flow* (see Figure 11.18 later). If, on the other hand, $\sigma_i \neq 0$ or $c_r \neq 0$ in the marginal state, then the instability sets in as traveling oscillations of growing amplitude. Following Eddington, such a mode of instability is frequently called *overstability* because the restoring forces are so strong that the system overshoots its corresponding position on the other side of equilibrium. We prefer to avoid this term and instead call it the *oscillatory mode* of instability.

The difference between the *neutrally stable state* and the *marginal state* should be noted as both have $\sigma_r = c_i = 0$. However, the marginal state has the additional constraint that it lies at the *borderline* between stable and unstable solutions. That is, a slight change of parameters (such as the Reynolds number) from the marginal state can take the system into an unstable regime where $\sigma_r > 0$. In many cases we shall find the stability criterion by simply setting $\sigma_r = 0$ or $c_i = 0$, without formally demonstrating that these conditions define the borderline between unstable and stable states.

11.3. KELVIN-HELMHOLTZ INSTABILITY

Instability at the interface between two horizontal parallel fluid streams with different velocities and densities is called the *Kelvin-Helmholtz instability*. This is an inertial instability and it can be readily analyzed assuming ideal flow in each stream. The name is also commonly used to describe the instability of the more general case where the variations of velocity and density are continuous and occur over a finite thickness (see Section 11.7).

The Kelvin-Helmholtz instability leads to enhanced momentum, heat, and moisture transport in the atmosphere, plus it is routinely exploited in a variety of geometries for mixing two or more fluid streams in engineering applications. The simplest version is analyzed here in two dimensions (x, z), where x is the stream-wise coordinate and z is the vertical coordinate. Consider two fluid layers of infinite depth that meet at a zero-thickness interface located at $z = \zeta(x, t)$. Let U_1 and ρ_1 be the horizontal velocity and density of the basic state in the upper half-space, and U_2 and ρ_2 be those of the basic state in the lower half-space (Figure 11.2). From Kelvin's circulation theorem, the perturbed flow must be irrotational in each half-space because the motion develops from an irrotational basic state, uniform velocity in each half-space. Thus, the infinitesimally perturbed flow above (subscript 1) and below (subscript 2) the interface can be described by the velocity potentials:

$$\tilde{\phi}_1 = U_1 x + \phi_1, \quad \text{and} \quad \tilde{\phi}_2 = U_2 x + \phi_2, \tag{11.2}$$

where the U_1 and U_2 terms represent the basic state, and tildes ($\sim$) denote the total flow potentials (background plus perturbations), a notation used throughout this chapter. Here $\tilde{\phi}_1$ and $\tilde{\phi}_2$ must satisfy the Laplace equation, so the perturbation potentials, ϕ_1 and ϕ_2, must also satisfy Laplace equations:

$$\nabla^2 \phi_1 = 0 \quad \text{and} \quad \nabla^2 \phi_2 = 0. \tag{11.3}$$

There are a total of four boundary conditions:

$$\phi_1 \to 0 \quad \text{as } z \to +\infty, \quad \phi_2 \to 0 \quad \text{as } z \to -\infty, \tag{11.4, 11.5}$$
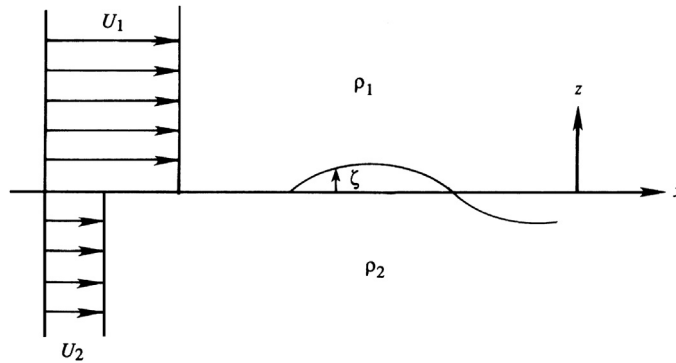

FIGURE 11.2 Basic flow configuration leading to the Kelvin-Helmholtz instability. Here the velocity and density profiles are discontinuous across an interface nominally located at $z = 0$. If the small vertical perturbation $\zeta(x,t)$ to this interface grows, then the flow is unstable.

$$\mathbf{n}\cdot\nabla\tilde{\phi}_1 = \mathbf{n}\cdot\mathbf{U}_s = \mathbf{n}\cdot\nabla\tilde{\phi}_2 \quad \text{on } z = \zeta, \text{ and} \tag{11.6}$$

$$p_1 = p_2 \quad \text{on } z = \zeta, \tag{11.7}$$

where $\mathbf{n}$ is the local normal to the interface, $\mathbf{U}_s$ is the velocity of the interface, and p_1 and p_2 are the pressures above and below the interface. Here, the kinematic and dynamic boundary conditions, (11.6) and (11.7), respectively, are conceptually similar to (7.14) and (7.20). The kinematic condition, (11.6), can be rewritten:

$$\mathbf{n}\cdot\left\{\frac{\partial\tilde{\phi}_1}{\partial x}\mathbf{e}_x + \frac{\partial\tilde{\phi}_1}{\partial z}\mathbf{e}_z\right\} = \mathbf{n}\cdot\left\{\frac{\partial\zeta}{\partial t}\mathbf{e}_z\right\} = \mathbf{n}\cdot\left\{\frac{\partial\tilde{\phi}_2}{\partial x}\mathbf{e}_x + \frac{\partial\tilde{\phi}_2}{\partial z}\mathbf{e}_z\right\} \quad \text{on } z = \zeta, \tag{11.8}$$

where $\mathbf{n} = \nabla f/|\nabla f| = [-(\partial\zeta/\partial x)\mathbf{e}_x + \mathbf{e}_z]/\sqrt{1 + (\partial\zeta/\partial x)^2}$ when $f(x,\ z,\ t) = z - \zeta(x,\ t) = 0$ defines the interface, and $\mathbf{U}_s = (\partial\zeta/\partial t)\mathbf{e}_z$ can be considered purely vertical. When the dot products are performed, the common square-root factor removed, and the derivatives of the potentials evaluated using (11.2), (11.8) reduces to:

$$-\left(U_1 + \frac{\partial\phi_1}{\partial x}\right)\frac{\partial\zeta}{\partial x} + \frac{\partial\phi_1}{\partial z} = \frac{\partial\zeta}{\partial t} = -\left(U_2 + \frac{\partial\phi_2}{\partial x}\right)\frac{\partial\zeta}{\partial x} + \frac{\partial\phi_2}{\partial z} \quad \text{on } z = \zeta.$$

This condition can be linearized by applying it at $z = 0$ instead of at $z = \zeta$ and by neglecting quadratic terms. Thus, the simplified version of (11.6) is:

$$-U_1\frac{\partial\zeta}{\partial x} + \frac{\partial\phi_1}{\partial z} = \frac{\partial\zeta}{\partial t} = -U_2\frac{\partial\zeta}{\partial x} + \frac{\partial\phi_2}{\partial z} \quad \text{on } z = 0. \tag{11.9}$$

The dynamic boundary condition at the interface requires the pressure to be continuous across the interface (when surface tension is neglected). The unsteady Bernoulli equations above and below the layer are:

$$\frac{\partial\tilde{\phi}_1}{\partial t} + \frac{1}{2}|\nabla\tilde{\phi}_1|^2 + \frac{p_1}{\rho_1} + gz = C_1, \quad \text{and} \quad \frac{\partial\tilde{\phi}_2}{\partial t} + \frac{1}{2}|\nabla\tilde{\phi}_2|^2 + \frac{p_2}{\rho_2} + gz = C_2. \tag{11.10}$$

So pressure matching requires:

$$p_1 = \rho_1\left(C_1 - \frac{\partial\tilde{\phi}_1}{\partial t} - \frac{1}{2}|\nabla\tilde{\phi}_1|^2 - gz\right) = \rho_2\left(C_2 - \frac{\partial\tilde{\phi}_2}{\partial t} - \frac{1}{2}|\nabla\tilde{\phi}_2|^2 - gz\right) = p_2 \text{ on } z = \zeta. \tag{11.11}$$

In the undisturbed state ($\phi_1 = \phi_2 = 0$, and $\zeta = 0$), (11.11) implies:

$$(p_1)_{undisturbed} = \rho_1\left(C_1 - \frac{1}{2}U_1^2\right) = \rho_2\left(C_2 - \frac{1}{2}U_2^2\right) = (p_2)_{undisturbed}. \tag{11.12}$$

Subtracting (11.11) from (11.12) and inserting (11.2) leads to:

$$\rho_1\left(\frac{\partial\phi_1}{\partial t} + U_1\frac{\partial\phi_1}{\partial x} + \frac{1}{2}|\nabla\phi_1|^2 + gz\right) = \rho_2\left(\frac{\partial\phi_2}{\partial t} + U_2\frac{\partial\phi_2}{\partial x} + \frac{1}{2}|\nabla\phi_2|^2 + gz\right) \text{ on } z = \zeta,$$

and this condition can be linearized by dropping quadratic terms and evaluating derivatives on $z = 0$ to find:

$$\rho_1 \left(\frac{\partial \phi_1}{\partial t} + U_1 \frac{\partial \phi_1}{\partial x} + g\zeta \right) = \rho_2 \left(\frac{\partial \phi_2}{\partial t} + U_2 \frac{\partial \phi_2}{\partial x} + g\zeta \right) \text{ on } z = 0. \tag{11.13}$$

Thus, field equations (11.3) and the conditions (11.4), (11.5), (11.9), and (11.13) specify the linear stability of a velocity discontinuity between uniform flows of different speeds and densities.

We now apply the method of normal modes and look for oscillatory solutions for ϕ_1' and ϕ_2' in the second exponential form of (11.1) with $\mathbf{K} = (k, 0, 0)$:

$$\phi_1(x, z, t) = A_1(z) \exp\{ik(x - ct)\}, \text{ and } \phi_2(x, z, t) = A_2(z) \exp\{ik(x - ct)\}. \tag{11.14}$$

Insertion of (11.14) into (11.3) produces:

$$-k^2 A_1 + \frac{d^2 A_1}{dz^2} = 0, \quad \text{and} \quad -k^2 A_2 + \frac{d^2 A_2}{dz^2} = 0,$$

after common factors are divided out. These equations have exponential solutions: $A_{\pm} \exp(\pm kz)$. The boundary conditions (11.4) and (11.5) require the minus sign for $z > 0$, and the positive sign for $z < 0$, so (11.14) reduces to:

$$\phi_1 = A_- \exp\{ik(x - ct) - kz\}, \quad \text{and} \quad \phi_2 = A_+ \exp\{ik(x - ct) + kz\}. \tag{11.15}$$

Inserting these two equations and a matching form for the interface shape, $\zeta = \zeta_o \exp\{ik(x - ct)\}$, into (11.9) and (11.13) leads to:

$$-iU_1 k\zeta_o - kA_- = -ikc\zeta_o = -iU_2 k\zeta_o + kA_+, \text{ and} \tag{11.16}$$

$$\rho_1(-ikcA_- + ikU_1 A_- + g\zeta_o) = \rho_2(-ikcA_+ + ikU_2 A_+ + g\zeta_o). \tag{11.17}$$

The remnant of the kinematic boundary condition (11.16) is sufficient to find $A_{\pm}$ in terms of ζ_o:

$$kA_- = -(ikU_1 - ikc)\zeta_o, \quad \text{and} \quad kA_+ = (ikU_2 - ikc)\zeta_o.$$

Substituting these into the remnant of the dynamic boundary condition (11.17) leads to a quadratic equation for c:

$$\rho_1 \left(-(-ikc + ikU_1)^2 + gk \right) = \rho_2 \left((-ikc + ikU_2)^2 + gk \right),$$

after the common factor of ζ_o has been divided out. The two solutions for c are:

$$c = \frac{\rho_2 U_2 + \rho_1 U_1}{\rho_2 + \rho_1} \pm \left[\left(\frac{\rho_2 - \rho_1}{\rho_2 + \rho_1} \right) \frac{g}{k} - \frac{\rho_2 \rho_1}{(\rho_2 + \rho_1)^2} (U_2 - U_1)^2 \right]^{1/2}. \tag{11.18}$$

Clearly, both possible values for c imply neutral stability ($c_i = 0$) as long as the second term within the square root is smaller than the first. However, one of these solutions will lead to exponential growth ($c_i > 0$) when

$$\left(\frac{\rho_2 - \rho_1}{\rho_2 + \rho_1}\right)\frac{g}{k} < \frac{\rho_2\rho_1}{(\rho_2 + \rho_1)^2}(U_2 - U_1)^2 \text{ or } g(\rho_2^2 - \rho_1^2) < k\rho_1\rho_2(U_2 - U_1)^2,$$

which occurs when the free-stream velocity difference is high enough, the density difference is small enough, or the wave number k (presumed positive real) is large enough. In addition, for each growing solution there is a corresponding decaying solution. This happens because the coefficients of the differential equation and the boundary conditions are all real (see Section 11.7).

Although it is somewhat complicated, (11.18) includes several limiting cases with simple interpretations. First of all, setting $U_1 = U_2 = 0$ simplifies (11.18) to

$$c = \pm\left[\left(\frac{\rho_2 - \rho_1}{\rho_2 + \rho_1}\right)\frac{g}{k}\right]^{1/2}, \tag{11.19}$$

which indicates a neutrally stable situation as long as $\rho_2 > \rho_1$. In this case, (11.19) is the dispersion relation for interface waves in an initially static medium; see (7.96). When $U_1 \neq U_2$, one can always find a value of k large enough to satisfy the requirement for instability. Because all wavelengths must be allowed in an instability analysis, we can say that the *flow is always unstable to short waves when* $U_1 \neq U_2$. When $\rho_1 = \rho_2$, the interface becomes a vortex sheet (see Section 5.8) with strength $\gamma = U_2 - U_1$, and (11.18) reduces to

$$c = \left(\frac{U_2 + U_1}{2}\right) \pm i\left(\frac{U_2 - U_1}{2}\right). \tag{11.20}$$

Here there is always a positive imaginary value of c for every k, so a vortex sheet is unstable to disturbances of any wavelength. It is also seen that the unstable wave moves with a phase velocity, c_r, equal to the average velocity of the basic flow. This must be true from symmetry considerations. In a frame of reference moving with the average velocity, the basic flow is symmetric and the wave therefore should have no preference between the positive and negative x directions (Figure 11.3).

The Kelvin-Helmholtz instability is caused by the destabilizing effect of shear, which overcomes the stabilizing effect of stratification. This kind of instability is easy to generate in the laboratory by filling a horizontal glass tube (of rectangular cross-section) containing two liquids of slightly different densities (one colored) and gently tilting it. This starts a current in the lower layer down the plane and a current in the upper layer up the plane. An example of instability generated in this manner is shown in Figure 11.4.

Shear instability of stratified fluids is ubiquitous in the atmosphere and the ocean and believed to be a major source of internal waves. Figure 11.5 is a striking photograph of a cloud pattern, which is clearly due to the existence of high shear across a sharp density gradient. Similar photographs of injected dye have been recorded in oceanic thermoclines (Woods, 1969).

Figures 11.4 and 11.5 show the advanced nonlinear stage of the instability in which the interface is a rolled-up layer of vorticity. Such an observed evolution of the interface is in agreement with results of numerical calculations in which the nonlinear terms are retained (Figure 11.6).

The source of energy for generating the Kelvin-Helmholtz instability is derived from the kinetic energy of the two streams. The disturbances evolve to smear out the gradients
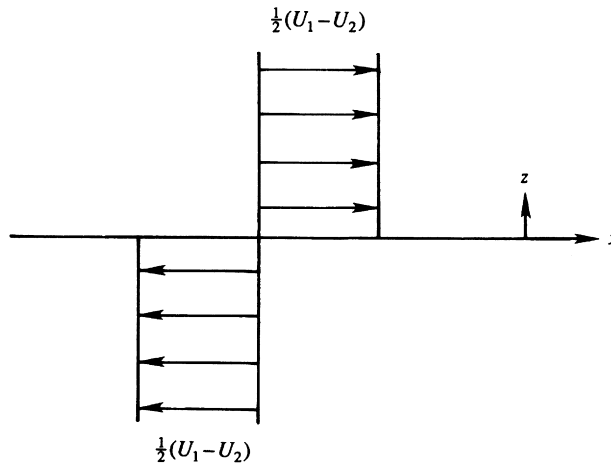
$$\tfrac{1}{2}(U_1 - U_2)$$

$$\tfrac{1}{2}(U_1 - U_2)$$

FIGURE 11.3 Background velocity field for the Kelvin-Helmholtz instability as seen by an observer traveling at the average velocity $(U_1 + U_2)/2$ of the two layers. When the densities of the two layers are equal, a disturbance to the interface will be stationary in this frame of reference.
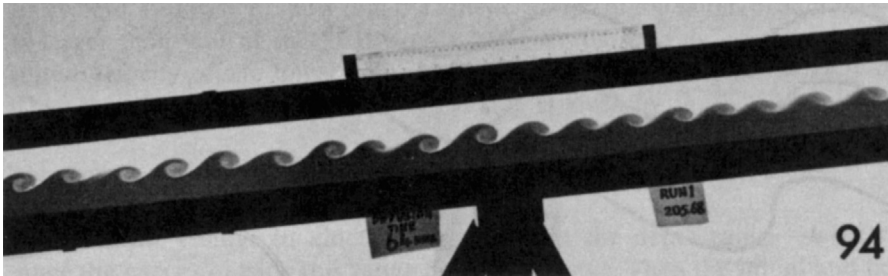

FIGURE 11.4 Kelvin-Helmholtz instability generated by tilting a horizontal channel containing two liquids of different densities. The lower layer is dyed and 18 wavelengths of the developing interfacial disturbance are shown. The mean flow in the lower layer is down the plane (to the left) and that in the upper layer is up the plane (to the right). *S. A. Thorpe,* Journal of Fluid Mechanics, *46, 299–319, 1971; reprinted with the permission of Cambridge University Press.*

until they cannot grow any longer. Figure 11.7 shows a typical behavior, in which the unstable waves at the interface have transformed the sharp density profile ACDF to ABEF and the sharp velocity profile MOPR to MNQR. The high-density fluid in the depth range DE has been raised upward (and mixed with the lower density fluid in the depth range BC), which means that the potential energy of the system has increased after the action of the instability. The required energy has been drawn from the kinetic energy of the basic field. It is easy to show that the kinetic energy of the initial profile MOPR is larger than that of the final profile MNQR. To see this, assume that the initial velocity of the lower layer is zero and that of the upper layer is U_1. Then the linear velocity profile after mixing is given by
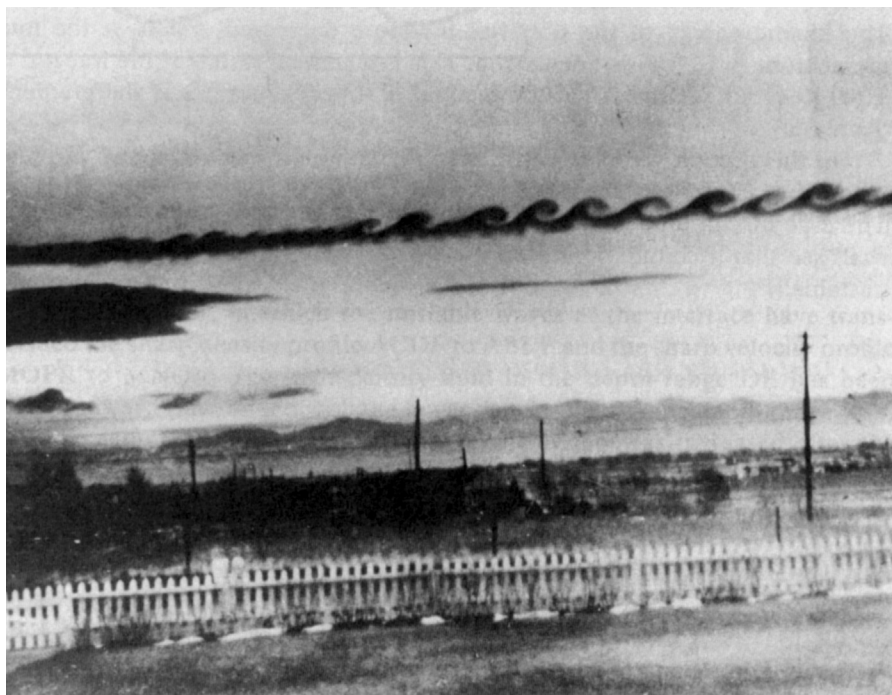
FIGURE 11.5   Overturning billow cloud near Denver, Colorado. The similarity in shape of the developing instability with that shown in Figure 11.4 is striking. *P. G. Drazin and W. H. Reid,* Hydrodynamic Stability, *1981; reprinted with the permission of Cambridge University Press.*

$$U(z) = U_1\left(\frac{1}{2} + \frac{z}{2h}\right) \quad \text{for} -h \leq z \leq h.$$

Consider the change in kinetic energy only in the depth range $-h < z < h$, as the energy outside this range does not change. Then the initial and final kinetic energies per unit width are:

$$
\begin{aligned}
E_{\text{initial}} &= \frac{\rho}{2}U_1^2 h, \\
E_{\text{final}} &= \frac{\rho}{2}\int_{-h}^{h} U^2(z) \ dz = \frac{\rho}{3}U_1^2 h.
\end{aligned}
$$

The kinetic energy of the flow has therefore decreased, although the total momentum $(= \int U dz)$ is unchanged. This is a general result: If the integral of $U(z)$ does not change, then the integral of $U^2(z)$ decreases if the gradients decrease.

In this section the case of a discontinuous variation across an infinitely thin interface is considered and the flow is always unstable. The case of continuous variation is considered in Section 11.7, and we shall see that one or more additional conditions must be satisfied in order for the flow to be unstable.

x/λ
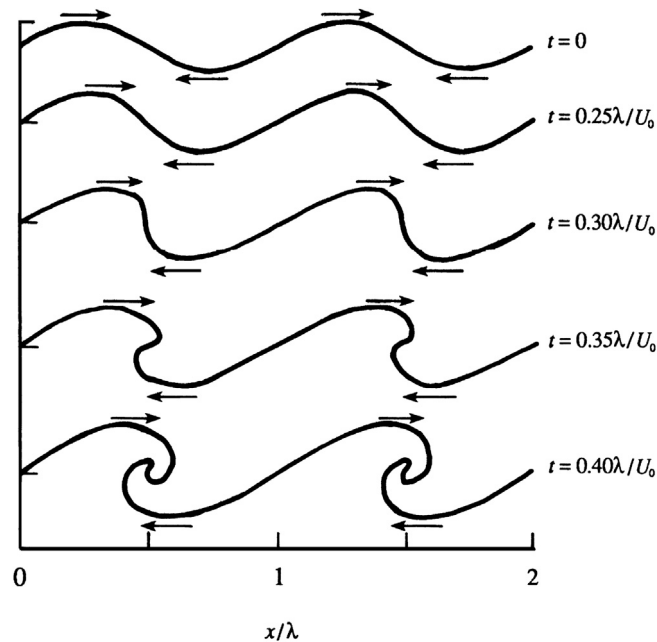
FIGURE 11.6 Nonlinear numerical calculation of the evolution of a vortex sheet that has been given a small transverse sinusoidal displacement with wavelength λ. The density difference across the interface is zero, and U_0 is the velocity difference across the vortex sheet. Here again, the similarity of the interface shape at the last time with the results shown in Figures 11.4 and 11.5 is striking. The smaller vertical displacements shown in Figures 11.4 and 11.5 are consistent with the effects of stratification that are absent from the calculations shown in this figure. *J. S. Turner, Buoyancy Effects in Fluids, 1973; reprinted with the permission of Cambridge University Press.*
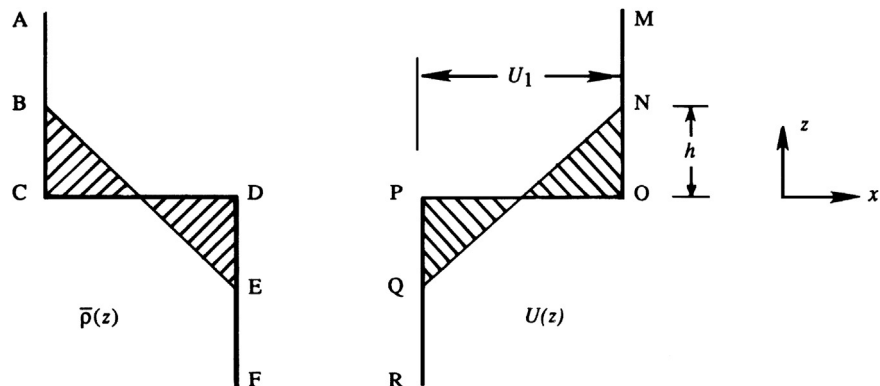
FIGURE 11.7 Smearing out of sharp density and velocity profiles, resulting in an increase of potential energy and a decrease of kinetic energy. When turbulent, the overturning eddies or billows shown in Figures 11.4 and 11.5 lead to cross-stream momentum transport and fluid mixing. The discontinuous profiles ACDF and MOPR evolve toward ABEF and MNQR as the instability develops.

11.4. THERMAL INSTABILITY: THE BÉNARD PROBLEM

In natural flows and engineering flows, heat addition to a nominally quiescent fluid from below can lead to a situation where cool, dense fluid overlies warmer, less dense fluid. Equation (11.19) indicates that such stratification will be unstable and lead to instability-driven motion when the fluid is ideal. However, when viscosity and thermal conduction are active, they may delay the onset of unstable convective motion, and only for large enough temperature gradients is the situation unstable. In this section, the conditions necessary for the onset of thermal instability in a layer of fluid are presented.

The first intensive experiments on instability caused by heating a layer of fluid from below were conducted by Bénard in 1900. Bénard experimented on only very thin layers (a millimeter or less) that had a free surface, and observed beautiful hexagonal cells when the convection developed. Stimulated by these experiments, Rayleigh in 1916 derived the theoretical requirement for the development of convective motion in a layer of fluid with two free surfaces. He showed that the instability would occur when the adverse temperature gradient was large enough to make the ratio,

$$\text{Ra} = g\alpha\Gamma d^4/\kappa\nu, \tag{11.21}$$

exceed a certain critical value. Here, g is the acceleration due to gravity, α is the fluid's coefficient of thermal expansion, $\Gamma = -d\overline{T}/dz$ is the vertical temperature gradient of the background state, d is the depth of the layer, κ is the fluid's thermal diffusivity, and ν is the fluid's kinematic viscosity. The parameter Ra is called the *Rayleigh number*, and it represents a ratio of the destabilizing effect of buoyancy to the stabilizing effect of viscosity. It has been recognized only recently that most of the *motions observed by Bénard were instabilities driven by the variation of surface tension with temperature and not the thermal instability due to a top-heavy density gradient* (Drazin & Reid, 1981, p. 34). The importance of instabilities driven by surface tension decreases as the layer becomes thicker. Later experiments on thermal convection in thicker layers (with or without a free surface) have obtained convective cells of many forms, not just hexagonal. Nevertheless, the phenomenon of thermal convection in a layer of fluid is still commonly called the *Bénard convection*. Rayleigh's solution of the thermal convection problem is considered a major triumph of linear stability theory. The concept of a critical Rayleigh number finds application in such geophysical problems as solar convection, cloud formation in the atmosphere, and the motion of the earth's core.

The formulation of the problem starts with a fluid layer of thickness d confined between two isothermal walls where the lower wall is maintained at a higher temperature, T_0, than the upper wall, $T_0 - \Delta T$, where $\Delta T > 0$ (see Figure 11.8). Use Cartesian coordinates centered in the middle of the fluid layer with the z-axis vertical; start from the Boussinesq set of equations,

$$\nabla \cdot \tilde{\mathbf{u}} = 0, \ \frac{\partial \tilde{\mathbf{u}}}{\partial t} + (\tilde{\mathbf{u}} \cdot \nabla)\tilde{\mathbf{u}} = -\frac{1}{\rho_0}\nabla\tilde{p} - g\left[1 - \alpha(\tilde{T} - T_0)\right]\mathbf{e}_z + \nu\nabla^2\tilde{\mathbf{u}}, \ \frac{\partial \tilde{T}}{\partial t} + (\tilde{\mathbf{u}} \cdot \nabla)\tilde{T} = \kappa\nabla^2\tilde{T},$$

$$\text{(4.10, 4.86, 4.89)}$$

and the simplified equation for the density in terms of the temperature: $\rho = \rho_o[1 - \alpha(\tilde{T} - T_0)]$, where ρ_0 and T_0 are the reference density and temperature. Here again, the total flow variables
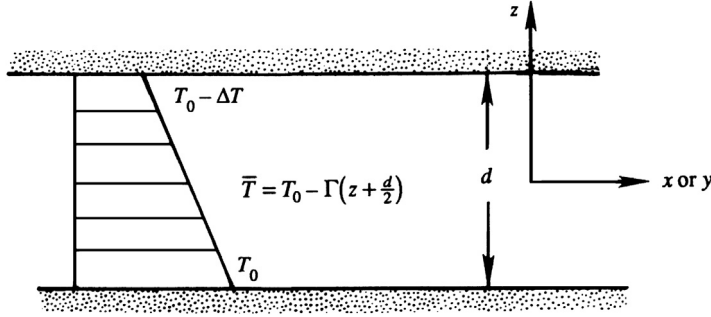
FIGURE 11.8   Flow geometry for the thermal convection between horizontal surfaces separated by a distance d. The lower surface is maintained at a higher temperature than the upper surface, and the coordinates are centered between them. For a given fluid and a fixed geometry, when the temperature difference ΔT is small, the fluid remains motionless and heat is transferred between the plates by thermal conduction. However, a sufficiently high ΔT will cause a cellular flow pattern to appear and thermal convection of heat to occur.

(background plus perturbation) carry a tilde ($\sim$). We decompose the total flow field into a motionless background plus perturbations:

$$\tilde{\mathbf{u}} = 0 + \mathbf{u}(\mathbf{x}, t), \quad \tilde{T} = \overline{T}(z) + T'(\mathbf{x}, t), \text{ and } \tilde{p} = P(z) + p(\mathbf{x}, t). \tag{11.22}$$

The basic state is represented by a quiescent fluid with temperature and pressure distributions $\overline{T}(z)$ and $P(z)$ that satisfy the equations,

$$0 = -\frac{1}{\rho_0}\nabla P - g[1 - \alpha(\overline{T} - T_0)]\,\mathbf{e}_z \quad \text{and} \quad 0 = \kappa\frac{\partial^2 \overline{T}}{\partial z^2}. \tag{11.23}$$

The preceding thermal equation gives the linear vertical temperature distribution:

$$\overline{T}(z) = T_0 - \frac{1}{2}\Delta T - \Gamma z, \tag{11.24}$$

where $\Gamma \equiv \Delta T/d$ is the magnitude of the vertical temperature gradient. Substituting (11.22) into the Boussinesq equation set and subtracting (11.23) produces:

$$\nabla \cdot \mathbf{u} = 0, \quad \frac{\partial \mathbf{u}}{\partial t} + (\mathbf{u} \cdot \nabla)\mathbf{u} = -\frac{1}{\rho_0}\nabla p + g\alpha T'\mathbf{e}_z + \nu\nabla^2 \mathbf{u}, \text{ and } \frac{\partial T'}{\partial t} - w\Gamma + (\mathbf{u} \cdot \nabla)T' = \kappa\nabla^2 T',$$

where w is the vertical component of the fluid velocity, and the $-w\Gamma$ term in the final equation comes from evaluating $(\mathbf{u} \cdot \nabla)\overline{T}$ using (11.24). For small perturbations, it is appropriate to linearize the second two equations by dropping quadratic and higher order terms:

$$\nabla \cdot \mathbf{u} = 0, \quad \frac{\partial \mathbf{u}}{\partial t} = -\frac{1}{\rho_0}\nabla p + g\alpha T'\mathbf{e}_z + \nu\nabla^2 \mathbf{u}, \text{ and } \frac{\partial T'}{\partial t} - w\Gamma = \kappa\nabla^2 T'. \tag{11.25, 11.26, 11.27}$$

These equations govern the behavior of perturbations to the basic state. A simple scaling analysis based on these equations leads to the Rayleigh number when $T' \sim \Delta T$, and $\nabla \sim 1/d$. From (11.27), the vertical velocity scale is found by equating the advective and diffusion terms:

$$w\Gamma \sim \kappa\nabla^2 T' \sim \kappa\frac{1}{d^2}\Delta T = \kappa\frac{1}{d}\frac{\Delta T}{d} = \kappa\frac{1}{d}\Gamma, \quad \text{so } w \sim \kappa/d.$$

Forming a ratio of the last two terms in (11.26) leads to:

$$\frac{buoyant\ force}{viscous\ force} \sim \frac{g\alpha T'}{\nu(1/d^2)w} \sim \frac{g\alpha(\Delta T/d)d}{\nu(1/d^2)(\kappa/d)} = \frac{g\alpha\Gamma d^4}{\nu\kappa} = \text{Ra}.$$

The perturbation equations can be written in terms of w and T' by taking the Laplacian of the z-component of (11.26):

$$\frac{\partial}{\partial t}\nabla^2 w = -\frac{1}{\rho_0}\nabla^2\frac{\partial p}{\partial z} + g\alpha\nabla^2 T' + \nu\nabla^4 w. \tag{11.28}$$

The pressure term in (11.28) can be eliminated by taking the divergence of (11.26), using (11.25),

$$\frac{\partial}{\partial t}\nabla\cdot\mathbf{u} = -\frac{1}{\rho_0}\nabla^2 p + g\alpha\frac{\partial}{\partial z}T' + \nu\nabla^2\nabla\cdot\mathbf{u}, \text{ or } 0 = -\frac{1}{\rho_0}\nabla^2 p + g\alpha\frac{\partial}{\partial z}T',$$

and then differentiating with respect to z to obtain:

$$0 = -\frac{1}{\rho_0}\nabla^2\frac{\partial p}{\partial z} + g\alpha\frac{\partial^2 T'}{\partial z^2},$$

which can be subtracted from (11.28) to find:

$$\frac{\partial}{\partial t}\nabla^2 w = +g\alpha\nabla_H^2 T' + \nu\nabla^4 w, \tag{11.29}$$

where $\nabla_H^2 = \partial^2/\partial x^2 + \partial^2/\partial y^2$ is the horizontal Laplacian operator.

Equations (11.27) and (11.29) govern the development of perturbations on the system. The boundary conditions on the upper and lower rigid surfaces are that the no-slip condition is satisfied and that the walls are maintained at constant temperatures. These conditions require $u = v = w = T' = 0$ at $z = \pm d/2$. Because the conditions on u and v hold for all x and y, it follows from the continuity equation that $\partial w/\partial z = 0$ at the walls. The boundary conditions therefore can be written as

$$w = \partial w/\partial z = T' = 0 \quad \text{on } z = \pm d/2. \tag{11.30}$$

Dimensionless independent variables are used in the rest of the analysis via the transformation:

$$t \to (d^2/\kappa)t \quad \text{and} \quad (x, y, z) \to (xd, yd, zd),$$

where the dimensional variables are on the left side and the new dimensionless variables are on the right-hand side; note that we are avoiding the introduction of new symbols for the dimensionless variables. Equations (11.27), (11.29), and (11.30) then become:

$$\left(\frac{\partial}{\partial t} - \nabla^2\right)T' = \frac{\Gamma d^2}{\kappa}w, \quad \left(\frac{1}{\text{Pr}}\frac{\partial}{\partial t} - \nabla^2\right)\nabla^2 w = \frac{g\alpha d^2}{\nu}\nabla_H^2 T', \text{ and}$$

$$w = \partial w/\partial z = T' = 0 \quad \text{on } z = \pm\frac{1}{2}. \tag{11.31, 11.32, 11.33}$$

where $\text{Pr} \equiv \nu/\kappa$ is the Prandtl number.

The method of normal modes is now introduced. Because the coefficients in (11.31) and (11.32) are independent of x, y, and t, solutions exponential in these variables are allowed. We therefore assume normal modes given by the first version of (11.1) with $\mathbf{K} = (k, l, 0)$:

$$w = \widehat{w}(z) \exp\{ikx + ily + \sigma t\}, \quad \text{and} \quad T' = \widehat{T}(z) \exp\{ikx + ily + \sigma t\}.$$

The requirement that solutions remain bounded as $x, y \to \infty$ implies that the wave numbers k and l must be real. In other words, the normal modes must be oscillatory in the directions of unboundedness. The temporal growth rate $\sigma = \sigma_r + i\sigma_i$ is allowed to be complex. With this dependence, the operators in (11.31) and (11.32) primarily transform to algebraic multipliers via:

$$\partial/\partial t \to \sigma, \quad \nabla_H^2 \to -k^2 - l^2 \equiv -K^2, \quad \text{and} \quad \nabla^2 \to -K^2 + d^2/dz^2,$$

where $K = |\mathbf{K}|$ is the magnitude of the (dimensionless) horizontal wave number. Equations (11.31) and (11.32) then become

$$\left(\sigma + K^2 - \frac{d^2}{dz^2}\right)\widehat{T} = \frac{\Gamma d^2}{\kappa}\widehat{w} \quad \text{and} \quad \left(\frac{\sigma}{\mathrm{Pr}} + K^2 - \frac{d^2}{dz^2}\right)\left(\frac{d^2}{dz^2} - K^2\right)\widehat{w} = -\frac{g\alpha d^2 K^2}{\nu}\widehat{T}.$$

$$(11.34, 11.35)$$

Making the substitution $W \equiv (\Gamma d^2/\kappa)\widehat{w}$, (11.34) and (11.35) reduce to:

$$\left(\sigma + K^2 - \frac{d^2}{dz^2}\right)\widehat{T} = W \quad \text{and} \quad \left(\frac{\sigma}{\mathrm{Pr}} + K^2 - \frac{d^2}{dz^2}\right)\left(\frac{d^2}{dz^2} - K^2\right)W = -\mathrm{Ra}K^2\widehat{T}. \quad (11.36, 11.37)$$

The boundary conditions (11.33) become

$$W = \partial W/\partial z = \widehat{T} = 0 \quad \text{on } z = \pm 1/2. \tag{11.38}$$

Here we note that σ is real for $\mathrm{Ra} > 0$ (see Exercise 11.6). The Bénard problem is one of two well-known problems in which σ is real. (The other one is Taylor-Couette flow between rotating cylinders, discussed in the following section.) In most other problems σ is complex, and the marginal state ($\sigma_r = 0$) contains propagating waves (as is true for the Kelvin-Helmholtz instability). In the Bénard and Taylor problems, however, the marginal state corresponds to $\sigma = 0$, and is therefore *stationary* and does not contain propagating waves. In these flows, the onset of instability is marked by a transition from the background state to another *steady* state. In such a case we commonly say that the *principle of exchange of stabilities* is valid, and the instability sets in as a *cellular convection*, which will be explained shortly.

Two solutions for Rayleigh-Bénard flow are presented in the remainder of this section. First, the solution is presented for the case that is easiest to realize in a laboratory experiment, namely, a layer of fluid confined between two rigid plates on which no-slip conditions are satisfied. The solution to this problem was first given by Jeffreys in 1928. The second solution for a layer of fluid with two stress-free surfaces is presented after the first.

For the marginal state $\sigma = 0$, the equation pair (11.36) and (11.37) become

$$\left(\frac{d^2}{dz^2} - K^2\right)\widehat{T} = -W \quad \text{and} \quad \left(\frac{d^2}{dz^2} - K^2\right)^2 W = \text{Ra}K^2\widehat{T}. \tag{11.39}$$

Eliminating $\widehat{T}$, we obtain

$$\left(\frac{d^2}{dz^2} - K^2\right)^3 W = -\text{Ra}K^2 W. \tag{11.40}$$

The boundary condition (11.38) becomes

$$W = \partial W/\partial z = (d^2/dz^2 - K^2)^2 W = 0 \quad \text{on } z = \pm 1/2. \tag{11.41}$$

We have a sixth-order homogeneous differential equation with six homogeneous boundary conditions. Nonzero solutions for such a system can only exist for a particular value of Ra (for a given K). It is therefore an eigenvalue problem. Note that the Prandtl number has dropped out of the marginal state.

The point to observe is that the problem is symmetric with respect to the two boundaries, thus the eigenfunctions fall into two distinct classes—those with the vertical velocity symmetric about the midplane $z = 0$, and those with the vertical velocity antisymmetric about the midplane (Figure 11.9). The gravest even mode therefore has one row of cells, and the gravest odd mode has two rows of cells. It can be shown that the smallest critical Rayleigh number is obtained by assuming disturbances in the form of the gravest even mode, which also agrees with experimental findings of a single row of cells.

Because the coefficients of the governing equation (11.40) are independent of z, the general solution can be expressed as a superposition of solutions of the form: $W \propto \exp(qz)$, where the six roots of q are found from

$$(q^2 - K^2)^3 = -\text{Ra}K^2.$$

The three roots of this equation for q^2 are:

$$q^2 = -K^2\left[\left(\frac{\text{Ra}}{K^4}\right)^{1/3} - 1\right] \quad \text{and} \quad q^2 = K^2\left[1 + \frac{1}{2}\left(\frac{\text{Ra}}{K^4}\right)^{1/3}(1 \pm i\sqrt{3})\right]. \tag{11.42}$$
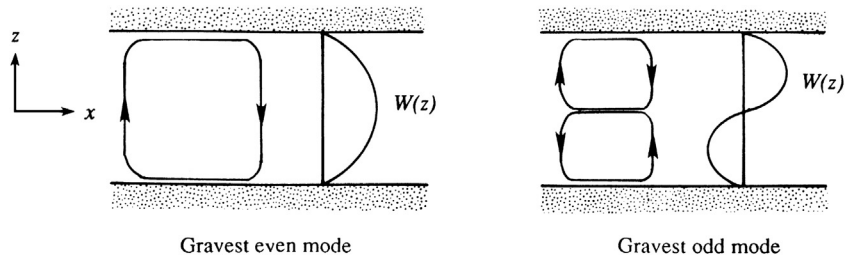
FIGURE 11.9 Flow pattern and eigenfunction structure of the gravest even mode and the gravest odd mode in the Bénard problem. The even mode is observed first as the temperature difference between the surfaces is increased.

Taking square roots, the six roots for q are $\pm iq_0$, $\pm q$, and $\pm q^*$, where

$$q_0 = K\left[\left(\frac{\text{Ra}}{K^4}\right)^{1/3} - 1\right]^{1/2}$$

and q and its conjugate q^* are given by the two roots of the second part of (11.42).

The even solution of (11.40) is therefore

$$W = A \cos q_0 z + B \cosh qz + C \cosh q^* z,$$

where A, B, and C are constants. To apply the boundary conditions on this solution, we find the following derivatives:

$$dW/dz = -Aq_0 \sin q_0 z + Bq \sinh qz + Cq^* \sinh q^* z, \text{ and}$$

$$\left(d^2/dz^2 - K^2\right)^2 W = A\left(q_0^2 + K^2\right)^2 \cos q_0 z + B\left(q^2 - K^2\right)^2 \cosh qz + B\left(q^{*2} - K^2\right)^2 \cosh q^* z.$$

The boundary conditions (11.41) then require:

$$\begin{bmatrix} \cos\dfrac{q_0}{2} & \cosh\dfrac{q}{2} & \cosh\dfrac{q^*}{2} \\[2mm] -q_0 \sin\dfrac{q_0}{2} & q \sinh\dfrac{q}{2} & q^* \sinh\dfrac{q^*}{2} \\[2mm] \left(q_0^2 + K^2\right)^2 \cos\dfrac{q_0}{2} & \left(q^2 - K^2\right)^2 \cosh\dfrac{q}{2} & \left(q^{*2} - K^2\right)^2 \cosh\dfrac{q^*}{2} \end{bmatrix} \begin{bmatrix} A \\ B \\ C \end{bmatrix} = 0.$$

Here, A, B, and C cannot all be zero if we want to have a nonzero solution, which requires that the determinant of the matrix must vanish. This gives a relation between Ra and the corresponding eigenvalue K (Figure 11.10). Points on the curve $K(Ra)$ represent marginally stable states, which separate regions of stability and instability. The lowest value of Ra for marginal stability is found to be $\text{Ra}_{\text{cr}} = 1708$, attained at $K_{\text{cr}} = 3.12$. As *all* values of K are allowed by the system, the flow first becomes unstable when the Rayleigh number reaches a value of

$$\text{Ra}_{\text{cr}} = 1708.$$

The wavelength at the onset of instability is: $\lambda_{cr} = 2\pi d/K_{cr} \cong 2d$. Laboratory experiments agree remarkably well with these predictions, and the solution of the Bénard problem is considered one of the major successes of the linear stability theory.

The solution for a fluid layer with stress-free surfaces is somewhat simpler and was first given by Rayleigh. This case can be approximately realized in a laboratory experiment if a layer of liquid is floating on top of a somewhat heavier liquid. Here the boundary conditions are $w = T' = \mu(\partial u/\partial z + \partial w/\partial x) = \mu(\partial v/\partial z + \partial w/\partial y) = 0$ at the surfaces, the latter two conditions resulting from zero stress. Because w vanishes (for all x and y) on the boundaries, it follows that the vanishing stress conditions require $\partial u/\partial z = \partial v/\partial z = 0$ at the boundaries. On differentiating the continuity equation with respect to z, it follows that $\partial^2 w/\partial z^2 = 0$ on the free surfaces. In terms of the complex amplitudes, the eigenvalue problem is therefore defined by (11.39) and with boundary conditions:

$$W = (d^2/dz^2 - K^2)^2 W = d^2 W/dz^2 = 0 \quad \text{on } z = \pm 1/2.$$
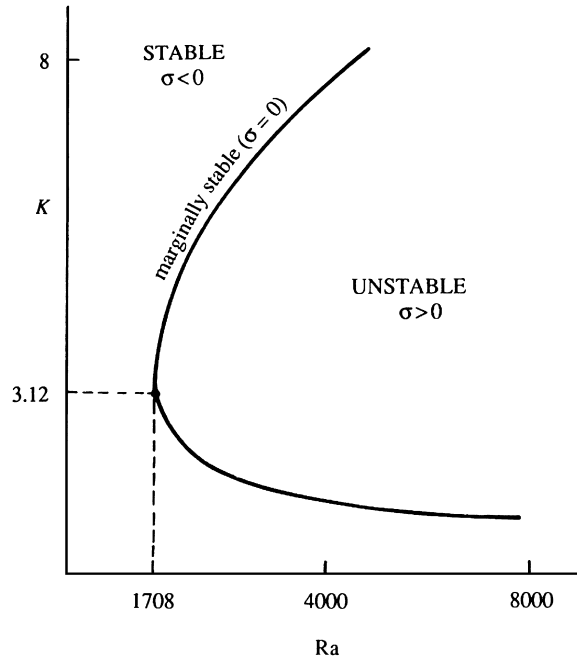
FIGURE 11.10   Stable and unstable regions for Bénard convection in a plot of the dimensionless wave number K vs. Ra, the Rayleigh number (11.21). The lowest possible Ra value for which the flow may be unstable is 1708, and the wave number of the first mode of instability is $3.12/d$, where d is the separation between the horizontal surfaces.

By expanding and simplifying the products of operators, the boundary conditions can be rewritten as

$$W = d^2W/dz^2 = d^4W/dz^4 = 0 \quad \text{on } z = \pm 1/2, \tag{11.43}$$

which should be compared with the conditions (11.41) for rigid boundaries.

Successive differentiation of (11.40) shows that *all* even derivatives of W vanish on the boundaries. The eigenfunctions must therefore be

$$W = A\sin(n\pi z),$$

where A is any constant and n is an integer. Substitution into equation (11.40) leads to the eigenvalue relation

$$Ra = \left(n^2\pi^2 + K^2\right)^3/K^2, \tag{11.44}$$

which gives the Rayleigh number in the marginal state. For a given K^2, the lowest value of Ra occurs when $n = 1$, which is the gravest mode. The critical Rayleigh number is obtained by finding the minimum value of Ra as K^2 is varied, that is, by setting $dRa/dK^2 = 0$:

$$\frac{dRa}{dK^2} = \frac{3\left(\pi^2 + K^2\right)^2}{K^2} - \frac{3\left(\pi^2 + K^2\right)^3}{K^4} = 0,$$

FIGURE 11.11 Two-dimensional convection rolls in Bénard convection. Fluid alternately ascends and descends between the rolls. The horizontal spacing between roll centers is nearly the same as the spacing between the horizontal surfaces.
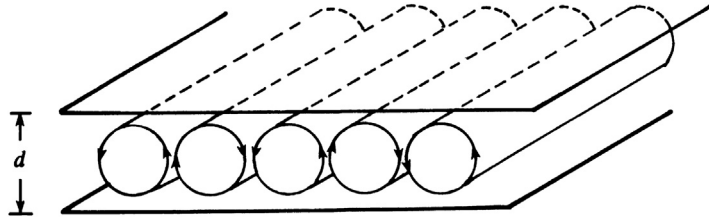
which requires $K_{cr}^2 = \pi^2/2$. The corresponding value of Ra is:

$$\text{Ra}_{cr} = (27/4)\pi^4 = 657.5.$$

For a layer with a free upper surface (where the stress is zero) and a rigid bottom wall, the solution of the eigenvalue problem gives $\text{Ra}_{cr} = 1101$ and $K_{cr} = 2.68$. This case is of interest in laboratory experiments having the most visual effects, as originally conducted by Bénard.

The linear theory specifies the horizontal wavelength at the onset of instability, but not the horizontal pattern of the convective cells. This is because a given wave number vector **K** can be decomposed into two orthogonal components in an infinite number of ways. If we assume that the experimental conditions are horizontally isotropic, with no preferred directions, then regular polygons in the form of equilateral triangles, squares, and regular hexagons are all possible structures. Bénard's original experiments showed only hexagonal patterns, but we now know that he was observing a different phenomenon. The observations summarized in Drazin and Reid (1981) indicate that hexagons frequently predominate initially. As Ra is increased, the cells tend to merge and form rolls, on the walls of which the fluid rises or sinks (Figure 11.11). The cell structure becomes more chaotic as Ra is increased further, and the flow becomes turbulent when $\text{Ra} > 5 \times 10^4$.

The magnitude or direction of flow in the cells cannot be predicted by linear theory. After a short time of exponential growth, the flow becomes fast enough for the nonlinear terms to be important and it reaches a nonlinear equilibrium stage. The flow pattern for a hexagonal cell is sketched in Figure 11.12. Particles in the middle of the cell usually rise in a liquid and
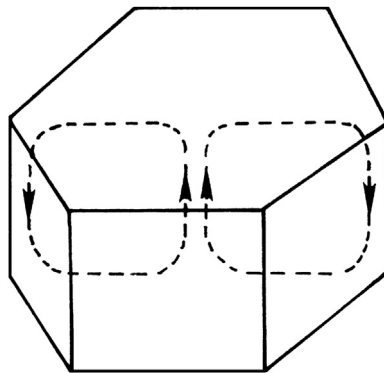

FIGURE 11.12 Above the critical Rayleigh number, complicated flow patterns may exist because a range of wave numbers is unstable for the first mode. A commonly observed Bénard-convection flow pattern involves hexagonal cells. Once such cell is shown here.

fall in a gas. This has been attributed to the property that the viscosity of a liquid decreases with temperature, whereas that of a gas increases with temperature. The rising fluid loses heat by thermal conduction at the top wall, travels horizontally, and then sinks. For a steady cellular pattern, the continuous generation of kinetic energy is balanced by viscous dissipation. The generation of kinetic energy is maintained by continuous release of potential energy due to heating at the bottom and cooling at the top.

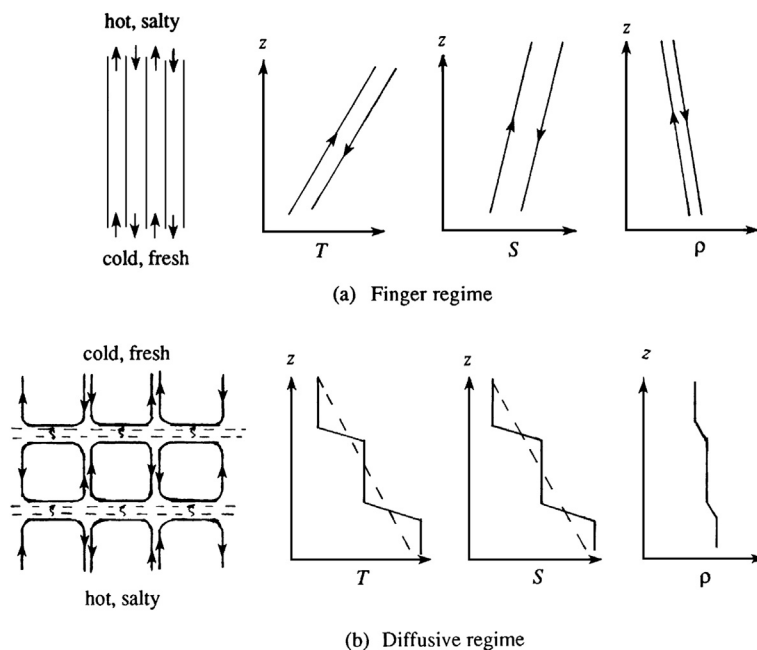## 11.5. DOUBLE-DIFFUSIVE INSTABILITY

An interesting instability results when the density of the fluid depends on two opposing gradients. The possibility of this phenomenon was first suggested by Stommel et al. (1956), but the dynamics of the process was first explained by Stern (1960). Turner (1973), review articles by Huppert and Turner (1981), and Turner (1985) discuss the dynamics of this phenomenon and its applications to various fields such as astrophysics, engineering, and geology. Historically, the phenomenon was first suggested with oceanic application in mind, and this is how we shall present it. For sea water the density depends on the temperature $\tilde{T}$ and salt content $\tilde{s}$ (kilograms of salt per kilograms of water), so that the density is given by:

$$\tilde{\rho} = \rho_0 \left[1 - \alpha(\tilde{T} - T_0) + \beta(\tilde{s} - s_0) \right],$$

where the value of α determines how fast the density decreases with temperature, and the value of β determines how fast the density increases with salinity. As defined here, both α and β are positive. The key factor in this instability is that the diffusivity κ_s of salt in water is only 1% of the thermal diffusivity κ. *Such a system can be unstable even when the density decreases upwards.* By means of the instability, the flow releases the potential energy of the *component* that is "heavy at the top." Therefore, the effect of diffusion in such a system can be to *destabilize* a stable density gradient. This is in contrast to a medium containing a single diffusing component, for which the analysis of the preceding section shows that the effect of diffusion is to *stabilize* the system even when it is heavy at the top.

Consider the two situations of Figure 11.13, both of which can be unstable although each is stably stratified in density ($d\bar{\rho}/dz < 0$). Consider first the case of hot and salty water lying over cold and fresh water (Figure 11.13a), that is, when the system is top heavy in salt. In this case both $d\overline{T}/dz$ and dS/dz are positive, and we can arrange the composition of water such that the density decreases upward. Because $\kappa_s \ll \kappa$, a displaced particle would be near thermal equilibrium with the surroundings, but would exchange negligible salt. A rising particle therefore would be constantly lighter than the surroundings because of the salinity deficit, and would continue to rise. A parcel displaced downward would similarly continue to plunge downward. The basic state shown in Figure 11.13a is therefore unstable. Laboratory observations show that the instability in this case appears in the form of a forest of long narrow convective cells, called *salt fingers* (Figure 11.14). Shadowgraph images in the deep ocean have confirmed their existence in nature.

We can derive a criterion for instability by generalizing our analysis of the Bénard convection so as to include salt diffusion. Assume a layer of depth d confined between stress-free boundaries maintained at constant temperature and constant salinity. If we repeat the

(a) Finger regime

(b) Diffusive regime

FIGURE 11.13 Two kinds of double-diffusive instabilities. (a) Finger instability, showing up- and down-going salt fingers and their temperature, salinity, and density. Arrows indicate the direction of fluid motion. (b) Oscillating instability, finally resulting in a series of convecting layers separated by "diffusive" interfaces. Across these interfaces T and S vary sharply, but heat is transported much faster than salt.
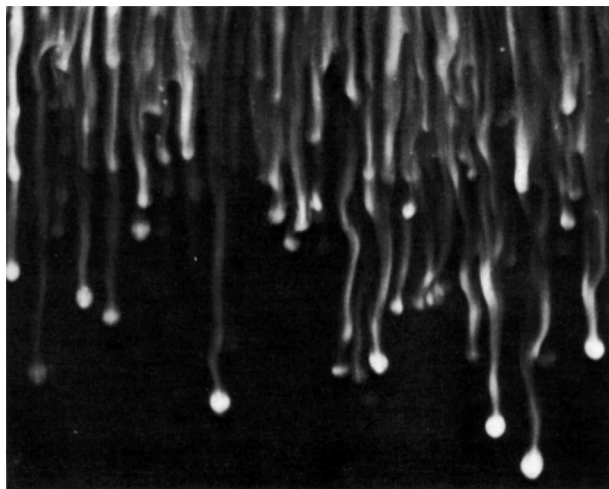
FIGURE 11.14 Salt fingers, produced by pouring a salt solution on top of a stable temperature gradient. Flow visualization by fluorescent dye and a horizontal beam of light. *J. Turner,* Naturwissenschaften, *72, 70–75, 1985; reprinted with the permission of Springer-Verlag GmbH & Co.*

derivation of the perturbation equations for the normal modes of the system, the equations that replace (11.39) are found to be:

$$\left(\frac{d^2}{dz^2} - K^2\right)\widehat{T} = -W, \ \frac{\kappa_s}{\kappa}\left(\frac{d^2}{dz^2} - K^2\right)\widehat{s} = -W, \ \text{and} \ \left(\frac{d^2}{dz^2} - K^2\right)^2 W = -\text{Ra}K^2\widehat{T} + \text{Rs}'K^2\widehat{s},$$

(11.45)

where $\widehat{s}\,(z)$ is the complex amplitude of the salinity perturbation, and we have defined

$$\text{Ra} \equiv \frac{g\alpha d^4(d\overline{T}/dz)}{\nu\kappa} \quad \text{and} \quad \text{Rs}' \equiv \frac{g\beta d^4(dS/dz)}{\nu\kappa}.$$

Note that κ (and not κ_s) appears in the definition of Rs'. In contrast to (11.45), a positive sign appeared in (11.39) in front of Ra because in the preceding section Ra was defined to be positive for a top-heavy situation.

It is seen from the first two equations of (11.45) that the equations for $\widehat{T}$ and $\widehat{s}\kappa_s/\kappa$ are the same. The boundary conditions are also the same for these variables:

$$\widehat{T} = \widehat{s}\kappa_s/\kappa = 0 \quad \text{at } z = \pm 1/2.$$

It follows that we must have $\widehat{T} = \kappa_s\widehat{s}/\kappa$ everywhere. Equations (11.45) therefore become:

$$(d^2/dz^2 - K^2)\widehat{T} = -W \quad \text{and} \quad (d^2/dz^2 - K^2)^2 W = (\text{Rs} - \text{Ra})K^2\widehat{T},$$

where

$$\text{Rs} \equiv \frac{\kappa}{\kappa_s}\text{Rs}' = \frac{g\beta d^4(dS/dz)}{\nu\kappa_s}.$$

The preceding set is now identical to the set (11.39) for the Bénard convection, with $(\text{Rs} - \text{Ra})$ replacing Ra. For stress-free boundaries, the solution of the preceding section shows that the critical value is

$$\text{Rs} - \text{Ra} = \frac{27}{4}\pi^4 = 657,$$

which can be written as

$$\frac{gd^4}{\nu}\left[\frac{\beta}{\kappa_s}\frac{dS}{dz} - \frac{\alpha}{\kappa}\frac{d\overline{T}}{dz}\right] = 657.$$

(11.46)

Even if $\alpha\,(d\overline{T}/dz) - \beta\,(dS/dz) > 0$ (i.e., $\overline{\rho}$ decreases upward), the condition (11.46) can be quite easily satisfied because κ_s is much smaller than κ. The flow can therefore be made unstable simply by ensuring that the factor within [ ] is positive and making d large enough.

The analysis predicts that the lateral width of the cell is of the order of d, but such wide cells are not observed at supercritical stages when $(\text{Rs} - \text{Ra})$ far exceeds 657. Instead, long thin salt fingers are observed, as shown in Figure 11.14. If the salinity gradient is large, then experiments as well as calculations show that a deep layer of salt fingers becomes unstable and breaks down into a series of convective layers, with fingers confined to the interfaces. Oceanographic observations frequently show a series of staircase-shaped vertical

distributions of salinity and temperature; with a positive overall dS/dz and $d\overline{T}/dz$ such distributions can indicate salt finger activity.

The double-diffusive instability may also occur when cold fresh water overlays hot salty water (Figure 11.13b). In this case both $d\overline{T}/dz$ and dS/dz are negative, and we can choose their values such that the density decreases upward. Again the system is unstable, but the dynamics are different. A particle displaced upward loses heat but no salt. Thus it becomes heavier than the surroundings and buoyancy forces it back toward its initial position, resulting in an oscillation. However, a stability calculation shows that less than perfect heat conduction results in a growing oscillation, although some energy is dissipated. In this case the growth rate σ is complex, in contrast to the situation of Figure 11.13a where it is real.

Laboratory experiments show that the initial oscillatory instability does not last long, and eventually results in the formation of a number of horizontal *convecting layers*, as sketched in Figure 11.13b. Consider the situation when a stable salinity gradient in an isothermal fluid is heated from below (Figure 11.9). The initial instability starts as a growing oscillation near the bottom. As the heating is continued beyond the initial appearance of the instability, a well-mixed layer develops, capped by a salinity step, a temperature step, and no density step. The heat flux through this step forms a thermal boundary layer, as shown in Figure 11.15. As the well-mixed layer grows, the temperature step across the thermal boundary layer becomes larger. Eventually, the Rayleigh number across the thermal boundary layer becomes critical, and a second convecting layer forms on top of the first. The second layer is maintained by heat flux (and negligible salt flux) across a sharp laminar interface on top of the first layer. This process continues until a stack of horizontal layers forms one upon another. From comparison with the Bénard convection, it is clear that inclusion of a stable salinity gradient has prevented a complete overturning from top to bottom.
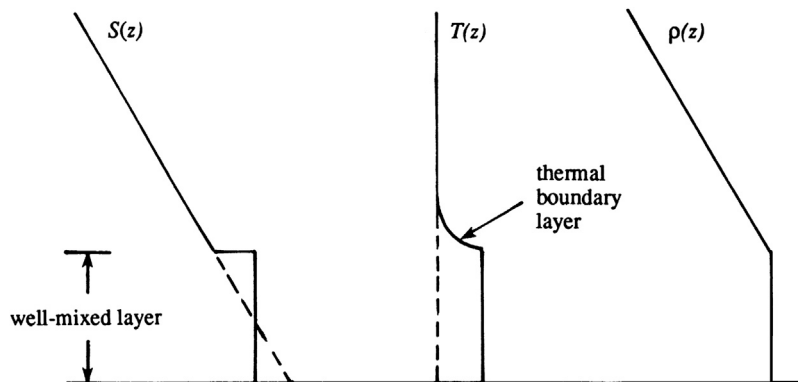

FIGURE 11.15   Distributions of salinity, temperature, and density generated by heating a linear salinity gradient from below. As heating continues the mixed layer depth will increase until a second mixed layer forms. Eventually, the flow pattern sketched and described in Figure 11.13b forms. Top to bottom overturning motion is not possible because of the overall stratification.

The two examples in this section show that in a double-component system in which the diffusivities for the two components are different, the effect of diffusion can be destabilizing, even if the system is judged hydrostatically stable. In contrast, diffusion is stabilizing in a single-component system, such as the Bénard system. The two requirements for the double-diffusive instability are that the diffusivities of the components be different, and that the components make opposite contributions to the vertical density gradient.

11.6. CENTRIFUGAL INSTABILITY: TAYLOR PROBLEM

In this section we shall consider the instability of a Couette flow between concentric rotating cylinders, a problem first solved by G. I. Taylor in 1923. In many ways the problem is similar to the Bénard problem, in which there is a potentially unstable arrangement of temperature. In the Couette-flow problem the source of the instability is the unstable arrangement of angular momentum. Whereas convection in a heated layer is brought about by buoyant forces becoming large enough to overcome the viscous resistance, the convection in a Couette flow is generated by the centrifugal forces being able to overcome the viscous forces. We shall first present Rayleigh's discovery of an inviscid stability criterion for the problem and then outline Taylor's solution of the viscous case. Experiments indicate that the instability initially appears in the form of axisymmetric disturbances, for which $\partial/\partial\theta = 0$. Accordingly, we shall limit ourselves only to the axisymmetric case.

The problem was first considered by Rayleigh in 1888. Neglecting viscous effects, he discovered the source of instability for this problem and demonstrated a necessary and sufficient condition for instability. Let $U_\theta(r)$ be the angular-directed velocity in the r-θ plane at any radial distance from the origin. For inviscid flows $U_\theta(r)$ can be any function, but only certain distributions can be stable. Imagine that two fluid rings with equal mass at radial distances r_1 and r_2 ($>r_1$) are interchanged. As the motion is inviscid, Kelvin's theorem requires that the circulation $\Gamma = 2\pi r U_\theta$ (proportional to the angular momentum $r U_\theta$) should remain constant during the interchange. That is, after the interchange, the fluid at r_2 will have the circulation (namely, Γ_1) that it had at r_1 before the interchange. Similarly, the fluid at r_1 will have the circulation (namely, Γ_2) that it had at r_2 before the interchange. Conservation of circulation requires that the kinetic energy E must change during the interchange. Because $E = U_\theta^2/2 = \Gamma^2/8\pi^2 r^2$ we have

$$E_{\text{final}} = \frac{1}{8\pi^2}\left[\frac{\Gamma_2^2}{r_1^2} + \frac{\Gamma_1^2}{r_2^2}\right],$$

$$E_{\text{initial}} = \frac{1}{8\pi^2}\left[\frac{\Gamma_1^2}{r_1^2} + \frac{\Gamma_2^2}{r_2^2}\right],$$

so that the kinetic energy change per unit mass is:

$$\Delta E = E_{\text{final}} - E_{\text{initial}} = \frac{1}{8\pi^2}(\Gamma_2^2 - \Gamma_1^2)\left(\frac{1}{r_1^2} - \frac{1}{r_2^2}\right).$$

Because $r_2 > r_1$, a velocity distribution for which $\Gamma_2^2 > \Gamma_1^2$ would make ΔE positive, and this implies that an external source of energy would be necessary to perform the interchange of

the fluid rings. Under this condition a *spontaneous* interchange of the rings is not possible, and the flow is stable. On the other hand, if Γ^2 decreases with r, then an interchange of rings will result in a release of energy; such a flow is unstable. It can be shown that in this situation the centrifugal force in the new location of an outwardly displaced ring is larger than the prevailing (radially inward) pressure gradient force.

Rayleigh's criterion can therefore be stated as follows: *An inviscid Couette flow is unstable if*

$$d\Gamma^2/dr < 0 \quad (\text{unstable}).$$

The criterion is analogous to the inviscid requirement for static instability in a density-stratified fluid:

$$d\overline{\rho}/dz > 0 \quad (\text{unstable}).$$

Therefore, the stratification of angular momentum in a Couette flow is unstable if it decreases radially outwards. When the outer cylinder is held stationary and the inner cylinder is rotated, $d\Gamma^2/dr < 0$ and Rayleigh's criterion implies that the flow is inviscidly unstable. As in the Bénard problem, however, merely having a potentially unstable arrangement does not cause instability in a viscous medium.

This inviscid Rayleigh criterion is modified in a viscous version of the problem. Taylor's solution of the viscous problem is outlined in what follows. Using cylindrical polar coordinates (R, φ, z) and assuming axial symmetry, the equations of motion are:

$$\frac{D\tilde{u}_R}{Dt} - \frac{\tilde{u}_\varphi^2}{R} = -\frac{1}{\rho}\frac{\partial \tilde{p}}{\partial R} + \nu\left(\nabla^2 \tilde{u}_R - \frac{\tilde{u}_R}{R^2}\right), \quad \frac{D\tilde{u}_\varphi}{Dt} + \frac{\tilde{u}_R \tilde{u}_\varphi}{R} = \nu\left(\nabla^2 \tilde{u}_\varphi - \frac{\tilde{u}_\varphi}{R^2}\right),$$

$$\frac{D\tilde{u}_z}{Dt} = -\frac{1}{\rho}\frac{\partial \tilde{p}}{\partial z} + \nu\nabla^2 \tilde{u}_z, \quad \text{and} \quad \frac{\partial}{\partial R}(R\tilde{u}_R) + \frac{\partial \tilde{u}_z}{\partial z} = 0, \tag{11.47}$$

where

$$\frac{D}{Dt} = \frac{\partial}{\partial t} + \tilde{u}_R\frac{\partial}{\partial R} + \tilde{u}_z\frac{\partial}{\partial z} \quad \text{and} \quad \nabla^2 = \frac{\partial^2}{\partial R^2} + \frac{1}{R}\frac{\partial}{\partial R} + \frac{\partial^2}{\partial z^2}.$$

We decompose the motion into a background state plus perturbation:

$$\tilde{\mathbf{u}} = \mathbf{U} + \mathbf{u} \quad \text{and} \quad \tilde{p} = P + p. \tag{11.48}$$

The background state is given by (see Section 8.2):

$$U_R = U_z = 0, \, U_\varphi = AR + B/R \quad \text{and} \quad \frac{1}{\rho}\frac{dP}{dR} = \frac{U_\varphi^2}{R}, \tag{11.49}$$

where

$$A \equiv \frac{\Omega_2 R_2^2 - \Omega_1 R_1^2}{R_2^2 - R_1^2}, \quad B \equiv \frac{(\Omega_1 - \Omega_2)R_1^2 R_2^2}{R_2^2 - R_1^2}.$$

Here, Ω_1 and Ω_2 are the angular speeds of the inner and outer cylinders, respectively, and R_1 and R_2 are their radii (Figure 11.16).
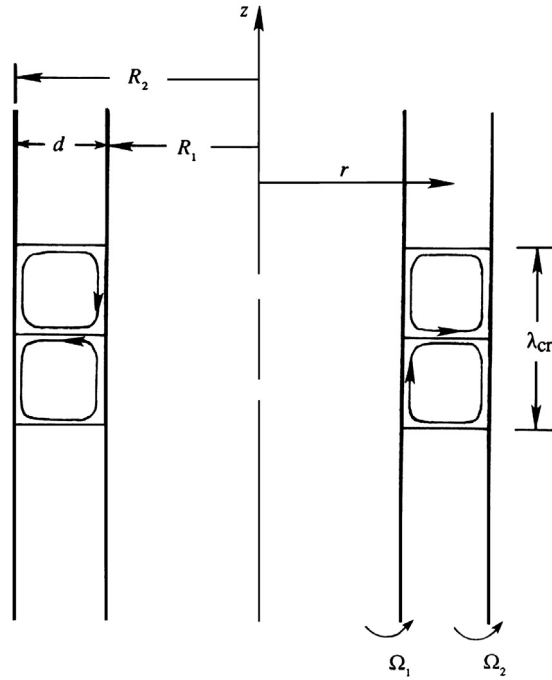
FIGURE 11.16 Geometry of the flow and the instability in rotating Couette flow. The fluid resides between rotating cylinders with radii R_1 and R_2. As for Bénard convection, the resulting instability forms as counter-rotating rolls with a wavelength that is approximately twice the gap between the cylinders.

Substituting (11.48) into (11.47), neglecting nonlinear terms, and subtracting the background state (11.49), we obtain the perturbation equations:

$$
\frac{\partial u_R}{\partial t} - \frac{2U_\varphi u_\varphi}{R} = -\frac{1}{\rho}\frac{\partial p}{\partial R} + \nu\left(\nabla^2 u_R - \frac{u_R}{R^2}\right), \quad \frac{\partial u_\varphi}{\partial t} + \left(\frac{dU_\varphi}{dR} + \frac{U_\varphi}{R}\right)u_R = \nu\left(\nabla^2 u_\varphi - \frac{u_\varphi}{R^2}\right),
$$
$$
\frac{\partial u_z}{\partial t} = -\frac{1}{\rho}\frac{\partial p}{\partial z} + \nu\nabla^2 u_z, \text{ and } \frac{\partial}{\partial R}(Ru_R) + \frac{\partial u_z}{\partial z} = 0. \tag{11.50}
$$

As the coefficients in these equations depend only on R, the equations admit solutions that depend on z and t exponentially. We therefore consider normal mode solutions of the form:

$$
(u_R, u_\varphi, u_z, p) = \left(\widehat{u}_R(R), \widehat{u}_\varphi(R), \widehat{u}_z(R), \widehat{p}(R)\right)\exp\{ikz + \sigma t\}.
$$

The requirement that the solutions remain bounded as $z \to \pm\infty$ implies that the axial wave number k must be real. After substituting the normal modes into (11.50) and eliminating $\widehat{u}_z$ and $\widehat{p}$, we get a coupled system of equations in $\widehat{u}_R$ and $\widehat{u}_\varphi$. Under the *narrow-gap approximation*, for which $d = R_2 - R_1$ is much smaller than $(R_1 + R_2)/2$, these equations finally become (see Chandrasekhar, 1961, for details):

$$(d^2/dR^2 - k^2 - \sigma)(d^2/dR^2 - k^2)\widehat{u}_R = (1 + \alpha x)\widehat{u}_\varphi, \text{ and}$$

$$(d^2/dR^2 - k^2 - \sigma)\widehat{u}_\varphi = -\text{Ta}k^2\widehat{u}_R, \tag{11.51}$$

where

$$\alpha \equiv (\Omega_2/\Omega_1) - 1, \ x \equiv (R - R_1)/d, \ d \equiv R_2 - R_1,$$

and Ta is the Taylor number

$$\text{Ta} \equiv 4\left(\frac{\Omega_1 R_1^2 - \Omega_2 R_2^2}{R_2^2 - R_1^2}\right)\frac{\Omega_1 d^4}{\nu^2}. \tag{11.52}$$

It is the ratio of the centrifugal force to viscous force, and equals $2(\Omega_1 R_1 d/\nu)^2(d/R_1)$ when only the inner cylinder is rotating and the gap is narrow.

The boundary conditions are

$$\widehat{u}_R = d\widehat{u}_R/dR = \widehat{u}_\varphi = 0 \quad \text{at } x = 0, 1. \tag{11.53}$$

The eigenvalues k at the marginal state are found by setting the real part of σ to zero. On the basis of experimental evidence, Taylor assumed that the marginal states are given by $\sigma = 0$. This was later proven to be true for cylinders rotating in the same directions, but a general demonstration for all conditions is still lacking.

A solution of the eigenvalue problem (11.51), subject to (11.53), was obtained by Taylor. Figure 11.17 shows the results of his calculations and his own experimental
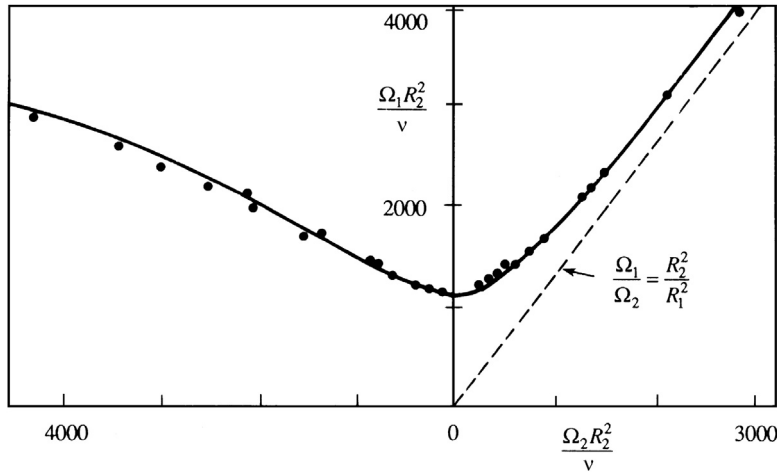
FIGURE 11.17   Taylor's observation and narrow-gap calculation of marginal stability in rotating Couette flow of water. The ratio of radii is $R_2/R_1 = 1.14$. The region above the curve is unstable. The dashed line represents Rayleigh's inviscid criterion, with the region to the left of the line representing instability. The experimental and theoretical results agree well and suggest that viscosity acts to stabilize the flow.
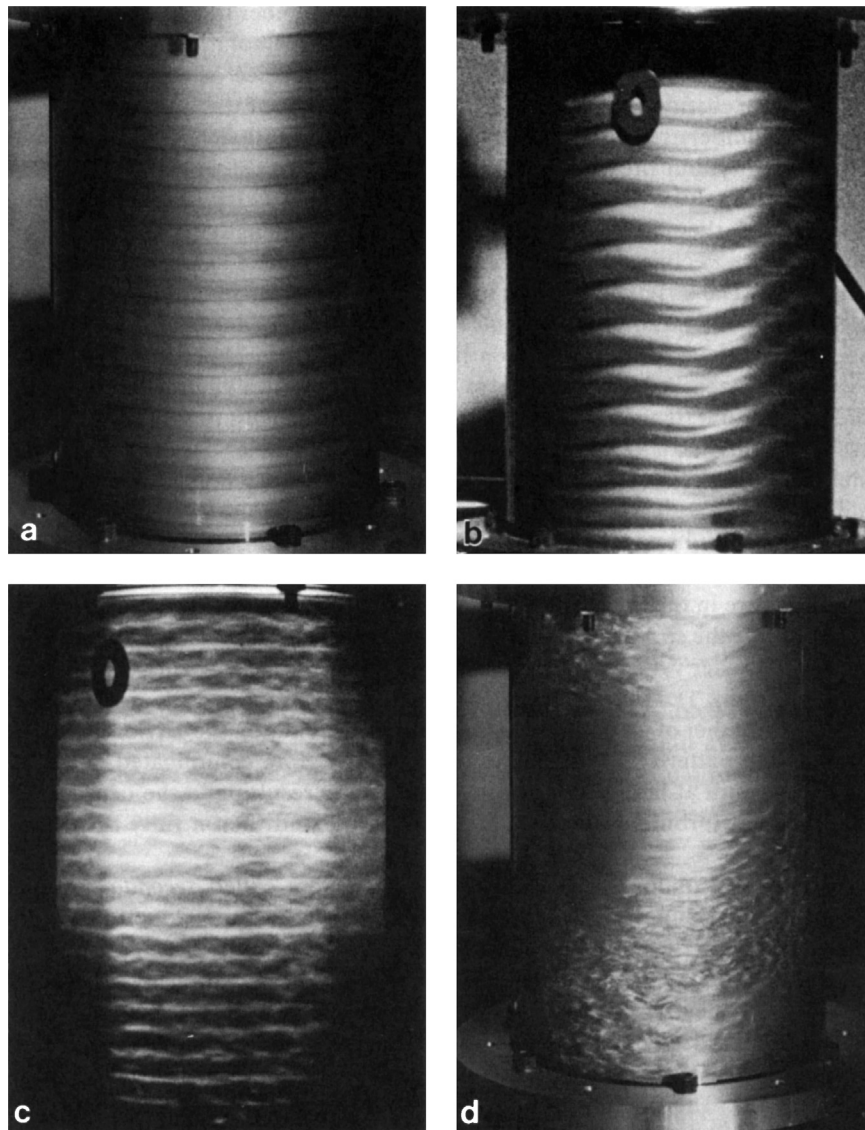
FIGURE 11.18   Instability of rotating Couette flow. Panels (a), (b), (c), and (d) correspond to increasing Taylor number. At first the instability appears as periodic rolls that do not vary with the azimuthal angle. Next, the rolls develop azimuthal waves with wavelengths that depend on the Taylor number. Eventually, the flow becomes turbulent. *D. Coles,* Journal of Fluid Mechanics, 21, *385–425, 1965; reprinted with the permission of Cambridge University Press.*

verification of the analysis. The vertical axis represents the angular velocity of the inner cylinder (taken positive), and the horizontal axis represents the angular velocity of the outer cylinder. Cylinders rotating in opposite directions are represented by a negative Ω_2. Taylor's solution of the marginal state is indicated, with the region above the curve

corresponding to instability. Rayleigh's inviscid criterion is also indicated by the straight dashed line. Taylor's viscous solution indicates that the flow remains stable until a critical Taylor number of

$$\text{Ta}_{cr} = \frac{1708}{(1/2)(1 + \Omega_2/\Omega_1)} \tag{11.54}$$

is attained. The nondimensional axial wave number at the onset of instability is found to be $k_{cr} = 3.12$, which implies that the wavelength at onset is $\lambda_{cr} = 2\pi d/k_{cr} \approx 2d$. The height of one cell is therefore nearly equal to d, so that the cross-section of a cell is nearly a square. In the limit $\Omega_2/\Omega_1 \rightarrow 1$, the critical Taylor number is identical to the critical Rayleigh number for thermal convection discussed in the preceding section, for which the solution was given by Jeffreys five years later. The agreement is expected, because in this limit $\alpha = 0$, and the eigenvalue problem (11.51) reduces to that of the Bénard problem (11.39). For cylinders rotating in opposite directions the Rayleigh criterion predicts instability, but the viscous solution can be stable.

Taylor's analysis of the problem was enormously satisfying, both experimentally and theoretically. He measured the wavelength at the onset of instability by injecting dye and obtained an almost exact agreement with his calculations. The observed onset of instability in the $\Omega_1 \Omega_2$-plane (Figure 11.17) was also in remarkable agreement. This has prompted remarks such as, "the closeness of the agreement between his theoretical and experimental results was without precedent in the history of fluid mechanics" (Drazin & Reid, 1981, p. 105). It even led some people to suggest happily that the agreement can be regarded as a verification of the underlying Navier-Stokes equations, which make a host of assumptions including a linearity between stress and strain rate.

The instability appears in the form of counter-rotating toroidal (or doughnut-shaped) vortices (Figure 11.18a) called *Taylor vortices*. The streamlines are in the form of helixes, with axes wrapping around the annulus, somewhat like the stripes on a barber's pole. These vortices themselves become unstable at higher values of Ta, when they give rise to wavy vortices for which $\partial/\partial\phi \neq 0$ (Figure 11.18b). In effect, the flow has now attained the next higher mode. The number of waves around the annulus depends on the Taylor number, and the wave pattern travels around the annulus. More complicated patterns of vortices result at a higher rate of rotation, finally resulting in the occasional appearance of turbulent patches (Figure 11.18d), and then a fully turbulent flow.

Phenomena analogous to the Taylor vortices are called *secondary flows* because they are superposed on a primary flow (such as the Couette flow in the present case). There are two other situations where a combination of curved streamlines (which give rise to centrifugal forces) and viscosity result in instability and steady secondary flows in the form of vortices. One is the flow through a curved channel, driven by a pressure gradient. The other is the appearance of *Görtler vortices* in a boundary-layer flow along a concave wall (Figure 11.19). The possibility of secondary flows signifies that the *solutions of the Navier-Stokes equations are nonunique* in the sense that more than one steady solution is allowed under the same boundary conditions. We can derive the form of the primary flow only if we exclude the secondary flow by appropriate assumptions. For example, we can derive the expression (11.50) for Couette flow by *assuming* $U_r = 0$ and $U_z = 0$ and thereby rule out the secondary flow.
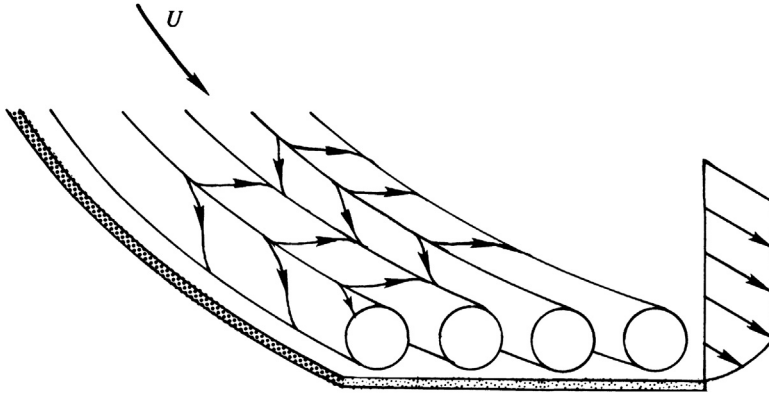
FIGURE 11.19 Görtler vortices in a boundary layer along a concave wall. The instability phenomenon here is essentially the same as that in Taylor-Couette flow, the only difference being the lack of the inner curved surface.

11.7. INSTABILITY OF CONTINUOUSLY STRATIFIED PARALLEL FLOWS

An instability of great geophysical importance is that of an inviscid stratified fluid in horizontal parallel flow. If the density and velocity vary discontinuously across an interface, the analysis in Section 11.3 shows that the flow is unconditionally unstable. Although only the discontinuous case was studied by Kelvin and Helmholtz, the more general case of continuous distribution is also commonly called the *Kelvin-Helmholtz instability.*

The problem has a long history. In 1915, Taylor, on the basis of his calculations with assumed distributions of velocity and density, *conjectured* that a gradient Richardson number (to be defined shortly) must be less than ¼ for instability. Other values of the critical Richardson number (ranging from 2 to ¼) were suggested by Prandtl, Goldstein, Richardson, Synge, and Chandrasekhar. Finally, Miles (1961) was able to prove Taylor's conjecture, and Howard (1961) immediately and elegantly generalized Miles' proof. A short record of the history is given in Miles (1986). In this section we shall prove the Richardson number criterion in the manner given by Howard.

Consider a horizontal parallel flow $U(z)$ directed along the x-axis. The z-axis is taken vertically upward. The basic flow is in equilibrium with the undisturbed density field $\overline{\rho}(z)$ and the basic pressure field $P(z)$. We shall only consider two-dimensional disturbances on this basic state, assuming that they are more unstable than three-dimensional disturbances; this is called *Squires' theorem* and is demonstrated in Section 11.8 in another context. The disturbed state has velocity, pressure, and density fields of:

$$\tilde{\mathbf{u}} = U\mathbf{e}_x + \mathbf{u} = (U + u, 0, w),\ \tilde{p} = P + p,\ \text{and}\ \tilde{\rho} = \overline{\rho} + \rho,$$

where, as before, the tilde indicates a total flow variable. The continuity equation reduces to $\partial u/\partial x + \partial w/\partial z = 0$, and the disturbed velocity field is assumed to satisfy the inviscid Boussinesq momentum equation:

$$\frac{\partial \tilde{\mathbf{u}}}{\partial t} + (\tilde{\mathbf{u}} \cdot \nabla)\tilde{\mathbf{u}} = -\frac{1}{\rho_0}\nabla\tilde{p} - g\frac{(\overline{\rho} + \rho)}{\rho_0}\mathbf{e}_z,$$

where the density variations are neglected except in the vertical component. Here, ρ_0 is a reference density. The basic flow satisfies

$$0 = -\frac{1}{\rho_0}\frac{\partial P}{\partial z} - g\frac{\overline{\rho}}{\rho_0}.$$

Subtracting the last two equations and dropping nonlinear terms, we obtain the perturbation equation of motion:

$$\frac{\partial \mathbf{u}}{\partial t} + (\mathbf{u}\cdot\nabla)(U\mathbf{e}_x) + U(\mathbf{e}_x\cdot\nabla)\mathbf{u} = -\frac{1}{\rho_0}\nabla p - g\frac{\rho}{\rho_0}\mathbf{e}_z.$$

The horizontal (x) and vertical (z) components of the preceding equation are

$$\frac{\partial u}{\partial t} + w\frac{\partial U}{\partial z} + U\frac{\partial u}{\partial x} = -\frac{1}{\rho_0}\frac{\partial p}{\partial x} \quad \text{and} \quad \frac{\partial w}{\partial t} + U\frac{\partial w}{\partial x} = -\frac{1}{\rho_0}\frac{\partial p}{\partial x} - g\frac{\rho}{\rho_0}. \tag{11.55}$$

In the absence of diffusion the density of fluid particles does not change: $D\tilde{\rho}/Dt = 0$, or

$$\frac{\partial}{\partial t}(\overline{\rho}+\rho) + (U+u)\frac{\partial}{\partial x}(\overline{\rho}+\rho) + w\frac{\partial}{\partial z}(\overline{\rho}+\rho) = 0.$$

Keeping only the linear terms, and using the fact that $\overline{\rho}$ is a function of z only, we obtain

$$\frac{\partial\rho}{\partial t} + U\frac{\partial\rho}{\partial x} + w\frac{\partial\overline{\rho}}{\partial z} = 0,$$

which can be written as

$$\frac{\partial\rho}{\partial t} + U\frac{\partial\rho}{\partial x} - \frac{\rho_0 N^2 w}{g} = 0, \tag{11.56}$$

where N is the buoyancy frequency in an incompressible flow:

$$N^2 \equiv -\frac{g}{\rho_0}\frac{d\overline{\rho}}{dz}. \tag{7.128}$$

The last term in equation (11.56) represents the density change at a point due to the vertical advection of the basic density field across the point.

The continuity equation can be satisfied with a stream function $u = \partial\psi/\partial z$ and $w = -\partial\psi/\partial x$. Equations (11.55) and (11.56) then become

$$\frac{\partial^2\psi}{\partial t\partial z} - \frac{\partial\psi}{\partial x}\frac{dU}{dz} + U\frac{\partial^2\psi}{\partial x\partial z} = -\frac{1}{\rho_0}\frac{\partial p}{\partial x}, \quad -\frac{\partial^2\psi}{\partial t\partial x} - U\frac{\partial^2\psi}{\partial x^2} = -\frac{g\rho}{\rho_0} - \frac{1}{\rho_0}\frac{\partial p}{\partial z},$$

$$\frac{\partial\rho}{\partial t} + U\frac{\partial\rho}{\partial x} + \frac{\rho_0 N^2}{g}\frac{\partial\psi}{\partial x} = 0. \tag{11.57}$$

Since the coefficients of derivatives in (11.57) are independent of x and t, exponential variations in these variables are allowed. Consequently, we assume traveling-wave normal mode solutions of the form:

$$[\rho, p, \psi] = [\hat{\rho}(z), \hat{p}(z), \hat{\psi}(z)]\exp\{ik(x-ct)\},$$

where quantities denoted by (^) are complex amplitudes. Because the flow is unbounded in x, the wave number k must be real. The eigenvalue $c = c_r + ic_i$ can be complex, and the solution is unstable if there exists a $c_i > 0$, similar to the development in Section 11.3. Substituting the normal modes, (11.57) becomes:

$$(U - c)\frac{\partial \widehat{\psi}}{\partial z} - \frac{\partial U}{\partial z}\widehat{\psi} = -\frac{1}{\rho_0}\widehat{p}, \quad k^2(U - c)\widehat{\psi} = -g\frac{\widehat{\rho}}{\rho_0} - \frac{1}{\rho_0}\frac{\partial \widehat{p}}{\partial z}, (U - c)\widehat{\rho} + \frac{\rho_0 N^2}{g}\widehat{\psi} = 0.$$

$$\text{(11.58, 11.59, 11.60)}$$

We seek a single equation for $\widehat{\psi}$. The pressure can be eliminated by taking the z-derivative of (11.58) and subtracting (11.59). The density can be eliminated via substitution from (11.60) to produce:

$$(U - c)\left(\frac{d^2}{dz^2} - k^2\right)\widehat{\psi} - \frac{\partial^2 U}{\partial z^2}\widehat{\psi} + \frac{N^2}{U - c}\widehat{\psi} = 0. \tag{11.61}$$

This is the *Taylor-Goldstein equation*, which governs the behavior of perturbations in a stratified parallel flow. Note that the complex conjugate of (11.61) is also a valid equation because we can take the imaginary part of the equation, change the sign, and add it to the real part of the equation. Now because the Taylor-Goldstein equation does not involve any i, a complex conjugate of the equation shows that if $\widehat{\psi}$ is an eigenfunction with eigenvalue c for some k, then $\widehat{\psi}^*$ is a possible eigenfunction with eigenvalue c^* for the same k. Therefore, to each eigenvalue with a positive c_i there is a corresponding eigenvalue with a negative c_i. In other words, *to each growing mode there is a corresponding decaying mode.* A nonzero c_i therefore ensures instability.

The boundary conditions are that $w = 0$ on rigid boundaries, presuming these are located at $z = 0$ and d. This requires $\partial \psi / \partial x = ik\widehat{\psi}\exp\{ik(x - ct)\} = 0$ at the walls, which is possible only if

$$\widehat{\psi}(0) = \widehat{\psi}(d) = 0. \tag{11.62}$$

A necessary condition involving the Richardson number for linear instability of inviscid stratified parallel flows can be derived by defining a new field variable ϕ (not the velocity potential) by

$$\phi \equiv \frac{\widehat{\psi}}{(U - c)^{1/2}} \quad \text{or} \quad \widehat{\psi} = (U - c)^{1/2}\phi. \tag{11.63}$$

Then we obtain the derivatives:

$$\frac{\partial \widehat{\psi}}{\partial z} = (U - c)^{1/2}\frac{\partial \phi}{\partial z} + \frac{\phi}{2(U - c)^{1/2}}\frac{dU}{dz},$$

$$\frac{\partial^2 \widehat{\psi}}{\partial z^2} = (U - c)^{1/2}\frac{\partial^2 \phi}{\partial z^2} + \frac{1}{(U - c)^{1/2}}\left(\frac{d\phi}{dz}\frac{dU}{dz} + \frac{1}{2}\phi\frac{d^2 U}{dz^2}\right) - \frac{\phi}{4(U - c)^{3/2}}\left(\frac{dU}{dz}\right)^2.$$

The Taylor-Goldstein equation then becomes, after some rearrangement:

$$\frac{d}{dz}\left[(U-c)\frac{d\phi}{dz}\right] - \left\{k^2(U-c) + \frac{1}{2}\frac{d^2U}{dz^2} + \frac{(1/4)(dU/dz)^2 - N^2}{U-c}\right\}\phi = 0.$$ (11.64)

Now multiply equation (11.64) by ϕ^* (the complex conjugate of ϕ), integrate from $z = 0$ to $z = d$, and use the boundary conditions $\phi(0) = \phi(d) = 0$. The first term gives:

$$\int_0^d \frac{d}{dz}\left\{(U-c)\frac{d\phi}{dz}\right\}\phi^* dz = \int_0^d \left[\frac{d}{dz}\left\{(U-c)\frac{d\phi}{dz}\phi^*\right\} - (U-c)\frac{d\phi}{dz}\frac{d\phi^*}{dz}\right] dz = -\int_0^d (U-c)\left|\frac{d\phi}{dz}\right|^2 dz.$$

Integrals of the other terms in (11.64) are also simple to manipulate. We finally obtain:

$$\int_0^d \left\{\frac{N^2 - (1/4)(dU/dz)^2}{U-c}\right\}|\phi|^2 dz = \int_0^d (U-c)\left\{\left|\frac{d\phi}{dz}\right|^2 + k^2|\phi|^2\right\} dz + \int_0^d \frac{1}{2}\frac{d^2U}{dz^2}|\phi|^2 dz.$$ (11.65)

The last term in the preceding equation is real. The imaginary part of the first term can be found by noting that:

$$\frac{1}{U-c} = \frac{U-c^*}{|U-c|^2} = \frac{U-c_r+ic_i}{|U-c|^2}.$$

Taking the imaginary part of (11.65) leads to:

$$c_i \int_0^d \left\{\frac{N^2 - (1/4)(dU/dz)^2}{|U-c|^2}\right\}|\phi|^2 dz = -c_i \int_0^d \left\{\left|\frac{d\phi}{dz}\right|^2 + k^2|\phi|^2\right\} dz.$$

The integral on the right side is positive. If the flow is such that $N^2 > (1/4)(dU/dz)^2$ everywhere, then the preceding equation states that c_i times a positive quantity equals c_i times a negative quantity; this is impossible and requires that $c_i = 0$ for such a case. Thus, defining the *gradient Richardson number:*

$$Ri(z) \equiv N^2/(dU/dz)^2,$$ (11.66)

we can say that linear stability is guaranteed if the inequality

$$Ri > \frac{1}{4} \left(\text{stable}\right)$$ (11.67)

is satisfied everywhere in the flow.

Note that the criterion does not state that the flow is necessarily unstable if $Ri < ¼$ somewhere, or even everywhere, in the flow. Thus $Ri < ¼$ is a *necessary* but not sufficient condition for instability. For example, in a jet-like velocity profile $u \propto \text{sech}^2 z$ and an exponential density profile, the flow does not become unstable until the Richardson number falls below 0.214. A critical Richardson number lower than ¼ is also found in the presence of boundaries, which stabilize the flow. In fact, there is no unique critical Richardson number that applies to all distributions of $U(z)$ and $N(z)$. However, several calculations show that in many shear layers

(having linear, tanh, or error function profiles for velocity and density), the flow does become unstable to disturbances of certain wavelengths if the minimum value of Ri in the flow (which is generally at the center of the shear layer where $|dU/dz|$ is greatest) is less than ¼. The *most unstable* wave, defined as the first to become unstable as Ri is reduced below ¼, is found to have a wavelength $\lambda \approx 7h$, where h is the thickness of the shear layer. Laboratory (Scotti & Corcos, 1972) as well as geophysical observations (Eriksen, 1978) show that the requirement

$$\mathrm{Ri}_{\min} < \frac{1}{4}$$

is a useful guide for the prediction of instability of a stratified shear layer.

Similar to the previous analysis, another useful result concerning the behavior of the complex phase speed c in an inviscid parallel shear flow can be determined by considering an alternative version of (11.63):

$$F \equiv \frac{\widehat{\psi}}{U - c},\qquad(11.68)$$

which leads to derivatives:

$$\frac{\partial \widehat{\psi}}{\partial z} = (U - c)\frac{\partial F}{\partial z} + \frac{dU}{dz}F,$$

$$\frac{\partial^2 \widehat{\psi}}{\partial z^2} = (U - c)\frac{\partial^2 F}{\partial z^2} + 2\frac{dU}{dz}\frac{dF}{dz} + \frac{d^2U}{dz^2}F.$$

When (11.68) is substituted into the Taylor-Goldstein equation (11.61), the result is:

$$(U - c)\left[(U - c)\frac{d^2F}{dz^2} + 2\frac{dU}{dz}\frac{dF}{dz} - k^2(U - c)F\right] + N^2F = 0,$$

and the terms involving d^2U/dz^2 have canceled out. This can be rearranged in the form

$$\frac{d}{dz}\left[(U - c)^2\frac{dF}{dz}\right] - k^2(U - c)F + N^2F = 0.$$

Multiplying by F^*, integrating (by parts when necessary) over the depth of flow, and using the boundary conditions, we obtain

$$-\int (U - c)^2\left|\frac{dF}{dz}\right|^2 dz - k^2\int (U - c)^2|F|^2 dz + \int N^2|F|^2 dz = 0,$$

which can be written as

$$\int (U - c)^2 Q dz = \int N^2|F|^2 dz \quad \text{where } Q \equiv |dF/dz|^2 + k^2|F|^2$$

is positive. Equating real and imaginary parts, we obtain

$$\int \left[(U - c_r)^2 - c_i^2\right]Q dz = \int N^2|F|^2 dz \quad \text{and} \quad c_i\int (U - c_r)Q dz = 0. \qquad (11.69, 11.70)$$

For instability $c_i \neq 0$, for which (11.70) shows that $(U - c_r)$ must change sign somewhere in the flow:

$$U_{min} < c_r < U_{max}, \tag{11.71}$$

which states that c_r lies in the range of U. Recall that we have assumed solutions of the form

$$\exp\{ik(x - ct)\} = \exp\{ik(x - c_r t\}\exp\{ + kc_i t\},$$

which means that c_r is the phase velocity in the positive x direction, and kc_i is the growth rate. Equation (11.71) shows that c_r is positive if U is everywhere positive, and is negative if U is everywhere negative. In these cases we can say that unstable waves propagate in the direction of the background flow.

Limits on the maximum growth rate can also be predicted. Equation (11.69) gives

$$\int \left[U^2 - 2Uc_r + c_r^2 - c_i^2 \right] Qdz > 0,$$

which, on using (11.70), becomes

$$\int \left[U^2 - c_r^2 - c_i^2 \right] Qdz > 0. \tag{11.72}$$

Now because $(U_{min} - U) < 0$ and $U_{max} - U > 0$, it is always true that

$$\int [U_{min} - U][U_{max} - U]dz \leq 0,$$

which can be recast as

$$\int \left[U_{max}U_{min} + U^2 - U(U_{max} + U_{min}) \right] Qdz \leq 0.$$

Using (11.72), this gives

$$\int \left[U_{max}U_{min} + c_r^2 + c_i^2 - U(U_{max} + U_{min}) \right] Qdz \leq 0,$$

and after using (11.70), this becomes

$$\int \left[U_{max}U_{min} + c_r^2 + c_i^2 - c_r(U_{max} + U_{min}) \right] Qdz \leq 0.$$

Because the quantity within [,]-brackets is independent of z, and $\int Qdz > 0$, we must have [ ] ≤ 0. With some rearrangement, this condition can be written as

$$\left[c_r - \frac{1}{2}(U_{max} + U_{min}) \right]^2 + c_i^2 \leq \left[\frac{1}{2}(U_{max} - U_{min}) \right]^2.$$

This shows that *the complex wave velocity, c, of any unstable mode of a disturbance in parallel flows of an inviscid fluid must lie inside the semicircle in the upper half of the c-plane, which has the range of U as the diameter* (Figure 11.20). This result was first derived by Howard
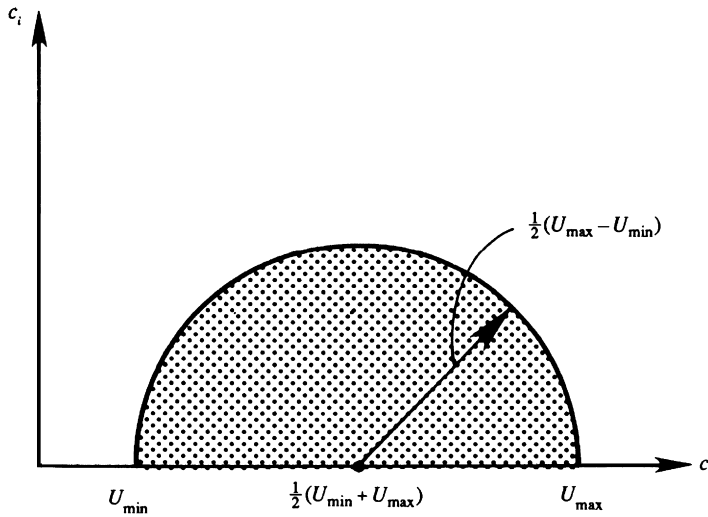
FIGURE 11.20　Depiction of the Howard semicircle theorem. In inviscid parallel flows the complex eigenvalue c must lie within the semicircle shown. This theorem limits both the real part (the phase speed) and the imaginary part (the growth rate divided by k) of the eigenvalue.

(1961) and is valid for flows with and without stratification. It is called the *Howard semicircle theorem* and states that the maximum growth rate is limited by:

$$kc_i < (k/2)(U_{\max} - U_{\min}).$$

The theorem is very useful in searching for eigenvalues $c(k)$ in numerical solution of instability problems.

11.8. SQUIRE'S THEOREM AND THE ORR-SOMMERFELD EQUATION

In our studies of the Bénard and Taylor problems, we encountered two flows in which viscosity has a stabilizing effect. Curiously, viscous effects can also be *destabilizing*, as indicated by several calculations of wall-bounded parallel flows. In this section we shall derive the equation governing the stability of parallel flows of a homogeneous viscous fluid. Let the primary flow be directed along the x direction and vary in the y direction so that $\mathbf{U} = (U(y), 0, 0)$. We decompose the total flow as the sum of the basic flow plus the perturbation:

$$\tilde{\mathbf{u}} = (U + u, v, w), \text{ and } \tilde{p} = P + p.$$

Both the background and the perturbed flows satisfy the Navier-Stokes equations. The perturbed flow satisfies the x-momentum equation:

$$\frac{\partial u}{\partial t} + (U + u)\frac{\partial}{\partial x}(U + u) + v\frac{\partial}{\partial y}(U + u) = -\frac{\partial}{\partial x}(P + p) + \frac{1}{Re}\nabla^2(U + u), \tag{11.73}$$

where the variables have been made dimensionless with a characteristic length scale L (say, the width of flow), and a characteristic velocity U_0 (say, the maximum velocity of the basic

flow); time is scaled by L/U_0 and the pressure is scaled by ρU_0^2. The Reynolds number is $Re = U_0 L/\nu$.

The background flow satisfies:

$$0 = -\frac{\partial P}{\partial x} + \frac{1}{Re}\nabla^2 U.$$

Subtracting this from (11.73) and neglecting terms nonlinear in the perturbations, we obtain the x-momentum equation for the perturbations:

$$\frac{\partial u}{\partial t} + U\frac{\partial u}{\partial x} + v\frac{\partial U}{\partial y} = -\frac{\partial p}{\partial x} + \frac{1}{Re}\nabla^2 u. \tag{11.74}$$

Similarly the y-momentum, z-momentum, and continuity equations for the perturbations are:

$$\frac{\partial v}{\partial t} + U\frac{\partial v}{\partial x} = -\frac{\partial p}{\partial y} + \frac{1}{Re}\nabla^2 v, \quad \frac{\partial w}{\partial t} + U\frac{\partial w}{\partial x} = -\frac{\partial p}{\partial z} + \frac{1}{Re}\nabla^2 w, \text{ and } \frac{\partial u}{\partial x} + \frac{\partial v}{\partial y} + \frac{\partial w}{\partial z} = 0. \tag{11.75}$$

The coefficients in (11.74) and (11.75) depend only on y, so that the equations admit solutions exponential in x, z, and t. Accordingly, we assume normal modes of the form:

$$[\mathbf{u}, p] = \left[\widehat{\mathbf{u}}(y), \widehat{p}(y)\right] \exp\{i(kx + mz - kct)\}. \tag{11.76}$$

As the flow is unbounded in x and z, the wave number components k and m must be real. However, the wave speed $c = c_r + ic_i$ may be complex. Without loss of generality, we can consider only positive values for k and m; the sense of propagation is then left open by keeping the sign of c_r unspecified. The normal modes represent waves that travel obliquely to the basic flow with a wave number magnitude $\sqrt{k^2 + m^2}$ and have an amplitude that varies as $\exp(kc_i t)$. Solutions are therefore stable if $c_i < 0$ and unstable if $c_i > 0$.

Substitution of (11.76) into the perturbation equations (11.74) and (11.75) produces:

$$ik(U - c)\widehat{u} + \widehat{v}(dU/dy) = -ikp + (1/Re)\left[d^2\widehat{u}/dy^2 - (k^2 + m^2)\widehat{u}\right],$$

$$ik(U - c)\widehat{v} = -d\widehat{p}/dy + (1/Re)\left[d^2\widehat{v}/dy^2 - (k^2 + m^2)\widehat{v}\right],$$

$$ik(U - c)\widehat{w} = -im\widehat{p} + (1/Re)\left[d^2\widehat{w}/dy^2 - (k^2 + m^2)\widehat{w}\right], \text{ and}$$

$$ik\widehat{u} + d\widehat{v}/dy + im\widehat{w} = 0.$$

$$\tag{11.77}$$

These are the normal mode equations for three-dimensional disturbances.

Before proceeding further, we shall first prove Squire's Theorem (1933) which states that *to each unstable three-dimensional disturbance there corresponds a more unstable two-dimensional one.* To prove this theorem, consider the *Squire transformation*:

$$\overline{k} = \sqrt{k^2 + m^2}, \overline{c} = c, \overline{k}\overline{u} = k\widehat{u} + m\widehat{w}, \overline{v} = \widehat{v}, \overline{p}/\overline{k} = \widehat{p}/k, \text{ and } \overline{k}\overline{Re} = k\text{Re}. \tag{11.78}$$

After substituting (11.78) into (11.77), and adding the first and third equations, the result is

$$i\bar{k}(U-c)\bar{u} + \bar{v}(dU/dy) = -i\bar{k}\bar{p} + (1/\overline{\text{Re}})\left[d^2\bar{u}/dy^2 - \bar{k}^2\bar{u}\right],$$

$$i\bar{k}(U-c)\bar{v} = -d\hat{p}/dy + (1/\overline{\text{Re}})\left[d^2\bar{v}/dy^2 - \bar{k}^2\bar{v}\right], \text{ and}$$

$$i\bar{k}\bar{u} + d\bar{v}/dy = 0.$$

These equations are exactly the same as (11.77), but with $m = \hat{w} = 0$. Thus, to each three-dimensional problem corresponds an equivalent two-dimensional one. Moreover, Squire's transformation (11.78) shows that the equivalent two-dimensional problem is associated with a *lower* Reynolds number since $\bar{k} > k$. It follows that the critical Reynolds number at which the instability starts is lower for two-dimensional disturbances. Therefore, we only need to consider a two-dimensional disturbance if we want to determine the minimum Reynolds number for the onset of instability.

The three-dimensional disturbance (11.76) is a wave propagating obliquely to the basic flow. If we orient the coordinate system with the new x-axis in this direction, the equations of motion are such that only the component of the basic flow in this direction affects the disturbance. Thus, the effective Reynolds number is reduced.

Interestingly, Squire's theorem also holds for several other problems that do not involve the Reynolds number. Equation (11.78) shows that the growth rate for a two-dimensional disturbance is $\exp(\bar{k}\bar{c}_i t)$, whereas (11.76) shows that the growth rate of a three-dimensional disturbance is $\exp(kc_i t)$. The two-dimensional growth rate is therefore larger because Squire's transformation requires $\bar{k} > k$ and $\bar{c} = c$. We can therefore say that the two-dimensional disturbances are more unstable.

Because of Squire's theorem, we only need consider the equation set (11.77) with $m = \hat{w} = 0$. The two-dimensionality allows the use of a stream function $\psi(x,y,t)$ for the perturbation field via the usual relationships: $u = \partial\psi/\partial y$ and $v = -\partial\psi/\partial x$. Again, we assume normal modes of the form:

$$[u, v, \psi] = [\hat{u}(y), \hat{v}(y), \phi(y)]\exp\{ik(x - ct)\}.$$

(To be consistent, we should denote the complex amplitude of ψ by $\hat{\psi}$; we are using ϕ [not the potential] instead to follow the standard notation for this variable in the literature.) Then we must have $\hat{u} = \partial\phi/\partial y$ and $\hat{v} = -ik\phi$, and a single equation in terms of ϕ can now be found by eliminating the pressure from (11.77). This effort yields a fourth-order ordinary differential equation:

$$(U-c)\left(\frac{d^2\phi}{dy^2} - k^2\phi\right) - \frac{d^2U}{dy^2}\phi = \frac{1}{ik\text{Re}}\left(\frac{d^4\phi}{dy^4} - 2k^2\frac{d^2\phi}{dy^2} + k^4\phi\right). \tag{11.79}$$

The boundary conditions are the no-slip conditions which require

$$\phi = d\phi/dy = 0 \quad \text{at } y = y_1 \text{ and } y_2. \tag{11.80}$$

Equation (11.79) is the well-known *Orr-Sommerfeld equation*, which governs the stability of nearly parallel viscous flows such as those in a straight channel or in a boundary layer. It is essentially a vorticity equation because the pressure has been eliminated. Analytical

solutions of the Orr-Sommerfeld equations are difficult to obtain, and only the results of some simple flows will be discussed in the later sections. However, we shall first present certain results obtained by ignoring the viscous terms on the right side of this equation.

11.9. INVISCID STABILITY OF PARALLEL FLOWS

Insight into the viscous stability of parallel flows can be obtained by first assuming that the disturbances obey inviscid dynamics. The governing equation can be found by letting $\text{Re} \to \infty$ in the Orr-Sommerfeld equation, giving

$$(U - c)\left(\frac{d^2\phi}{dy^2} - k^2\phi\right) - \frac{d^2U}{dy^2}\phi = 0, \tag{11.81}$$

which is called the *Rayleigh equation*. If the flow is bounded by walls at y_1 and y_2 where $v = 0$, then the boundary conditions are

$$\phi = 0 \quad \text{at } y = y_1 \text{ and } y_2. \tag{11.82}$$

The set (11.81) and (11.82) defines an eigenvalue problem, with $c(k)$ as the eigenvalue and ϕ as the eigenfunction. As these equations do not involve i, taking the complex conjugate shows that if ϕ is an eigenfunction with eigenvalue c for some k, then ϕ^* is also an eigenfunction with eigenvalue c^* for the same k. Therefore, to each eigenvalue with a positive c_i there is a corresponding eigenvalue with a negative c_i. In other words, *to each growing mode there is a corresponding decaying mode*. Stable solutions therefore can have only a real c. Note that this is true of inviscid flows only. The viscous term in the full Orr-Sommerfeld equation (11.79) involves an i, and the foregoing conclusion is no longer valid.

We shall now show that certain velocity distributions $U(y)$ are potentially unstable according to the inviscid Rayleigh equation (11.81). In this discussion it should be noted that we are only assuming that the *disturbances* obey inviscid dynamics; the background flow profile $U(y)$ may be that of a steady laminar viscous flow.

The first deduction that can be made from (11.81) is Rayleigh's inflection point criterion that states that *a necessary (but not sufficient) criterion for instability of an inviscid parallel flow is that the basic velocity profile $U(y)$ has a point of inflection*. To prove the theorem, rewrite the Rayleigh equation (11.81) in the form

$$\frac{d^2\phi}{dy^2} - k^2\phi - \frac{1}{U-c}\frac{d^2U}{dy^2}\phi = 0,$$

and consider the unstable mode for which $c_i > 0$, and therefore $U - c \neq 0$. Multiply this equation by ϕ^*, integrate from y_1 to y_2, by parts where necessary, and apply the boundary condition (11.82). The first term transforms as follows:

$$\int \phi^*(d^2\phi/dy^2)dy = [\phi^*(d\phi/dy)]_{y_1}^{y_2} - \int (d\phi^*/dy)(d\phi/dy)dy = -\int |d\phi/dy|^2 dy,$$

where the limits on the integrals have not been explicitly written. The Rayleigh equation then gives

$$\int (|d\phi/dy|^2 + k^2|\phi|^2)dy + \int \frac{1}{U-c}\frac{d^2U}{dy^2}|\phi|^2dy \ = \ 0. \tag{11.83}$$

The first term is real. The second term in (11.83) is complex, and its imaginary part can be found by multiplying the numerator and denominator by $(U - c^*)$. Thus, the imaginary part of (11.83) implies:

$$c_i \int \frac{1}{|U-c|^2}\frac{d^2U}{dy^2}|\phi|^2dy \ = \ 0. \tag{11.84}$$

For the unstable case, for which $c_i \neq 0$, (11.84) can be satisfied only if d^2U/dy^2 changes sign at least once in the *open* interval $y_1 < y < y_2$. In other words, for instability the background velocity distribution must have at least one point of inflection (where $d^2U/dy^2 = 0$) within the flow. Clearly, the existence of a point of inflection does not guarantee a nonzero c_i. The inflection point is therefore a necessary but not sufficient condition for inviscid instability.

Some seventy years after Rayleigh's discovery, the Swedish meteorologist Fjortoft in 1950 discovered a stronger necessary condition for the instability of inviscid parallel flows. He showed that *a necessary condition for instability of inviscid parallel flows is that* $(U - U_1)(d^2U/dy^2) < 0$ *somewhere in the flow*, where U_1 is the value of U at the point of inflection. To prove the theorem, take the real part of (11.83):

$$\int \frac{U-c_r}{|U-c|^2}\frac{d^2U}{dy^2}|\phi|^2dy \ = \ -\int(|d\phi/dy|^2 + k^2|\phi|^2)dy < 0. \tag{11.85}$$

Suppose that the flow is unstable, so that $c_i \neq 0$, and a point of inflection does exist according to the Rayleigh criterion. Then it follows from (11.84) that

$$(c_r - U_1)\int \frac{1}{|U-c|^2}\frac{d^2U}{dy^2}|\phi|^2dy \ = \ 0. \tag{11.86}$$

Adding equations (11.85) and (11.86), we obtain

$$\int \frac{U-U_1}{|U-c|^2}\frac{d^2U}{dy^2}|\phi|^2dy < 0,$$

so that $(U - U_1)(d^2U/dy^2)$ must be negative somewhere in the flow.

Some common velocity profiles are shown in Figure 11.21. Only the two flows shown in the bottom row can possibly be unstable, for only they satisfy Fjortoft's theorem. Flows (a), (b), and (c) do not have an inflection point: flow (d) does satisfy Rayleigh's condition but not Fjortoft's because $(U - U_1)(d^2U/dy^2)$ is positive. Note that an alternate way of stating Fjortoft's theorem is that *the magnitude of vorticity of the basic flow must have a maximum within the region of flow,* not at the boundary. In flow (d), the maximum magnitude of vorticity occurs at the walls.

The criteria of Rayleigh and Fjortoft essentially point to the importance of having a point of inflection in the velocity profile. They show that flows in jets, wakes, shear layers, and boundary layers with adverse pressure gradients, all of which have a point of inflection and satisfy Fjortoft's theorem, are potentially unstable. On the other hand,
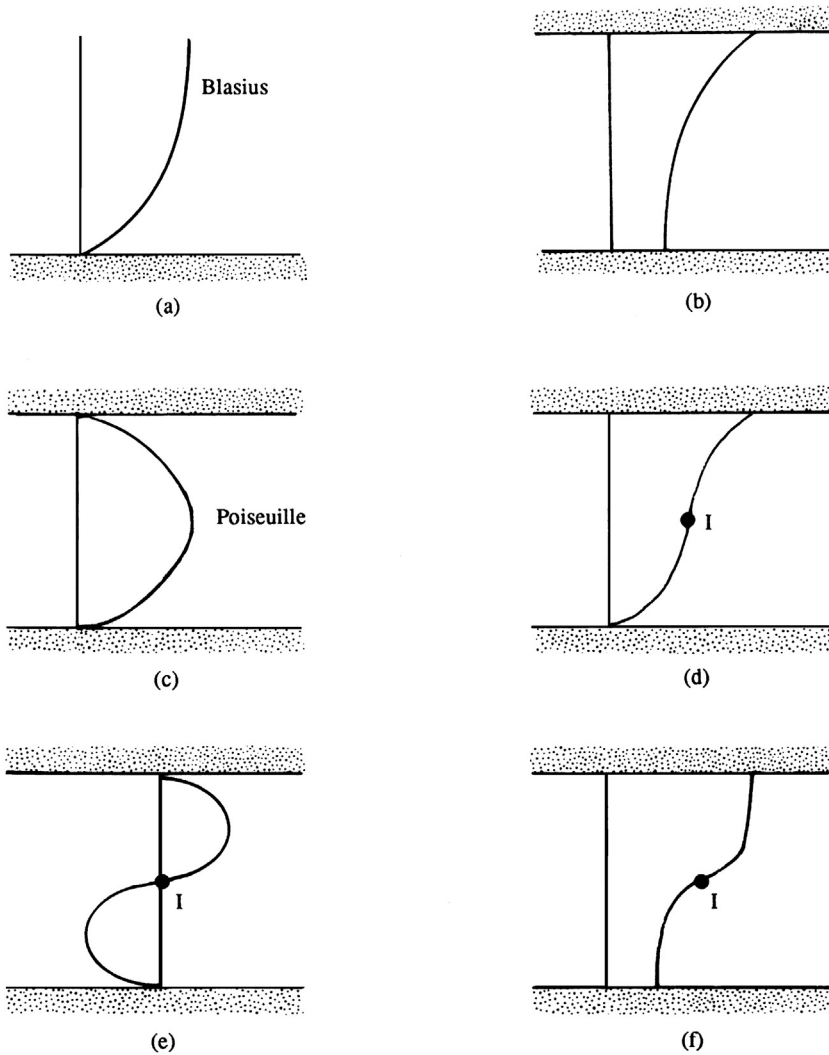
FIGURE 11.21   Examples of parallel flows. Points of inflection are denoted by I. Profiles (a), (b), and (c) are inviscidly stable. Profiles (d), (e), and (f) may be inviscidly unstable by Rayleigh's inflection point criterion. Only profiles (e) and (f) satisfy Fjortoft's criterion of inviscid instability.

plane Couette flow, Poiseuille flow, and a boundary-layer flow with zero or favorable pressure gradient have no point of inflection in the velocity profile and are stable in the inviscid limit.

However, neither of the two conditions is sufficient for instability. An example is the sinusoidal profile $U = \sin(y)$, with boundaries at $y = \pm b$. It has been shown that the flow is stable if the width is restricted to $2b < \pi$, although it has an inflection point at $y = 0$.

Invisicd parallel flows satisfy Howard's semicircle theorem, which was proved in Section 11.7 for the more general case of a stratified shear flow. The theorem states that the phase speed c_r of an unstable mode with wave number k has a value that lies between the minimum and the maximum values of $U(y)$ in the flow field. Growing and decaying modes are characterized by a nonzero c_i, whereas neutral modes can have only a real $c = c_r$. Thus, it follows that neutral modes must have $U = c$ somewhere in the flow field. The neighborhood y around y_c at which $U = c = c_r$ is called a *critical layer*. The location y_c is a critical point of the inviscid governing equation (11.81), because the highest derivative drops out at this value of y, and the eigenfunction for this k and c may be discontinuous across this layer. The full Orr-Sommerfeld equation (11.79) has no such critical layer because the highest-order derivative does not drop out when $U = c$. It is apparent that in a real flow a viscous boundary layer must form at the location where $U = c$, and that the layer becomes thinner as $Re \rightarrow \infty$.

The streamline pattern in the neighborhood of the critical layer where $U = c$ was given by Kelvin in 1888, and indicates the nature of the nearby unstable modes having the same k but small positive c_i. The discussion provided here is adapted from Drazin and Reid (1981). Consider a flow viewed by an observer moving with the phase velocity $c = c_r$. Then the basic velocity field seen by this observer is $(U - c)$, so that the stream function due to the basic flow is

$$\Psi = \int (U - c)dy.$$

The total stream function is obtained by adding the perturbation:

$$\widehat{\psi} = \int (U - c)dy + A\phi(y) \exp\{ikx\}. \tag{11.87}$$

where A is an arbitrary constant, and the time factor in the second term is omitted because the disturbance is neutrally stable. Near the critical layer $y = y_c$, a Taylor series expansion of the real part of (11.87) is approximately

$$\widehat{\psi} \cong \frac{(y - y_c)^2}{2}\left[\frac{dU}{dy}\right]_{y=y_c} + A\phi(y_c)\cos(kx),$$

where $\phi(y_c)$ is assumed to be real. The streamline pattern corresponding to this equation is sketched in Figure 11.22, showing the so-called *Kelvin cat's eye pattern* that is
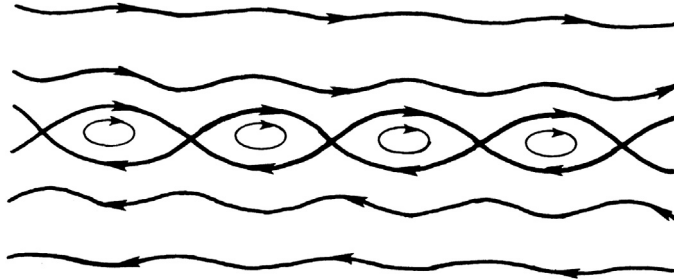
FIGURE 11.22   The Kelvin cat's eye pattern near a critical layer, showing streamlines as seen by an observer moving with a neutrally stable wave having $c = c_r$. This flow pattern is reminiscent of those shown in Figures 11.4–11.6.

visually similar to the illustrations of the Kelvin-Helmholtz instability given in Figures 11.4 through11.6.

## 11.10. RESULTS FOR PARALLEL AND NEARLY PARALLEL VISCOUS FLOWS

The dominant intuitive expectation is that viscous effects are stabilizing. The stability of thermal and centrifugal convections discussed in Sections 11.4 and 11.6 confirm this expectation. However, the actual situation is more complicated. Consider the Poiseuille-flow and Blasius boundary-layer velocity profiles in Figure 11.21. Neither has an inflection point so both are inviscidly stable. Yet, in experiments, these flows are known to undergo transition to turbulence at some Reynolds number, and this suggests that viscous effects are destabilizing in these flows. Thus, fluid viscosity may be stabilizing as well as destabilizing, a duality confirmed by stability calculations of parallel viscous flows.

Analytical solution of the Orr-Sommerfeld equation is notoriously complicated and will not be presented here. The viscous term in (11.79) contains the highest-order derivative, and therefore the eigenfunction may contain regions of rapid variation in which the viscous effects become important. Sophisticated asymptotic techniques are therefore needed to treat these boundary layers. Alternatively, solutions can be obtained numerically. For our purposes, we shall discuss only certain features of these calculations for the two-stream shear layer, plane Poiseuille flow, plane Couette flow, pipe flow, and boundary layers with pressure gradients. This section concludes with an explanation of how viscosity can act to destabilize a flow. Additional information can be found in Drazin and Reid (1981), and in the review article by Bayly, Orszag, and Herbert (1988).

Two-Stream Shear Layer

Consider a shear layer with the velocity profile $U(y) = U_0\tanh(y/L)$, so that $U(y) \to \pm U_0$ as $y/L \to \pm\infty$. This profile has its peak vorticity at its inflection point and is of the type shown in Figure 11.21f. A stability diagram for solution of the Orr-Sommerfeld equation for this velocity distribution is sketched in Figure 11.23. At all Reynolds numbers the flow is unstable to waves having low wave numbers in the range $0 < k < k_u$, where the upper limit k_u depends on the Reynolds number $\mathrm{Re} = U_0L/\nu$. For high values of Re, the range of unstable wave numbers increases to $0 < k < 1/L$, which corresponds to a wavelength range of $\infty > \lambda > 2\pi L$. It is therefore essentially a long-wavelength instability. In the limit $kL \to 0$, these results simplify to those given in Section 11.3 for a vortex sheet.

Figure 11.23 implies that the critical Reynolds number for the onset of instability in a shear layer is zero. In fact, viscous calculations for all flows with *inflectional profiles* show a small critical Reynolds number; for example, for a jet of the form $u = U\mathrm{sech}^2(y/L)$, it is $\mathrm{Re}_{cr} = 4$. These wall-free shear flows therefore become unstable very quickly, and the inviscid prediction that these flows are always unstable is a fairly good description. The reason the inviscid analysis works well in describing the stability characteristics of free shear flows can be explained as follows. For flows with inflection points the eigenfunction of the inviscid solution is smooth. On this zero-order approximation, the viscous term acts as a *regular*
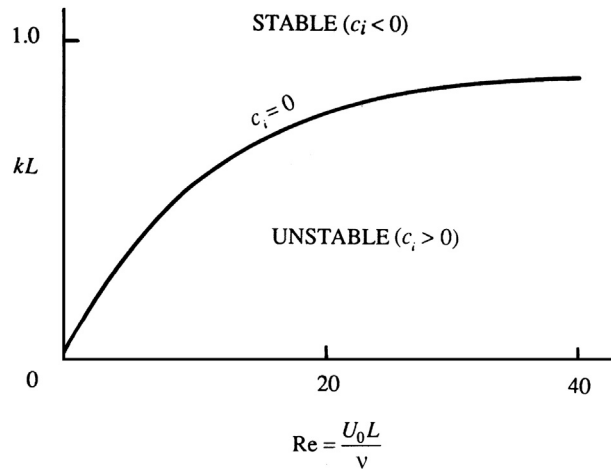
FIGURE 11.23   Marginal stability curve for a shear layer with a velocity profile of $U_0\tanh(y/L)$ in terms of the Reynolds number U_0L/ν and the dimensionless wave number kL of the disturbance. This flow is only unstable to low wave number disturbances.

perturbation, and the resulting correction to the eigenfunction and eigenvalues can be computed as a perturbation expansion in powers of the small parameter $1/\mathrm{Re}$. This is true even though the viscous term in the Orr-Sommerfeld equation contains the highest-order derivative.

The instability in flows with inflection points is observed to form rolled-up regions of vorticity, much like in the calculations of Figure 11.6 or in the photographs in Figures 11.4 and 11.5. This behavior is robust and insensitive to the detailed experimental conditions. They are therefore easily observed. In contrast, the unstable waves in a wall-bounded shear flow are extremely difficult to observe, as discussed in the next section.

Plane Poiseuille Flow

The flow in a channel with parabolic velocity distribution has no point of inflection and is inviscidly stable. However, linear viscous calculations show that the flow becomes unstable at a critical Reynolds number of 5780. Nonlinear calculations, which consider the distortion of the basic profile by the finite amplitude of the perturbations, give a critical Reynolds number of 2510, which agrees better with the observations of transition. In any case, the interesting point is that viscosity is *destabilizing* for this flow. The solution of the Orr-Sommerfeld equation for Poiseuille flow and other parallel flows with rigid boundaries, which do not have an inflection point, is complicated. In contrast to flows with inflection points, the viscosity here acts as a *singular* perturbation, and the eigenfunction has viscous boundary layers on the channel walls and around critical layers where $U = c_r$. The disturbances that cause instability in these flows are called *Tollmien-Schlichting* waves, and their experimental detection is discussed in the next section. In his 1979 text, Yih gives a thorough discussion of the solution of the Orr-Sommerfeld equation using asymptotic expansions in the limit

sequence Re $\rightarrow \infty$, then $k \rightarrow 0$ (but kRe $\gg$ 1). He follows closely the analysis of Heisenberg (1924). Yih presents Lin's (1955) improvements on Heisenberg's analysis with Shen's (1954) calculations of the stability curves.

Plane Couette Flow

This is the flow confined between two parallel plates; it is driven by the motion of one of the plates parallel to itself. The basic velocity profile is linear, with $U \propto y$. Contrary to the experimentally observed fact that the flow does become turbulent at high Reynolds numbers, all linear analyses have shown that the flow is stable to small disturbances. It is now believed that the observed instability is caused by disturbances of finite magnitude.

Pipe Flow

The absence of an inflection point in the velocity profile signifies that the flow is inviscidly stable. All linear stability calculations of the *viscous* problem have also shown that the flow is stable to small disturbances. In contrast, most experiments show that the transition to turbulence takes place at a Reynolds number of about Re $= U_{max}d/v \sim 3000$. However, careful experiments, some of them performed by Reynolds in his classic investigation of the onset of turbulence, have been able to maintain laminar flow up to Re $= 50,000$. Beyond this the observed flow is invariably turbulent. The observed transition has been attributed to one of the following effects: 1) It could be a finite amplitude effect; 2) the turbulence may be initiated at the entrance of the tube by boundary-layer instability (Figure 9.2); and 3) the instability could be caused by a slow rotation of the inlet flow which, when added to the Poiseuille distribution, has been shown to result in instability. This is still under investigation. New insights into the instability and transition of pipe flow were described by Eckhardt et al. (2007) by analysis via dynamical systems theory and comparison with recent very carefully crafted experiments by them and others. They characterized the turbulent state as a *chaotic saddle in state space*. The boundary between laminar and turbulent flow was found to be exquisitely sensitive to initial conditions. Because pipe flow is linearly stable, finite amplitude disturbances are necessary to cause transition, but as Reynolds number increases, the amplitude of the critical disturbance diminishes. The boundary between laminar and turbulent states appears to be characterized by a pair of vortices closer to the walls that give the strongest amplification of the initial disturbance.

Boundary Layers with Pressure Gradients

Recall from Section 9.7 that when pressure decreases in the direction of flow the pressure gradient is said to be *favorable*, and when pressure increases in the direction of flow the pressure gradient is said to be *adverse*. It was shown there that boundary layers with an adverse pressure gradient have a point of inflection in the velocity profile. This has a dramatic effect on stability characteristics. A schematic plot of the marginal stability curve for a boundary layer with favorable and adverse gradients of pressure is shown in Figure 11.24. The ordinate in the plot represents the longitudinal wave number, and the abscissa represents the Reynolds number based on the free-stream velocity and the displacement thickness δ^* of
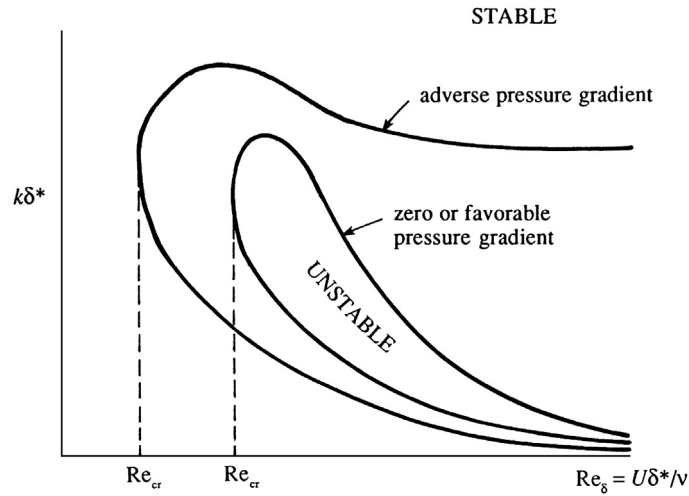
FIGURE 11.24 Sketch of marginal stability curves for laminar boundary layers with favorable and adverse pressure gradients in terms of the displacement-thickness Reynolds number $U_o\delta^*/\nu$ and the dimensionless wave number $k\delta^*$ of the disturbance. The addition of the inflection point in the adverse-pressure gradient case increases the parametric realm of instability.

the boundary layer. The marginal stability curve divides stable and unstable regions, with the region within the loop representing instability. Because the boundary layer thickness grows along the direction of flow, Re_δ increases with x, and points at various downstream distances are represented by larger values of Re_δ.

The following features can be noted in the figure. Boundary-layer flows are stable for low Reynolds numbers, but may become unstable as the Reynolds number increases. The effect of increasing viscosity is therefore stabilizing in this range. For boundary layers with a zero pressure gradient (Blasius flow) or a favorable pressure gradient, the instability loop shrinks to zero as $Re_\delta \rightarrow \infty$. This is consistent with the fact that these flows do not have a point of inflection in the velocity profile and are therefore inviscidly stable. In contrast, for boundary layers with an adverse pressure gradient, the instability loop does not shrink to zero; the upper branch of the marginal stability curve now becomes flat with a limiting value of k_∞ as $Re_\delta \rightarrow \infty$. The flow is then unstable to disturbances with wave numbers in the range $0 < k < k_\infty$. This is consistent with the existence of a point of inflection in the velocity profile, and the results of the shear layer calculations (Figure 11.23). Note also that the critical Reynolds number is lower for flows with adverse pressure gradients.

Table 11.1 summarizes the results of the linear stability analyses of some common parallel viscous flows. The first two flows in the table have points of inflection in the velocity profile and are inviscidly unstable; the viscous solution shows either a zero or a small critical Reynolds number. The remaining flows are stable in the inviscid limit. Of these, the Blasius boundary layer and the plane Poiseuille flow are unstable in the presence of viscosity, but have high critical Reynolds numbers. Although the idealized *tanh* profile for a shear layer, assuming straight and parallel streamlines, is immediately unstable, more recent work by Bhattacharya et al. (2006), which allowed for the basic

**TABLE 11.1**   Linear Stability Results of Common Viscous Parallel Flows

Flow	$U(y)/U_0$	Re_{cr}	Remarks
Jet	$sech^2(y/L)$	4	
Shear layer	$tanh(y/L)$	0	Always unstable
Blasius		520	Re based on δ^*
Plane Poiseuille	$1 - (y/L)^2$	5780	$L =$ half $-$ width
Pipe flow	$1 - (r/R)^2$	∞	Always stable
Plane Couette	y/L	∞	Always stable

flow to be two dimensional, has yielded a finite critical Reynolds number, modifying somewhat Table 11.1.

While the results presented in the preceding paragraphs document flows where viscous effects are destabilizing, the mechanism of this destabilization has not been identified. One means of describing the destabilization mechanism relies on use of the equation for integrated kinetic energy of the disturbance:

$$\frac{d}{dt}\int \frac{1}{2}u_i^2 dV = -\int u_i u_j \frac{\partial U_i}{\partial x_j}dV - \Lambda, \tag{11.88}$$

where V is a stationary volume having stream-wise control surfaces chosen to coincide with the walls where no-slip conditions are satisfied or where $u_i \to 0$, and having a length (in the stream-wise direction) that is an integer number of disturbance wavelengths (see Figure 11.25). In (11.88), $\Lambda = \nu \int (\partial u_i/\partial x_j)^2 dV$ is the total viscous dissipation rate of kinetic energy in V. This disturbance kinetic energy equation can be derived from the incompressible Navier-Stokes momentum equation for the flow (see Exercise 11.13).
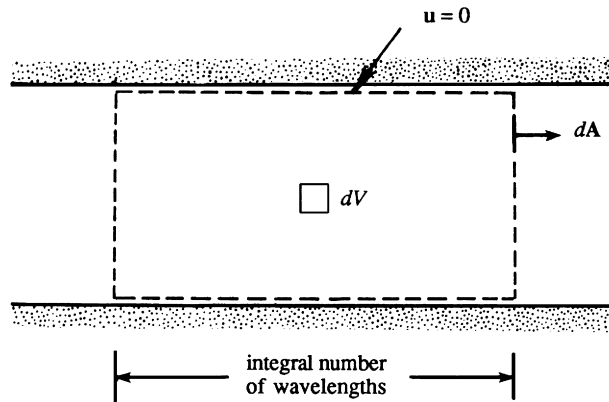
FIGURE 11.25   A control volume for deriving (11.88). Here there is zero net flux across boundaries. This control volume can be extended to boundary-layer flow stability, when the boundary layer forms on the lower wall, by placing the upper control surface far enough from the lower wall so that the disturbance velocity $u_i \to 0$ on this control surface, even if this control surface may not abut the upper wall.

For two-dimensional disturbances in a shear flow defined by $\mathbf{U} = [U(y), 0, 0]$, the disturbance energy equation becomes:

$$\frac{d}{dt}\int \frac{1}{2}(u^2 + v^2)dV = -\int uv\frac{\partial U}{\partial y}dV - \Lambda,$$

and has a simple interpretation. The first term is the rate of change of kinetic energy of the two-dimensional disturbance, and the second term is the rate of production of disturbance energy by the interaction of the product uv (also known as the *Reynolds shear stress*) and the mean shear $\partial U/\partial y$. (The concept of Reynolds stresses is explained in Chapter 12.) The point to note here is that the value of the product uv averaged over a period is zero if the velocity components u and v are out of phase; for example, the mean value of uv is zero if $u = \sin t$ and $v = \cos t$. In inviscid parallel flows without a point of inflection in the velocity profile, the u and v components are such that the disturbance field cannot extract energy from the basic shear flow, thus resulting in stability. The presence of viscosity, however, changes the phase relationship between u and v, which causes the spatial integral of $-uv(\partial U/\partial y)$ to be positive and larger than the viscous dissipation rate. This is how viscous effects can cause instability.

11.11. EXPERIMENTAL VERIFICATION OF BOUNDARY-LAYER INSTABILITY

This section presents the results of stability calculations of the Blasius boundary-layer profile and compares them with experiments. Because of the nearly parallel nature of the Blasius flow, most stability calculations are based on an analysis of the Orr-Sommerfeld equation, which assumes a parallel flow. The first calculations were performed by Tollmien in 1929 and Schlichting in 1933. Instead of assuming exactly the Blasius profile (which can be specified only numerically), they used the profile

$$\frac{U}{U_\infty} = \begin{cases} 1.7(y/\delta) & 0 \le y/\delta \le 0.1724 \\ 1 - 1.03\left[1 - (y/\delta)^2\right] & 0.1724 \le y/\delta \le 1 \\ 1 & y/\delta \ge 1 \end{cases},$$

which, like the Blasius profile, has a zero curvature at the wall. The calculations of Tollmien and Schlichting showed that unstable waves appear when the Reynolds number is high enough; the unstable waves in a viscous boundary layer are called *Tollmien-Schlichting waves*. Until 1947 these waves remained undetected, and the experimentalists of the period believed that the transition in a real boundary layer was probably a finite-amplitude effect. The speculation was that large disturbances cause locally adverse pressure gradients, which resulted in a local separation and consequent transition. The theoretical view, in contrast, was that small disturbances of the right frequency or wavelength can amplify if the Reynolds number is large enough.

Verification of the theory was finally provided by some clever experiments conducted by Schubauer and Skramstad in 1947. The experiments were conducted in a wind tunnel specially designed to suppress fluctuations in the free-stream flow. The experimental technique used was novel. Instead of depending on natural disturbances, they introduced

periodic disturbances of known frequency by means of a vibrating metallic ribbon stretched across the flow close to the wall. The ribbon was vibrated by passing an alternating current through it in the field of a magnet. The subsequent development of the disturbance was measured downstream via hot-wire anemometry. Such techniques later become standard.

The experimental data are shown in Figure 11.26, which also shows the calculations of Schlichting and the more accurate calculations of Shen (1954). Instead of the wave number, the ordinate represents the frequency of the disturbance, which is easier to measure. It is apparent that the agreement between Shen's calculations and the experimental data is very good.

The prediction of the Tollmien-Schlichting waves is regarded as a major accomplishment of linear stability theory. The ideal conditions for their existence are two dimensionality and negligible fluctuations in the free stream. These waves have been found to be very sensitive to small deviations from the ideal conditions, and that is why they can be observed only under very carefully controlled experimental conditions with artificial excitation. People who care about historical fairness have suggested that the waves should only be referred to as TS waves, to honor Tollmien, Schlichting, Schubauer, and Skramstad. TS waves have also been observed in natural flow (Bayly et al., 1988).
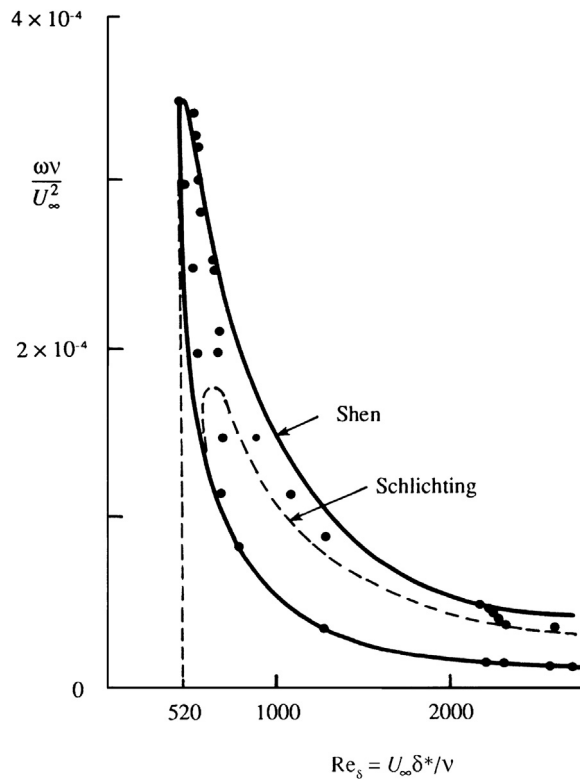

FIGURE 11.26 Marginal stability curve for a Blasius boundary layer. Theoretical solutions of Shen and Schlichting are compared with experimental data of Schubauer and Skramstad.

Nayfeh and Saric (1975) treated Falkner-Skan flows in a study of nonparallel stability and found that generally there is a decrease in the critical Reynolds number. The decrease is least for favorable pressure gradients, about 10% for zero pressure gradients, and grows rapidly as the pressure gradient becomes more adverse. Grabowski (1980) applied linear stability theory to the boundary layer near a stagnation point on a body of revolution. His stability predictions were found to be close to those of parallel-flow stability theory obtained from solutions of the Orr-Sommerfeld equation. Reshotko (2001) provides a review of temporally and spatially transient growth as a path from subcritical (Tollmien-Schlichting) disturbances to transition. Growth or decay is studied from the Orr-Sommerfeld and Squire equations. Growth may occur because eigenfunctions of these equations are not orthogonal as the operators are not self-adjoint. Results for Poiseuille pipe flow and compressible blunt body flows are given.

Fransson and Alfredsson (2003) have shown that the asymptotic suction profile (solved in Exercise 9.26) significantly delays transition stimulated by free-stream turbulence or by Tollmien-Schlichting waves. Specifically, the value of $\text{Re}_{cr} = 520$ based on δ^* in Table 11.1 is increased for suction velocity ratio $v_0/U_\infty = -.00288$ to more than 54,000. The very large stabilizing effect is a result of the change in the shape of the stream-wise velocity profile from the Blasius profile to an exponential.

11.12. COMMENTS ON NONLINEAR EFFECTS

To this point we have discussed only linear stability theory, which considers infinitesimal perturbations and predicts exponential growth when the relevant parameter exceeds a critical value. The effect of the perturbations on the basic field is neglected in the linear theory. An examination of (11.88) shows that the perturbation field must be such that the average uv (the average taken over a wavelength) must be nonzero for the perturbations to extract energy from the basic shear; similarly, the heat flux, the average of uT', must be nonzero in a thermal convection problem. These rectified fluxes of momentum and heat change the *basic* velocity and temperature fields. Linear instability theory neglects these changes of the basic state. A consequence of the constancy of the basic state is that the growth rate of the perturbations is also constant, leading to predictions of exponential growth. However, after some time, the perturbations eventually become so large that the rectified fluxes of momentum and heat significantly change the basic state, which in turn alters the growth of the perturbations.

A frequent effect of nonlinearity is to change the basic state in such a way as to arrest the growth of the disturbances after they have reached significant amplitude via their initial exponential growth. (Note, however, that the effect of nonlinearity can sometimes be destabilizing; for example, the instability in a pipe flow may be a finite-amplitude effect because the flow is stable to infinitesimal disturbances.) Consider the thermal convection in the annular space between two vertical cylinders rotating at the same speed. The outer wall of the annulus is heated and the inner wall is cooled. For small heating rates the flow is steady. For large heating rates a system of regularly spaced waves develop and progress azimuthally at a uniform speed without changing their shape. (This is the equilibrated form of baroclinic instability, discussed in Section 13.17.) At still larger heating rates an irregular, aperiodic, or chaotic flow develops. The chaotic response to constant forcing (in this case the heating rate) is an interesting nonlinear effect and is discussed further in Section 11.14. Meanwhile, a brief description of the transition from laminar to turbulent flow is given in the next section.

11.13. TRANSITION

The process by which a laminar flow changes to a turbulent one is called *transition*. Instability of a laminar flow does not immediately lead to turbulence, which is a severely nonlinear and chaotic flow state. After the initial breakdown of laminar flow because of amplification of small disturbances, the flow goes through a complex sequence of changes, finally resulting in the chaotic state we call turbulence. The process of transition is greatly affected by such experimental conditions as intensity of fluctuations of the free stream, roughness of the walls, and shape of the inlet. The sequence of events that leads to turbulence is also greatly dependent on boundary geometry. For example, the scenario of transition in wall-bounded shear flows is different from that in free shear flows such as jets and wakes.

Early stages of transition consist of a succession of instabilities on increasingly complex basic flows, an idea first suggested by Landau in 1944 (see Landau and Lifshitz, 1959). The basic state of wall-bounded parallel shear flows becomes unstable to two-dimensional TS waves, which grow and eventually reach equilibrium at some finite amplitude. This steady state can be considered a new background state, and calculations show that it is generally unstable to *three-dimensional* waves of short wavelength, which vary in the cross-stream or *span-wise* direction. (If x denotes the stream-wise flow direction and y denotes the wall-normal direction, then the z-axis lies in the *span-wise* direction.) We shall call this the *secondary instability*. Interestingly, the secondary instability does not reach equilibrium at finite amplitude but directly evolves to a fully turbulent flow. Recent calculations of the secondary instability have been quite successful in reproducing critical Reynolds numbers for various wall-bounded flows, as well as predicting three-dimensional structures observed in experiments.

A key experiment on the three-dimensional nature of the transition process in a boundary layer was performed by Klebanoff, Tidstrom, and Sargent (1962). They conducted a series of controlled experiments by which they introduced three-dimensional disturbances on a field of TS waves in a boundary layer. The TS waves were as usual artificially generated by an electromagnetically vibrated ribbon, and the three dimensionality of a particular span-wise wavelength was introduced by placing spacers (small pieces of transparent tape) at equal intervals underneath the vibrating ribbon (Figure 11.27). When the amplitude of the TS waves became roughly 1% of the free-stream velocity, the three-dimensional perturbations grew rapidly and resulted in a span-wise irregularity of the stream-wise velocity displaying peaks and valleys in the amplitude of u. The three-dimensional disturbances continued to grow until the boundary layer became fully turbulent. The chaotic flow seems to result from the nonlinear evolution of the secondary instability, and numerical calculations have accurately reproduced several characteristic features of real flows (see Figures 7 and 8 in Bayly et al., 1988).

It is interesting to compare the chaos observed in turbulent shear flows with that in controlled low-order dynamical systems such as the Bérnard convection or Taylor vortex flow. In these low-order flows only a very small number of modes participate in the dynamics because of the strong constraint of the boundary conditions. All but a few low modes are identically zero, and the chaos develops in an orderly way. As the constraints are relaxed (we can think of this as increasing the number of allowed Fourier modes), the evolution toward apparent chaos becomes less orderly.
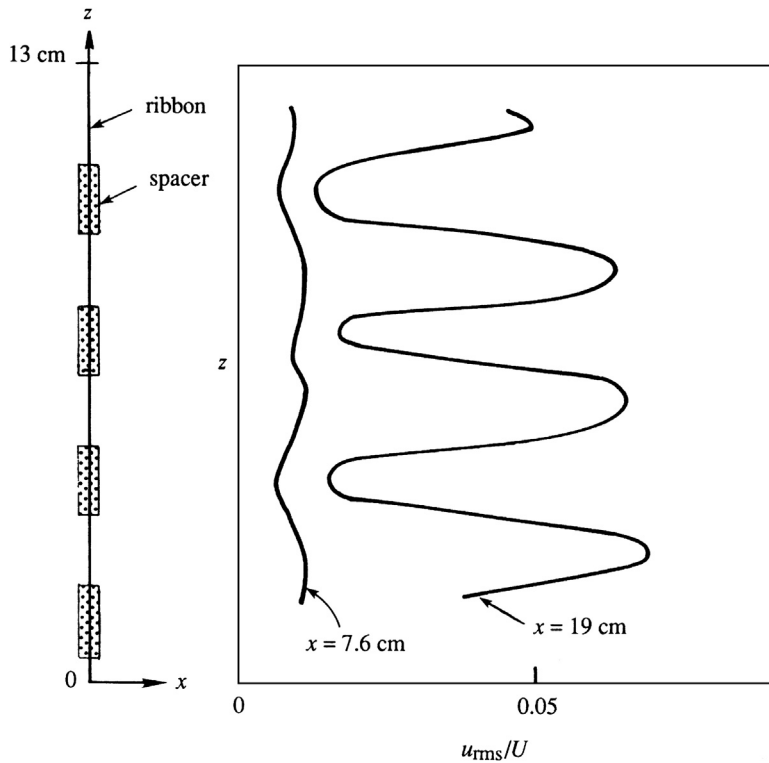
FIGURE 11.27 Three-dimensional unstable waves initiated by a vibrating ribbon. Measured distributions of intensity of the u-fluctuation at two distances from the ribbon are shown. Clearly the span-wise variation enhances the signature of the instability. *P. S. Klebanoff et al.,* Journal of Fluid Mechanics, 12, *1–34, 1962; reprinted with the permission of Cambridge University Press.*

Transition in a free shear layer, such as a jet or a wake, occurs in a different manner. Because of the inflectional velocity profiles involved, these flows are unstable at very low Reynolds numbers, that is, of order 10 compared to about 10^3 for wall-bounded flows. The breakdown of the laminar flow therefore occurs quite readily and close to the origin of such a flow. Transition in a free shear layer is characterized by the appearance of a rolled-up row of vortices, whose wavelength corresponds to the one with the largest growth rate. Frequently, these pairs of vortices regroup themselves and result in a dominant wavelength twice that of the original wavelength. Small-scale turbulence develops in the strain fields between and within these larger scale vortices, finally leading to turbulence.

11.14. DETERMINISTIC CHAOS

The discussion in the previous section has shown that dissipative nonlinear systems such as fluid flows reach a random or chaotic state when the parameter measuring nonlinearity

(say, the Reynolds number or the Rayleigh number) is large. The evolution from laminar flow to the chaotic state generally takes place through a sequence of transitions, with the exact route depending on the flow geometry and other characteristics. It has been realized that chaotic behavior not only occurs in continuous systems having an infinite number of degrees of freedom, but also in discrete nonlinear systems having only a small number of degrees of freedom, governed by ordinary nonlinear differential equations. In this context, a *chaotic system* is defined as one in which the solution is *extremely sensitive to initial conditions*. That is, solutions with arbitrarily close initial conditions evolve into quite different states. Other symptoms of a chaotic system are that the solutions are *aperiodic*, and that the spectrum of fluctuations is broadband instead of being composed of a few discrete frequencies or wave numbers.

Numerical integrations (to be shown later in this section) have recently demonstrated that nonlinear systems governed by a finite set of deterministic ordinary differential equations allow chaotic solutions in response to a steady forcing. This fact is interesting because in a dissipative *linear* system a constant forcing ultimately (after the decay of the transients) leads to a constant response, a periodic forcing leads to a periodic response, and a random forcing leads to a random response. In the presence of nonlinearity, however, a constant forcing can lead to a variable response, both periodic and aperiodic. Consider again the experiment mentioned in Section 11.12, namely, the thermal convection in the annular space between two vertical cylinders rotating at the same speed. The outer wall of the annulus is heated and the inner wall is cooled. For small heating rates the flow is steady. For large heating rates a system of regularly spaced waves develops and progresses azimuthally at a uniform speed, without the waves changing shape. At still larger heating rates an irregular, aperiodic, or chaotic flow develops. This experiment shows that both periodic and aperiodic flow can result in a nonlinear system even when the forcing (in this case the heating rate) is constant. Another example is the periodic oscillation in the flow behind a blunt body at Re ~ 40 (associated with the initial appearance of the von Karman vortex street) and the breakdown of the oscillation into turbulent flow at larger values of the Reynolds number.

It has been found that transition to chaos in the solution of ordinary nonlinear differential equations displays a certain *universal* behavior and proceeds in one of a few different ways. Transition to turbulence in fluid flows may be related to the development of chaos in the solutions of these simple systems. In this section we shall discuss some of the elementary ideas involved, starting with the definitions for phase space and attractors, moving on to the Lorenz model of thermal convection and scenarios for transition to chaos, and then concluding with a description of the implications of such phenomena. An introduction to the subject of chaos is given by Bergé, Pomeau, and Vidal (1984); a useful review is given in Lanford (1982). The subject has far-reaching cosmic consequences in physics and evolutionary biology, as discussed by Davies (1988).

Very few nonlinear equations have analytical solutions. For nonlinear systems, a typical procedure is to find a numerical solution and display its properties in a space whose axes are the *dependent* variables. Consider the equation governing the motion of a simple pendulum of length l:

$$\ddot{X} + (g/l)\sin X = 0,$$

where X is the *angular* displacement and $\ddot{X}$ is the angular acceleration. The equation is nonlinear because of the $\sin X$ term. The second-order equation can be split into two coupled first-order equations:

$$\dot{X} = Y \quad \text{and} \quad \dot{Y} = -(g/l)\sin X. \tag{11.89}$$

Starting with some initial conditions on X and Y, one can integrate (11.89) forward in time. The behavior of the system can be studied by describing how the variables $Y\,(=\dot{X})$ and X vary as functions of time. For the pendulum problem, the space whose axes are $\dot{X}$ and X is called a *phase space,* and the evolution of the system is described by a *trajectory* in this space. The dimension of the phase space is called the *degree of freedom* of the system; it equals the number of independent initial conditions necessary to specify the system. For example, the degree of freedom for the set (11.89) is two.

Dissipative systems are characterized by the existence of *attractors,* which are structures in the phase space toward which neighboring trajectories approach as $t \to \infty$. An attractor can be a *fixed point* representing a stable steady flow or a closed curve (called a *limit cycle*) representing a stable oscillation (Figure 11.28a, b). The nature of the attractor depends on the value of the nonlinearity parameter, which will be denoted by R in this section. As R is increased, the fixed point representing a steady solution may change from being an attractor to a repeller with spirally outgoing trajectories, signifying that the steady flow has become unstable to infinitesimal perturbations. Frequently, the trajectories are then attracted by a limit cycle, which means that the unstable steady solution gives way to a steady oscillation (Figure 11.28b). For example, the steady flow behind a blunt body becomes oscillatory as Re is increased, resulting in the periodic von Karman vortex street (Figure 9.17).

The branching of a solution at a critical value R_{cr} of the nonlinearity parameter is called a *bifurcation*. Thus, we say that the stable steady solution of Figure 11.28a bifurcates to a stable limit cycle as R increases through R_{cr}. This can be represented on the graph of a dependent variable (say, X) versus R (Figure 11.28c). At $R = R_{cr}$, the solution curve branches into two paths; the two values of X on these branches (say, X_1 and X_2) correspond to the maximum and minimum values of X in Figure 11.28b. It is seen that the size of the limit cycle grows larger as $(R - R_{cr})$ becomes larger. Limit cycles, representing oscillatory response with amplitude independent of initial conditions, are characteristic features of nonlinear systems. Linear stability theory predicts an exponential growth of the perturbations if $R > R_{cr}$, but a nonlinear theory frequently shows that the perturbations eventually equilibrate to a steady oscillation whose amplitude increases with $(R - R_{cr})$.

A famous fluid-flow example involving these concepts comes from thermal convection in a layer heated from below (the Bénard problem). Lorenz (1963) demonstrated that the development of chaos is associated with the flow's attractor acquiring certain strange properties. He considered a layer with stress-free boundaries. Assuming nonlinear disturbances in the form of rolls invariant in the y direction, and defining a disturbance stream function in the x-z plane by $u = -\partial\psi/\partial z$ and $w = \partial\psi/\partial x$, he substituted solutions of the form

$$\psi \propto X(t)\cos(\pi z)\sin(kx) \quad \text{and} \quad T' \propto Y(t)\cos(\pi z)\cos(kx) + Z(t)\sin(2\pi z) \tag{11.90}$$

into the equations of motion. Here, T' is the departure of temperature from the state of no convection, k is the wave number of the perturbation, and the boundaries are at $z = \pm\frac{1}{2}$. It is clear that X is proportional to the speed of convective motion, Y is proportional to
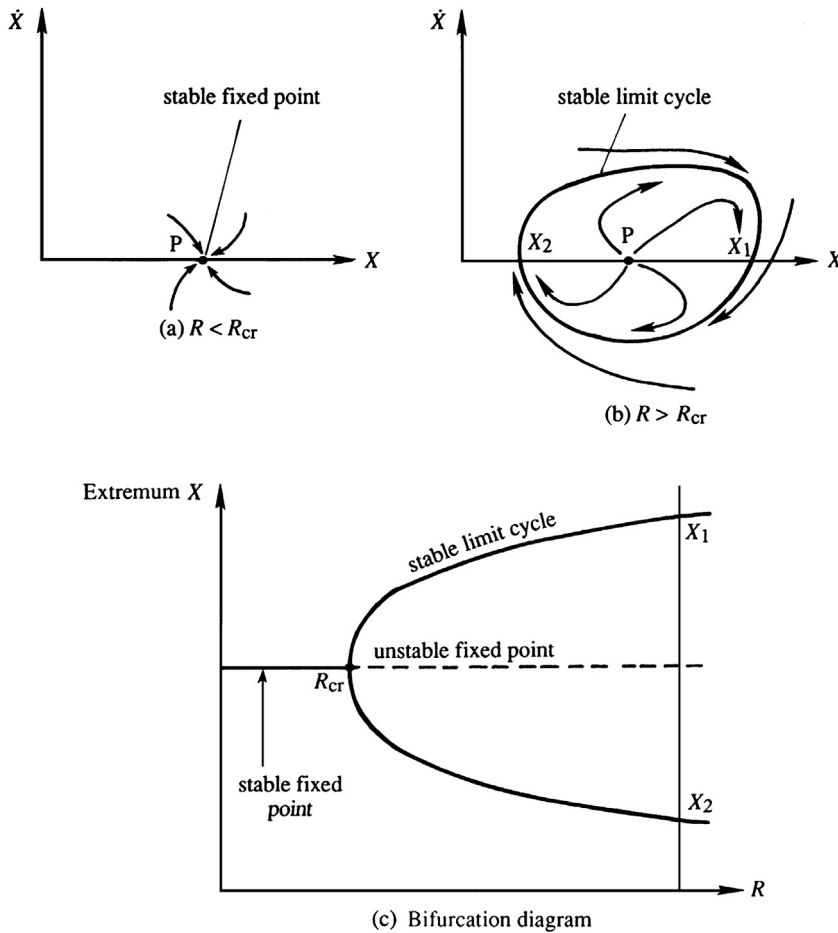
FIGURE 11.28 Attractors in a phase plane of X and $\dot{X}$. In (a), point P is an attractor. For a larger value of R, the nonlinearity parameter, panel (b) shows that P becomes an unstable fixed point (a *repeller*), and the trajectories are attracted to an orbit or limit cycle that encircles P. Panel (c) is the bifurcation diagram corresponding to this situation.

the temperature difference between the ascending and descending currents, and Z is proportional to the distortion of the average vertical profile of temperature from linearity. (Note in (11.90) that the x-average of the term multiplied by $Y(t)$ is zero, so that this term does not cause distortion of the basic temperature profile.) As discussed in Section 11.4, Rayleigh's linear analysis showed that solutions of the form (11.90), with X and Y constants and $Z = 0$, would develop if Ra slightly exceeds the critical value $\text{Ra}_{cr} = 27\pi^4/4$. Equations (11.90) are expected to give realistic results when Ra is slightly supercritical but not when strong convection occurs because only the lowest wave number terms are retained.

On substitution of (11.90) into the equations of motion, Lorenz finally obtained the system:

$$\dot{X} = \text{Pr}(Y - X), \ \dot{Y} = -XZ + rX - Y, \text{ and } \dot{Z} = XY - bZ, \tag{11.91}$$

where Pr is the Prandtl number, $r = \text{Ra}/\text{Ra}_{cr}$, and $b = 4\pi^2/(\pi^2 + k^2)$. Equations (11.91) are a set of nonlinear equations with three degrees of freedom, which means that the phase space is three dimensional.

Equations (11.91) allow the steady solution $X = Y = Z = 0$, representing the state of no convection. For $r > 1$ the system possesses two additional steady-state solutions, which we shall denote by $\overline{X} = \overline{Y} = \pm\sqrt{b(r - 1)}$, $\overline{Z} = r - 1$; the two signs correspond to the two possible senses of rotation of the rolls. (The fact that these steady solutions satisfy (11.91) can easily be checked by substitution and setting $\dot{X} = \dot{Y} = \dot{Z} = 0$.) Lorenz showed that the steady-state convection becomes unstable if r is large. Choosing $\text{Pr} = 10$, $b = 8/3$, and $r = 28$, he numerically integrated the set and found that the solution never repeats itself; it is aperiodic and wanders about in a chaotic manner. Figure 11.29 shows the variation of $X(t)$, starting with some initial conditions. (The variables $Y(t)$ and $Z(t)$ also behave in a similar way.) It is seen that the amplitude of the convecting motion initially oscillates around one of the steady values $\overline{X} = \pm\sqrt{b(r - 1)}$, with the oscillations growing in magnitude. When it is large enough, the amplitude suddenly goes through zero to start oscillations of opposite sign about the other value of $\overline{X}$. That is, the motion switches in a chaotic manner between two oscillatory limit cycles, with the number of oscillations between transitions seemingly random. Calculations show that the variables X, Y, and Z have continuous spectra and that the solution is extremely sensitive to initial conditions.

The trajectories in the phase space of the Lorenz model of thermal convection are shown in Figure 11.30. The centers of the two loops represent the two steady convections
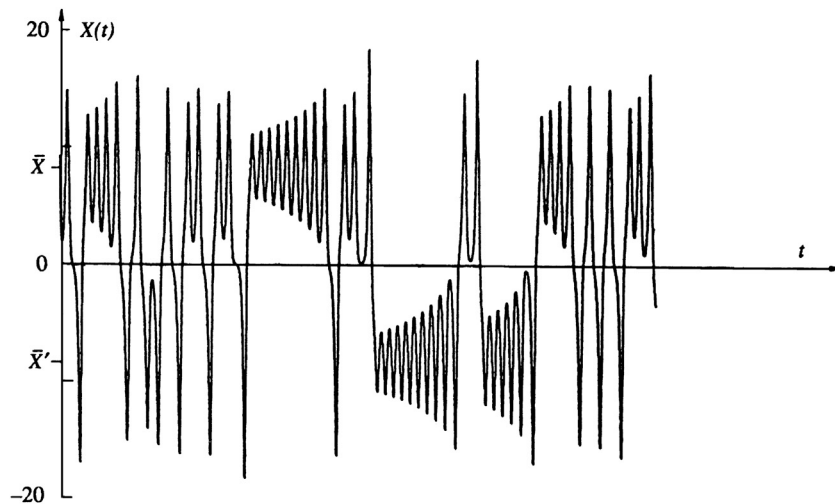
FIGURE 11.29 Variation of $X(t)$ in the Lorenz model. Note that the solution oscillates erratically around the two steady values $\overline{X}$ and $\overline{X}'$ and does not have a reliable period. *P. Bergé, Y. Pomeau, and C. Vidal,* Order Within Chaos, *1984; reprinting permitted by Heinemann Educational, a division of Reed Educational & Professional Publishing Ltd.*
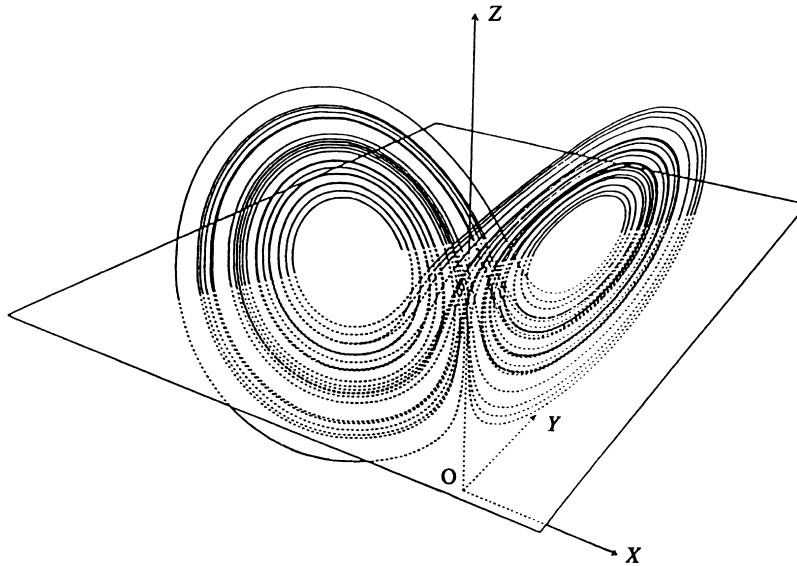
FIGURE 11.30   The Lorenz attractor. All nearby initial conditions are attracted to this double loop structure, but any two such trajectories will eventually diverge, even if they begin very close together. The centers of the two loops represent the two steady solutions $(\overline{X}, \overline{Y}, \overline{Z})$.

$\overline{X} = \overline{Y} = \pm\sqrt{b(r-1)}$ and $\overline{Z} = r - 1$. The structure resembles two rather flat loops of ribbon, one lying slightly in front of the other along a central band, with the two joined together at the bottom of that band. The trajectories go clockwise around the left loop and counterclockwise around the right loop; two trajectories never intersect. The structure shown in Figure 11.30 is an attractor because orbits starting with initial conditions *outside of the attractor* merge onto it and then follow it. The attraction is a result of dissipation in the system. The aperiodic attractor, however, is unlike the normal attractor in the form of a fixed point (representing steady motion) or a closed curve (representing a limit cycle). This is because two trajectories *on the aperiodic attractor*, with infinitesimally different initial conditions, follow each other closely only for a while, eventually diverging to very different final states. This is the basic reason for sensitivity to initial conditions.

For these reasons the aperiodic attractor is called a *strange attractor*. The idea of a strange attractor is not intuitive because it has the dual property of attraction and divergence. Trajectories starting from the neighboring regions in phase space are drawn toward it, but once on the attractor the trajectories eventually diverge and result in chaos. An ordinary attractor in phase space allows the trajectories from slightly different initial conditions to merge, so that the *memory* of initial conditions is lost. However, the strange attractor ultimately accentuates small initial condition differences. The idea of the strange attractor was first conceived by Lorenz, and since then attractors of other chaotic systems have also been studied. They all have the common property of aperiodicity, continuous spectra, and sensitivity to initial conditions.

Thus far we have described a discrete dynamical system having only a small number of degrees of freedom and seen that aperiodic or chaotic solutions result when the nonlinearity

parameter is large. Several routes or scenarios of transition to chaos in such systems have been identified. Two of these are described briefly here.

(1) *Transition through subharmonic cascade*: As R is increased, a typical nonlinear system develops a limit cycle of a certain frequency ω. With further increase of R, several systems are found to generate additional frequencies $\omega/2$, $\omega/4$, $\omega/8$, ... The addition of frequencies in the form of *subharmonics* does not change the periodic nature of the solution, but the period doubles each time a lower harmonic is added. The period doubling takes place more and more rapidly as R is increased, until an *accumulation point* (Figure 11.31) is reached, beyond which the solution wanders about in a chaotic manner. At this point the peaks disappear from the temporal-frequency spectrum, which becomes broadband. Many systems approach chaotic behavior through period doubling. Feigenbaum (1978) proved the important result that this kind of transition develops in a *universal* way, independent of the particular nonlinear systems studied. If R_n represents the value for development of a new subharmonic, then R_n converges in a geometric series with

$$\frac{R_n - R_{n-1}}{R_{n+1} - R_n} \to 4.6692 \quad \text{as } n \to \infty$$

That is, the horizontal gap between two bifurcation points is about a fifth of the previous gap. The vertical gap between the branches of the bifurcation diagram also decreases, with each gap about two-fifths of the previous gap. In other words, the bifurcation
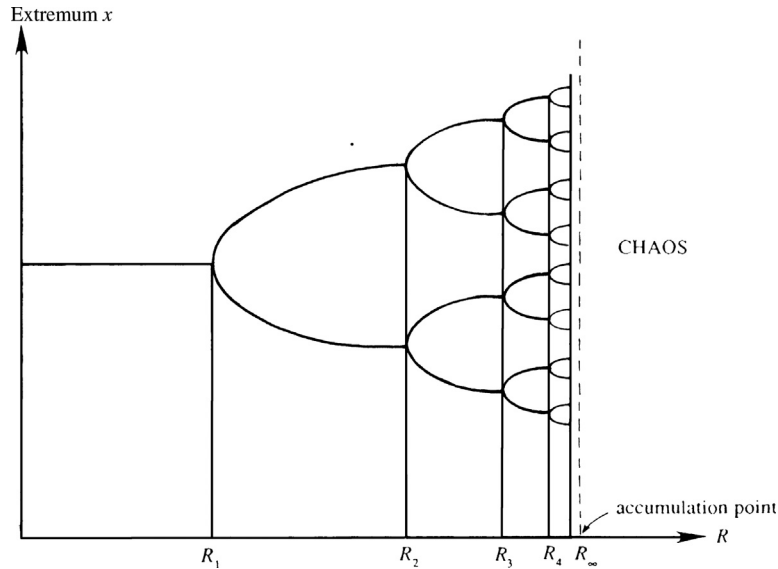

FIGURE 11.31   Bifurcation diagram during period doubling. The period doubles at each value R_n of the nonlinearity parameter. For large n the "bifurcation tree" becomes self-similar. Chaos sets in beyond the accumulation point R_∞. This process may mimic the transition from laminar to turbulent flow under some circumstances.

diagram (Figure 11.31) becomes "self-similar" as the accumulation point is approached. (Note that Figure 11.31 has not been drawn to scale, for illustrative purposes.) Experiments in low Prandtl number fluids (such as liquid metals) indicate that Bénard convection in the form of rolls develops oscillatory motion of a certain frequency ω at $Ra = 2Ra_{cr}$. As Ra is further increased, additional frequencies $\omega/2$, $\omega/4$, $\omega/8$, $\omega/16$, and $\omega/32$ have been observed. The convergence ratio has been measured to be 4.4, close to the value of 4.669 predicted by Feigenbaum's theory. The experimental evidence is discussed further in Bergé, Pomeau, and Vidal (1984).

(2) *Transition through quasi-periodic regime*: Ruelle and Takens (1971) have mathematically proven that certain systems need only a *small number* of bifurcations to produce chaotic solutions. As the nonlinearity parameter is increased, the steady solution loses stability and bifurcates to an oscillatory limit cycle with frequency ω_1. As R is increased, two more frequencies (ω_2 and ω_3) appear through additional bifurcations. In this scenario the ratios of the three frequencies (such as ω_1/ω_2) are *irrational* numbers, so that the motion consisting of the three frequencies is not exactly periodic. (When the ratios are rational numbers, the motion is exactly periodic. To see this, think of the Fourier series of a periodic function in which the various terms represent sinusoids of the fundamental frequency ω and its harmonics 2ω, 3ω, … . Some of the Fourier coefficients could be zero.) The spectrum for these systems suddenly develops broadband characteristics of chaotic motion as soon as the third frequency ω_3 appears. The exact point at which chaos sets in is not easy to detect in a measurement; in fact the third frequency may not be identifiable in the spectrum before it becomes broadband. The Ruelle-Takens theory is fundamentally different from that of Landau, who conjectured that turbulence develops due to an *infinite* number of bifurcations, each generating a new higher frequency, so that the spectrum becomes saturated with peaks and resembles a continuous one. According to Bergé, Pomeau, and Vidal (1984), the Bénard convection experiments in *water* seem to suggest that turbulence in this case probably sets in according to the Ruelle-Takens scenario.

The development of chaos in the Lorenz attractor is more complicated and does not follow either of the two routes mentioned in the preceding discussion.

Closure

Perhaps the most intriguing characteristic of a chaotic system is the extreme *sensitivity to initial conditions*. That is, solutions with arbitrarily close initial conditions evolve into two quite different states. Most nonlinear systems are susceptible to chaotic behavior. The extreme sensitivity to initial conditions implies that nonlinear phenomena (including the weather, in which Lorenz was primarily interested when he studied the convection problem) are essentially unpredictable, no matter how well we know the governing equations or the initial conditions. Although the subject of chaos has become a scientific revolution recently, the central idea was conceived by Henri Poincaré in 1908. He did not, of course, have the computing facilities to demonstrate it through numerical integration.

It is important to realize that the behavior of chaotic systems is not *intrinsically* nondeterministic; as such the implication of deterministic chaos is different from that of the uncertainty principle of quantum mechanics. In any case, the extreme sensitivity to initial

conditions implies that the *future is essentially unknowable* because it is never possible to know the initial conditions *exactly.* As discussed by Davies (1988), this fact has interesting philosophical implications regarding the evolution of the universe, including that of living species.

  We have examined certain elementary ideas about how chaotic behavior may result in simple nonlinear systems having only a small number of degrees of freedom. Turbulence in a continuous fluid medium is capable of displaying an infinite number of degrees of freedom, and it is unclear whether the study of chaos can throw a great deal of light on more complicated transitions such as those in pipe or boundary-layer flow. However, the fact that nonlinear systems can have chaotic solutions for a large value of the nonlinearity parameter (see Figure 11.29) is an important result by itself.

EXERCISES

11.1. A perturbed vortex sheet nominally located at $y = 0$ separates inviscid flows of differing density in the presence of gravity with downward acceleration g. The upper stream is semi-infinite and has density ρ_1 and horizontal velocity U_1. The lower stream has thickness h density ρ_2, and horizontal velocity U_2. A smooth flat impenetrable surface located at $y = -h$ lies below the second layer. The interfacial tension between the two fluids is σ. Assume a disturbance occurs on the vortex sheet with wave number $k = 2\pi/\lambda$, and complex wave speed c, i.e., $[y]_{sheet} = f(x,t) = f_o \operatorname{Re}\{e^{ik(x-ct)}\}$. The four boundary conditions are:

1) $u_1, v_1 \to 0$ as $y \to +\infty$.
2) $v_2 = 0$ on $y = -h$.
3) $\mathbf{u_1} \cdot \mathbf{n} = \mathbf{u_2} \cdot \mathbf{n} = $ normal velocity of the vortex sheet on both sides of the vortex sheet.
4) $p_1 - p_2 = \sigma\dfrac{\partial^2 f}{\partial x^2}$ on the vortex sheet ($\sigma = $ interfacial surface tension).

   a) Following the development in Section 11.3, show that:

$$c = \frac{\rho_1 U_1 + \rho_2 U_2 \coth(kh)}{\rho_1 + \rho_2 \coth(kh)} \pm \left[\frac{(g/k)(\rho_2 - \rho_1) + \sigma k}{\rho_1 + \rho_2 \coth(kh)} - \frac{\rho_1 \rho_2 (U_1 - U_2)^2 \coth(kh)}{(\rho_1 + \rho_2 \coth(kh))^2}\right]^{1/2}.$$

   b) Use the result of part a) to show that the vortex sheet is *unstable* when:

$$\left(\tanh(kh) + \frac{\rho_2}{\rho_1}\right)\left(\frac{g}{k}\frac{(\rho_2 - \rho_1)}{\rho_2} + \frac{\sigma k}{\rho_2}\right) < (U_1 - U_2)^2.$$

   c) Will the sheet be stable or unstable to long wavelength disturbances ($k \to 0$) when $\rho_2 > \rho_1$ for a fixed velocity difference?
   d) Will the sheet be stable or unstable to short wavelength disturbances ($k \to \infty$) for a fixed velocity difference?
   e) Will the sheet ever be unstable when $U_1 = U_2$?
   f) Under what conditions will the thickness h matter?

11.2. Consider a fluid layer of depth h and density ρ_2 lying under a lighter, infinitely deep fluid of density $\rho_1 < \rho_2$. By setting $U_1 = U_2 = 0$, in the results of Exercise 11.1, the following formula for the phase speed is found:

$$c = \pm \left[\frac{(g/k)(\rho_2 - \rho_1) + \sigma k}{\rho_1 + \rho_2 \coth(kh)} \right]^{1/2}.$$

Now invert the sign of gravity and consider why drops form when a liquid is splashed on the underside of a flat surface. Are long or short waves more unstable? Does a professional painter want interior ceiling paint with high or low surface tension? For a smooth finish should the painter apply thin or thick coats of paint? Assuming the liquid has the properties of water (surface tension ≈ 0.072 N/m, density $\approx 10^3$ kg/m) and that the lighter fluid is air, what is the longest neutrally stable wavelength on the underside of a horizontal surface? [This is the *Rayleigh-Taylor instability* and it occurs when density and pressure gradients point in opposite directions. It may be readily observed by accelerating rapidly downward an upward-open cup of water.]

11.3. Inviscid horizontal flow in the half space $y > 0$ moves at speed U over a porous surface located at $y = 0$. Here the fluid density ρ is constant and gravity plays no roll. A weak vertical velocity fluctuation occurs at the porous surface:
$[v]_{surface} = v_o \operatorname{Re}\{e^{ik(x-ct)}\}$, where $v_o \ll U$.
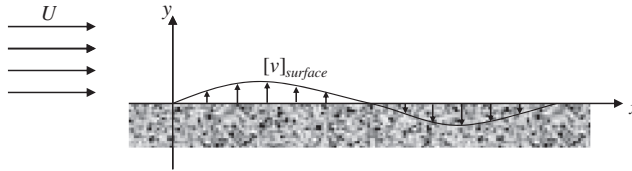
a) The velocity potential for the flow may be written $\tilde{\phi} = Ux + \phi$, where ϕ leads to $[v]_{surface}$ at $y = 0$ and ϕ vanishes as $y \to +\infty$. Determine the perturbation potential ϕ in terms of v_o, U, ρ, k, c, and the independent variables (x,y,t).

b) The porous surface responds to pressure fluctuations in the fluid via:
$[p - p_s]_{y=0} = -\gamma[v]_{surface}$, where p is the pressure in the fluid, p_s is the steady static pressure that is felt on the surface when the vertical velocity fluctuations are absent, and γ is a real material parameter that defines the porous surface's flow resistance. Determine a formula for c in terms of U, γ, ρ, and k.

c) What is the propagation velocity, $\operatorname{Re}\{c\}$, of the surface velocity fluctuation?

d) What sign should γ have for the flow to be stable? Interpret your answer.

11.4. Repeat Exercise 11.3 for a compliant surface nominally lying at $y = 0$ that is perturbed from equilibrium by a small surface wave: $[y]_{surface} = \zeta(x,t) = \zeta_o \operatorname{Re}\{e^{ik(x-ct)}\}$.

a) Determine the perturbation potential ϕ in terms of U, ρ, k, and c by assuming that ϕ vanishes as $y \rightarrow +\infty$, and that there is no flow through the compliant surface. Ignore gravity.

b) The compliant surface responds to pressure fluctuations in the fluid via: $[p - p_s]_{y=0} = -\gamma\zeta(x,t)$, where p is the pressure in the fluid, p_s is the steady pressure that is felt on the surface when the surface wave is absent, and γ is a real material parameter that defines the surface's compliance. Determine a formula for c in terms of U, γ, ρ, and k.

c) What is the propagation velocity, Re$\{c\}$, of the surface waves?

d) If γ is positive, is the flow stable? Interpret your answer.

11.5. As a simplified version of flag waving, consider the stability of a simple membrane in a uniform flow. Here, the undisturbed membrane lies in the x-z plane at $y = 0$, the flow is parallel to the x-axis at speed U, and the fluid has density ρ. The membrane has mass per unit area $= \rho_m$ and uniform tension per unit length $= T$. The membrane satisfies a dynamic equation based on pressure forces and internal tension combined with its local surface curvature:

$$\rho_m \frac{\partial^2 \zeta}{\partial t^2} = p_2 - p_1 + T\left(\frac{\partial^2 \zeta}{\partial x^2} + \frac{\partial^2 \zeta}{\partial z^2}\right).$$

Here, the vertical membrane displacement is given by $y = \zeta(x,z,t)$, and p_1 and p_2 are the pressures acting on the membrane from above and below, respectively. The velocity potentials for the undisturbed flow above (1) and below (2) the membrane are $\phi_1 = \phi_2 = Ux$. For the following items, assume a small amplitude wave is present on the membrane $\zeta(x,t) = \zeta_o \text{Re}\{e^{ik(x-ct)}\}$ with k a real parameter, and assume that all deflections and other fluctuations are uniform in the z-direction and small enough for the usual linear simplifications. In addition, assume the static pressures above and below the membrane, in the absence of membrane motion, are matched.
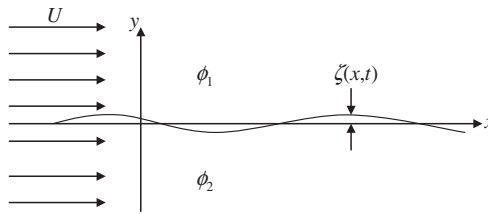
a) Using the membrane equation, determine the propagation speed of the membrane waves, Re$\{c\}$, in the absence of fluid loading (i.e., when $p_2 - p_1 = \rho = 0$).

b) Assuming inviscid flow above and below the membrane, determine a formula for c in terms of T, ρ_m, ρ, U, and k.

c) Is the membrane more or less unstable if U, T, ρ, and ρ_m are individually increased with the others held constant?

d) What is the propagation speed of the membrane waves when $U = 0$? Compare this to your answer for part a) and explain any differences.

11.6. Prove that $\sigma_r > 0$ for the thermal instability discussed in Section 11.4 via the following steps that include integration by parts and use of the boundary conditions (11.38).

  a) Multiply (11.36) by $\widehat{T}^*$ and integrate the result from $z = -1/2$ to $z = +1/2$, where z is the dimensionless vertical coordinate, to find: $\sigma I_1 + I_2 = \int \widehat{T}^* W dz$, where $I_1 \equiv \int |\widehat{T}|^2 dz$, $I_2 \equiv \int [|d\widehat{T}/dz|^2 + K^2 |\widehat{T}|^2] dz$, and the limits of the integrations have been suppressed for clarity.

  b) Multiply (11.37) by W^* and integrate from $z = -½$ to $z = +½$ to find:

  $$\frac{\sigma}{\text{Pr}} J_1 + J_2 = \text{Ra} K^2 \int W^* \widehat{T} dz \text{ where } J_1 \equiv \int [|dW/dz|^2 + K^2 |W|^2] dz,$$

  $J_2 \equiv \int [|d^2 W/dz^2|^2 + 2K^2 |dW/dz|^2 + K^4 |W|^2] dz$, and again the limits of the integrations have been suppressed.

  c) Combine the results of parts a) and b) to eliminate the mixed integral of W and $\widehat{T}$, and use the result of this combination to show that $\sigma_i = 0$ for Ra > 0. [*Note*: The integrals I_1, I_2, J_1, and J_2 are all positive definite.]

11.7. Consider the thermal instability of a fluid confined between two rigid plates, as discussed in Section 11.4. It was stated there without proof that the minimum critical Rayleigh number of $\text{Ra}_{\text{cr}} = 1708$ is obtained for the gravest *even* mode. To verify this, consider the gravest *odd* mode for which

$$W = A \sin q_0 z + B \sinh q z + C \sinh q^* z.$$

(Compare this with the gravest even mode structure: $W = A \cos q_0 z + B \cosh q z + C \cosh q^* z$.) Following Chandrasekhar (1961, p. 39), show that the minimum Rayleigh number is now 17,610, reached at the wave number $K_{\text{cr}} = 5.365$.

11.8. Consider the centrifugal instability problem of Section 11.6. Making the narrow-gap approximation, work out the algebra of going from (11.50) to (11.51).

11.9. Consider the centrifugal instability problem of Section 11.6. From (11.51) and (11.53), the eigenvalue problem for determining the marginal state ($\sigma = 0$) is

$$(d^2/dR^2 - k^2)^2 \widehat{u}_R = (1 + \alpha x) \widehat{u}_\varphi, \left(d^2/dR^2 - k^2 \right)^2 \widehat{u}_\varphi = -\text{Ta} k^2 \widehat{u}_R, \qquad (11.92, 11.93)$$

with $\widehat{u}_R = d\widehat{u}_R/dR = \widehat{u}_\varphi = 0$ at $x = 0$ and 1. Conditions on $\widehat{u}_\varphi$ are satisfied by assuming solutions of the form

$$\widehat{u}_\varphi = \sum_{m=1}^{\infty} C_m \sin(m\pi x). \qquad (11.94)$$

Inserting this into (11.92), obtain an equation for $\widehat{u}_R$, and arrange so that the solution satisfies the four remaining conditions on $\widehat{u}_R$. With $\widehat{u}_R$ determined in this manner and $\widehat{u}_\varphi$ given by (11.94), (11.93) leads to an eigenvalue problem for Ta(k). Following Chandrasekhar (1961, p. 300), show that the minimum Taylor number is given by (11.54) and is reached at $k_{\text{cr}} = 3.12$.

11.10. For a Kelvin-Helmholtz instability in a continuously stratified ocean, obtain a globally integrated energy equation in the form

$$\frac{1}{2}\frac{d}{dt}\int (u^2 + w^2 + g^2\rho^2/\rho_0^2N^2)dV = -\int uw\frac{\partial U}{\partial z}dV.$$

(As in Figure 11.25, the integration in x takes place over an integer number of wavelengths.) Discuss the physical meaning of each term and the mechanism of instability.

11.11. [1]Consider the inviscid stability of a constant vorticity layer of thickness h between uniform streams with flow speeds U_1 and U_3. Region 1 lies above the layer, $y > h/2$ with $U(y) = U_1$. Region 2 lies within the layer, $|y| \le h/2$, $U(y) = 1/2(U_1 + U_3) + (U_1 - U_3)(y/h)$. Region 3 lies below the layer, $y < -h/2$ with $U(y) = U_3$.
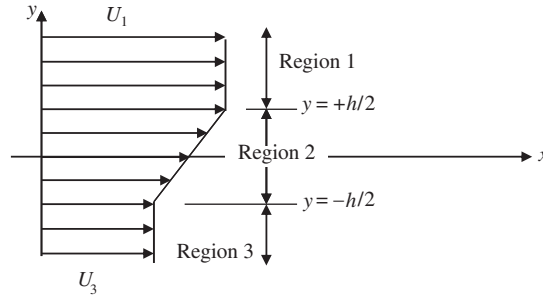
a) Solve the Rayleigh equation, $f'' - k^2f - \dfrac{fU''}{U - c} = 0$, in each region, then use appropriate boundary and matching conditions to obtain:

$$\begin{aligned}
f_1(y) &= (A\cosh(kh/2) + B\sinh(kh/2))e^{-k(y-h/2)} \quad \text{for } y > +h/2, \\
f_2(y) &= A\cosh(ky) + B\sinh(ky) \quad \text{for } |y| \le h/2, \\
f_3(y) &= (A\cosh(kh/2) - B\sinh(kh/2))e^{+k(y+h/2)} \quad \text{for } y < -h/2.
\end{aligned}$$

where f defines the spatial extent of the disturbance: $v' = f(y)e^{ik(x-ct)}$ and $u' = -(f'/ik)e^{ik(x-ct)}$, and A and B are undetermined constants.

b) The linearized horizontal momentum equation is: $\dfrac{\partial u'}{\partial t} + U\dfrac{\partial u'}{\partial x} + v'\dfrac{\partial U}{\partial y} = -\dfrac{1}{\rho}\dfrac{\partial p'}{\partial x}$.

Integrate this equation with respect to x, require the pressure to be continuous at $y = \pm h/2$, and simplify your results to find two additional constraint equations:

$$(c - U_1)f_1'(+h/2) = (c - U_1)f_2'(+h/2) + \frac{U_1 - U_3}{h}f_2(+h/2), \text{ and}$$

$$(c - U_3)f_3'(-h/2) = (c - U_3)f_2'(-h/2) + \frac{U_1 - U_3}{h}f_2(-h/2).$$

---

[1]Developed from Sherman, F. S. (1990).*Viscous Fluid Flow.* New York: McGraw-Hill, pp. 466−467.

c) Define $c_o = c - (1/2)(U_1 + U_3)$ (this is the phase speed of the disturbance waves in a frame of reference moving at the average speed), and use the results of parts a) and b) to determine a single equation for c_o:

$$c_o^2 = \left(\frac{U_1 - U_3}{2kh}\right)^2 \left\{(kh - 1)^2 - e^{-2kh}\right\}.$$

[This part of this problem requires patience and algebraic skill.]

d) From the result of part c), c_o will be real for $kh \gg 1$ (short wave disturbances), so the flow is stable or neutrally stable. However, for $kh \ll 1$ (long wave disturbances), use the result of part c) to show that:

$$c_o \cong \pm i\left(\frac{U_1 - U_3}{2}\right)\sqrt{1 - \frac{4}{3}kh + \ldots}$$

e) Determine the largest value of kh at which the flow is unstable.

11.12. Consider the inviscid instability of parallel flows given by the Rayleigh equation:

$$(U - c)\left(\frac{d^2\widehat{v}}{dy^2} - k^2\widehat{v}\right) - \frac{d^2U}{dy^2}\widehat{v} = 0, \tag{11.95}$$

where the y-component of the perturbation velocity is $v = \widehat{v}(y)\exp\{ik(x - ct)\}$.

a) Note that this equation is identical to the Rayleigh equation (11.81) for the stream function amplitude ϕ, as it must be because $\widehat{v}(y) = -ik\phi$. For a flow bounded by walls at y_1 and y_2, note that the boundary conditions are identical in terms of ϕ and $\widehat{v}$.

b) Show that if c is an eigenvalue of (11.95), then so is its conjugate $c^* = c_r - ic_i$. What aspect of (11.95) allows this result to be valid?

c) Let $U(y)$ be *antisymmetric*, so that $U(y) = -U(-y)$. Demonstrate that if $c(k)$ is an eigenvalue, then $-c(k)$ is also an eigenvalue. Explain the result physically in terms of the possible directions of propagation of perturbations in such an antisymmetric flow.

d) Let $U(y)$ be *symmetric* so that $U(y) = U(-y)$. Show that in this case $\widehat{v}$ is either symmetric or antisymmetric about $y = 0$.

[*Hint*: Letting $y \to -y$, show that the solution $\widehat{v}(-y)$ satisfies (11.95) with the same eigenvalue c. Form a symmetric solution, $S(y) = \widehat{v}(y) + \widehat{v}(-y) = S(-y)$, and an antisymmetric solution, $A(y) = \widehat{v}(y) - \widehat{v}(-y) = -A(-y)$. Then write $A[S\text{-}eqn] - S[A\text{-}eqn] = 0$ where S-eqn indicates the differential equation (11.95) in terms of S. Canceling terms this reduces to $(SA' - AS')' = 0$, where the prime (′) indicates a y-derivative. Integration gives $SA' - AS' = 0$, where the constant of integration is zero because of the boundary conditions. Another integration gives $S = bA$, where b is a constant of integration. Because the symmetric and antisymmetric functions cannot be proportional, it follows that one of them must be zero.]

Comments: If v is symmetric, then the cross-stream velocity has the same sign across the entire flow, although the sign alternates every half wavelength along the flow. This mode is consequently called *sinuous*. On the other hand, if v is

antisymmetric, then the shape of the jet expands and contracts along the length. This mode is now generally called the *sausage* instability because it resembles a line of linked sausages.

11.13. Derive (11.88) starting from the incompressible Navier-Stokes momentum equation for the disturbed flow:

$$\frac{\partial}{\partial t}(U_i + u_i) + (U_j + u_j)\frac{\partial}{\partial x_j}(U_i + u_i) = -\frac{1}{\rho}\frac{\partial}{\partial x_i}(P + p) + \nu\frac{\partial^2}{\partial x_j \partial x_j}(U_i + u_i), \qquad (11.96)$$

where U_i and u_i represent the basic flow and the disturbance, respectively. Subtract the equation of motion for the basic state from (11.96), multiply by u_i, and integrate the result within a stationary volume having stream-wise control surfaces chosen to coincide with the walls where no-slip conditions are satisfied or where $u_i \to 0$, and having a length (in the stream-wise direction) that is an integer number of disturbance wavelengths.

11.14. [2]The process of transition from laminar to turbulent flow may be driven both by exterior flow fluctuations and nonlinearity. Both of these effects can be simulated with the simple nonlinear logistic map $x_{n+1} = Ax_n(1 - x_n)$ and a computer spreadsheet program. Here, x_n can be considered to be the flow speed at the point of interest with A playing the role of the nonlinearity parameter (Reynolds number), x_0 (the initial condition) playing the role of an external disturbance, and iteration of the equation playing the role of increasing time. The essential feature illustrated by this problem is that increasing the nonlinearity parameter or changing the initial condition in the presence of nonlinearity may fully alter the character of the resulting sequence of x_n values. Plotting x_n vs. n should aid understanding for parts b) through e).

a) Determine the background solution of the logistic map that occurs when $x_{n+1} = x_n$ in terms of A.

Now, using a spreadsheet program, set up a column that computes x_{n+1} for $n = 1$ to 100 for user selectable values of x_0 and A for $0 < x_0 < 1$, and $0 < A < 4$.

b) For $A = 1.0, 1.5, 2.0,$ and 2.9, choose a few different values of x_0 and numerically determine if the background solution is reached by $n = 100$. Is the flow *stable* for these values of A, i.e., does it converge toward the background solution?

c) For the slightly larger value, $A = 3.2$, choose $x_0 = 0.6875, 0.6874,$ and 0.6876. Is the flow stable or oscillatory in these three cases? If it is oscillatory, how many iterations are needed for it to repeat?

d) For $A = 3.5$, is the flow stable or oscillatory? If it is oscillatory, how many iterations are needed for it to repeat? Does any value of x_0 lead to a stable solution?

e) For $A = 3.9$, is the flow stable, oscillatory, or chaotic? Does any value of x_0 lead to a stable solution?

---

[2]Provided to the third author by Professor Werner Dahm.

Literature Cited

Bayly, B. J., Orszag, S. A., & Herbert, T. (1988). Instability mechanisms in shear-flow transition. *Annual Review of Fluid Mechanics, 20*, 359–391.

Bergé, P., Pomeau, Y., & Vidal, C. (1984). *Order Within Chaos*. New York: Wiley.

Bhattacharya, P., Manoharan, M. P., Govindarajan, R., & Narasimha, R. (2006). The critical Reynolds number of a laminar incompressible mixing layer from minimal composite theory. *Journal of Fluid Mechanics, 565*, 105–114.

Chandrasekhar, S. (1961). *Hydrodynamic and Hydromagnetic Stability*. London: Oxford University Press. New York: Dover reprint, 1981.

Coles, D. (1965). Transition in circular Couette flow. *Journal of Fluid Mechanics, 21*, 385–425.

Davies, P. (1988). *Cosmic Blueprint*. New York: Simon and Schuster.

Drazin, P. G., & Reid, W. H. (1981). *Hydrodynamic Stability*. London: Cambridge University Press.

Eckhardt, B., Schneider, T. M., Hof, B., & Westerweel, J. (2007). Turbulence transition in pipe flow. *Annual Review of Fluid Mechanics, 39*, 447–468.

Eriksen, C. C. (1978). Measurements and models of fine structure, internal gravity waves, and wave breaking in the deep ocean. *Journal of Geophysical Research, 83*, 2989–3009.

Feigenbaum, M. J. (1978). Quantitative universality for a class of nonlinear transformations. *Journal of Statistical Physics, 19*, 25–52.

Fjørtoft, R. (1950). Application of integral theorems in deriving criteria of instability for laminar flows and for the baroclinic circular vortex. *Geofysiske Publikasjoner Oslo, 17*(6), 1–52.

Fransson, J. H. M., & Alfredsson, P. H. (2003). On the disturbance growth in an asymptotic suction boundary layer. *Journal of Fluid Mechanics, 482*, 51–90.

Grabowski, W. J. (1980). Nonparallel stability analysis of axisymmetric stagnation point flow. *Physics of Fluids, 23*, 1954–1960.

Heisenberg, W. (1924). Über Stabilität und Turbulenz von Flüssigkeitsströmen. *Annalen der Physik (Leipzig), 74*(4), 577–627.

Howard, L. N. (1961). Note on a paper of John W. Miles. *Journal of Fluid Mechanics, 13*, 158–160.

Huerre, P., & Monkewitz, P. A. (1990). Local and global instabilities in spatially developing flows. *Annual Review of Fluid Mechanics, 22*, 473–537.

Huppert, H. E., & Turner, J. S. (1981). Double-diffusive convection. *Journal of Fluid Mechanics, 106*, 299–329.

Jefferies, H. (1928). Some cases of instability in fluid motion. *Proceedings of the Royal Society London A, 118*, 195–208.

Klebanoff, P. S., Tidstrom, K. D., & Sargent, L. H. (1962). The three-dimensional nature of boundary layer instability. *Journal of Fluid Mechanics, 12*, 1–34.

Landau, L. D., & Lifshitz, E. M. (1959). *Fluid Mechanics*. Oxford, England: Pergamon Press.

Lanford, O. E. (1982). The strange attractor theory of turbulence. *Annual Review of Fluid Mechanics, 14*, 347–364.

Lin, C. C. (1955). *The Theory of Hydrodynamic Stability*. London: Cambridge University Press.

Lorenz, E. (1963). Deterministic nonperiodic flows. *Journal of Atmospheric Sciences, 20*, 130–141.

Miles, J. W. (1961). On the stability of heterogeneous shear flows. *Journal of Fluid Mechanics, 10*, 496–508.

Miles, J. W. (1986). Richardson's criterion for the stability of stratified flow. *Physics of Fluids, 29*, 3470–3471.

Nayfeh, A. H., & Saric, W. S. (1975). Nonparallel stability of boundary layer flows. *Physics of Fluids, 18*, 945–950.

Reshotko, E. (2001). Transient growth: A factor in bypass transition. *Physics of Fluids, 13*, 1067–1075.

Ruelle, D., & Takens, F. (1971). On the nature of turbulence. *Communications in Mathematical Physics, 20*, 167–192.

Schubauer, G. B., & Skramstad, H. K. (1947). Laminar boundary-layer oscillations and transition on a flat plate. *Journal of Research of the National Bureau of Standards, 38*, 251–292.

Scotti, R. S., & Corcos, G. M. (1972). An experiment on the stability of small disturbances in a stratified free shear layer. *Journal of Fluid Mechanics, 52*, 499–528.

Shen, S. F. (1954). Calculated amplified oscillations in plane Poiseuille and Blasius Flows. *Journal of the Aeronautical Sciences, 21*, 62–64.

Squire, H. B. (1933). On the stability of three dimensional disturbances of viscous flows between parallel walls. *Proceedings of the Royal Society London A, 142*, 621–628.

Stern, M. E. (1960). The salt fountain and thermohaline convection. *Tellus, 12*, 172–175.

Stommel, H., Arons, A. B., & Blanchard, D. (1956). An oceanographic curiosity: The perpetual salt fountain. *Deep-Sea Research, 3,* 152—153.

Thorpe, S. A. (1971). Experiments on the instability of stratified shear flows: Miscible fluids. *Journal of Fluid Mechanics, 46,* 299—319.

Turner, J. S. (1973). *Buoyancy Effects in Fluids.* London: Cambridge University Press.

Turner, J. S. (1985). Convection in multicomponent systems. *Naturwissenschaften, 72,* 70—75.

Woods, J. D. (1969). On Richardson's number as a criterion for turbulent—laminar transition in the atmosphere and ocean. *Radio Science, 4,* 1289—1298.

Yih, C. S. (1979). *Fluid Mechanics: A Concise Introduction to the Theory.* Ann Arbor, MI: West River Press.